LBNL-41308

ERNEST ORLANDO LAWRENCE
BERKELEY NATIONAL LABORATORY

Anion Photoelectron Spectroscopy of Semiconductor Clusters

Cangshan Xu

Chemical Sciences Division

December 1997

Ph.D. Thesis

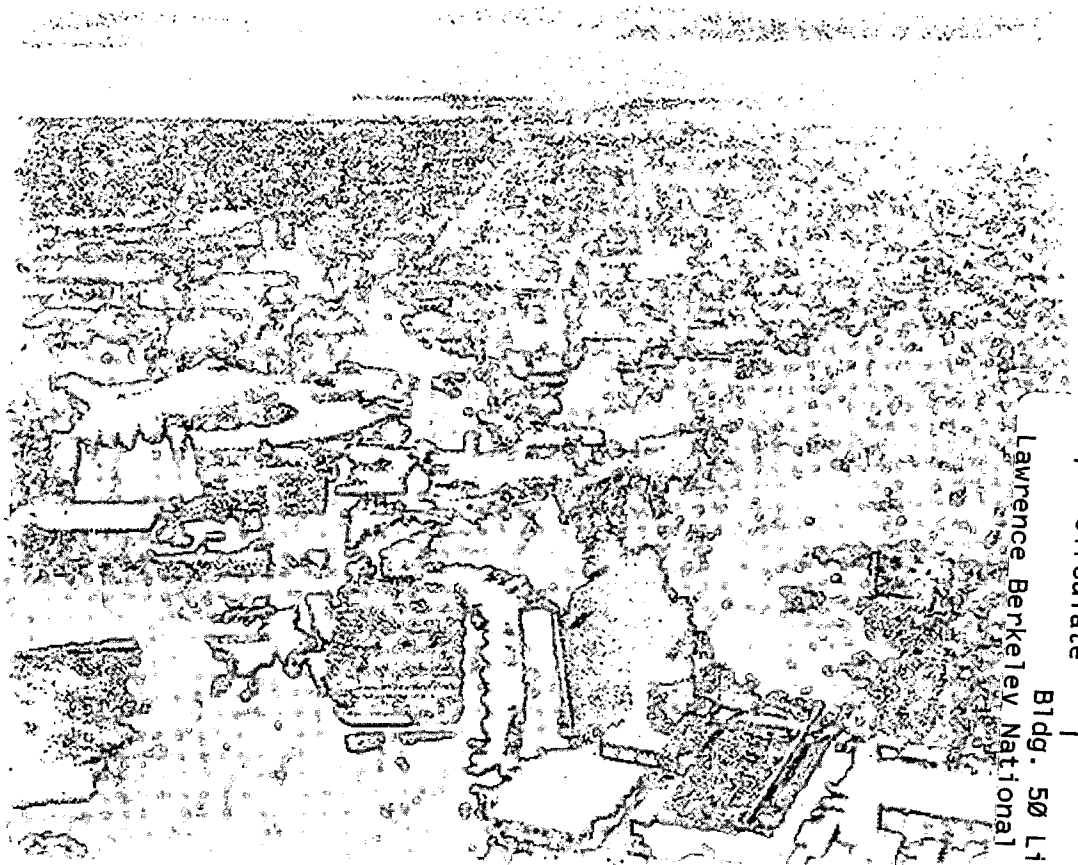

DISCLAIMER

LBNL-41308

Anion Photoelectron Spectroscopy of Semiconductor Clusters

Cangshan Xu
Ph.D. Thesis

Department of Chemistry
University of California, Berkeley

and

Chemical Sciences Division
Ernest Orlando Lawrence Berkeley National Laboratory
University of California
Berkeley, CA 94720

December 1997

This work was supported in part by the Director, Office of Energy Research, Office of Basic Energy Sciences, Chemical Sciences Division, of the U.S. Department of Energy under Contract No. DE-AC03-76SF00098, and by the National Science Foundation.

Anion Photoelectron Spectroscopy of Semiconductor Clusters

by

Cangshan Xu

B.S. (University of Science and Technology of China) 1992

A dissertation submitted in partial satisfaction of the

requirements for the degree of

Doctor of Philosophy
in

Chemistry

in the

GRADUATE DIVISION

of the

UNIVERSITY OF CALIFORNIA, BERKELEY

Committee in charge:

Professor Daniel M. Neumark, Chair
Professor A. Paul Alivisatos
Professor Roger W. Falcone

Fall 1997

This work was supported in part by the Director, Office of Energy Research, Office of Basic Energy Sciences, Chemical Sciences Division, of the U.S. Department of Energy under Contract No. DE-AC03-76SF00098, and in part by the National Science Foundation.

Anion Photoelectron Spectroscopy of Semiconductor Clusters

by

Cangshan Xu

ABSTRACT

Anion Photoelectron Spectroscopy of Semiconductor Clusters

by

Cangshan Xu

Doctor of Philosophy in Chemistry

University of California, Berkeley

Professor Daniel M. Neumark, Chair

Semiconductor and related clusters are studied by anion photoelectron spectroscopy. Vibrationally-resolved photoelectron spectra of carbon (C_4^-, C_6^-, and C_8^-) and silicon (Si_3^- - Si_7^-) clusters were measured at various photodetachment wavelengths. Electron affinities, term energies, and vibrational frequencies for the ground and excited electronic states of the neutral clusters have been obtained. The assignments of excited electronic states were aided by *ab initio* calculations, as well as measurements of photoelectron angular distributions.

Besides clusters of pure elements, mixed group III-V clusters are also investigated. Small indium phosphide clusters having 2-8 atoms are studied using anion photoelectron spectroscopy of $In_xP_y^-$ (x,y = 1-4). Both ground and low-lying electronic states of the neutral clusters are observed. Electron affinities are determined from the spectra. An electronic gap is shown in the even cluster anion spectra.

Other related clusters, Si_nH (n = 2-4) and PO_2 were also studied. The electron affinities and ground state vibrational frequencies are obtained from the spectral assignments, aided by *ab initio* calculations and photoelectron angular distributions. The anion geometry of PO_2 is also obtained from Franck-Condon analysis.

TABLE OF CONTENTS

Acknowledgments

I would first like to express my sincere gratitude to Professor Daniel Neumark for his guidance and support throughout the years. Dan's knowledge and enthusiasm for science have provided me with inspiration and motivation. It was a great fortune to have a research advisor like Dan who entrusted me to disassemble a machine, built by himself, and then rebuild it (hopefully improving it)! I am also grateful for his efforts in helping me to improve my experimental and linguistic skills.

Dr. Don Arnold taught me how to operate and understand the wonderful anion photoelectron spectrometer and to analyze data using his PES simulation code. I still remember his words, "To talk to the ions", which benefited me a lot during the long hours of data accumulation. He also gave me valuable suggestions and help on designing the linear mass reflectron.

Working with Dr. Gordon Burton, the tallest man I have ever worked with, was absolutely enjoyable. He gave me the chance to be exposed to many jokes I had never heard of (and probably will not in the future). The "KISS" (keep it silly simple) gas degreaser Gordon made had significant contribution for cleaning the parts from the machine shop.

Travis Taylor joined the PES project in 1994 from Utah State University (USU), and soon built his USU box (a dual channel micro motor controller). Travis has been a good co-worker to work with, despite his couple months of "sabbatical" due to a bike injury. The pursuing of cyclic C_6^- and the creative approaches of MALDI certainly made

the times more unforgettable. I still owe him a special thank you for lending me a sleeping bag during a cold -20°C camping-rafting trip in the late Spring.

Dr. Knut Asmis, a talented post-doc from Switzerland, joined the project in 1996 and contributed immediately to the $I_2(Ar)_n^-$ cluster experiments. I am also very grateful to other Neumark group members, both past and present, who have constantly provided me with help and guidance.

Dr. Esther deBeer deserves special credit for helping me to explore the indium phosphide world, along with Eun Ha Kim who patiently explained vibronic coupling to me.

Professor Caroline Jarrold, University of Illinois at Chicago, led me into the world of semiconductor clusters by helping me collect my first indium phosphide cluster spectrum. She also taught me the tricks to keep the "baby" YAG happy and running for most of the time.

I would also like to thank Dr. Doug Cyr for pioneering the discharge ion source, which made the studies of carbon, silicon, and silicon hydride clusters possible.

Dr. Yuexing Zhao taught me valuable lessons during the graduate school years as my fellow country man. The collaborated experiment between PES and ZEKE labs had involved probably the longest laser beam path in the Neumark group. Moreover, he helped me find my first job and continues to educate me at the company!

Dr. David Osborn has been such an effective system administrator, he even inspired me to become a PC and UNIX lover. I also thank him for a wonderful Thanksgiving lunch.

Ivan Yourshaw joined the group at the same time that I did, and will soon become Dr. Yourshaw. I am glad that he was in the same statistical mechanics and quantum mechanics classes with me; I could always find an answer when I was stuck by the tricky homeworks. Jeff Greenblatt, probably the only American in the group who understands and speaks (!) Chinese, had given me a hard time by asking me a lot of China-related questions. Fortunately, it was balanced out by my stupid questions of American culture. Jeff has been working hard with Marty Zanni building and fine-tuning the Femto-second Photoelectron Spectrometer. They have been rewarded by several exciting results. Mike Furlanetto has been taking care of all the UNIX workstations for a year. The nice setup of the new SGI, by Mike, made my Gaussian jobs a lot smoother and faster. Ryan Bise deserves special mention for teaching me skate-boarding. Hyeon Choi had brought extra fun for the annual dim-sum trips, which I enjoyed a lot. I wish them all the best.

Dr. David Mordaunt and Dr. Thomas Lenzer, two brilliant post-docs, brought not only fresh ideas and dedicated hard work, but also, fantasy homepages to the group.

As I was writing the thesis, Dan's group bloomed again. Four new graduate students: Alison Davis, Harry Gomez, Nick Pivonka, Jason Robinson and a new post-doc, Weizhong Sun joined the group. I wish them tremoundous success in the future.

I would like to thank Cheryn Gliebe and Noreen Buyers, two wonderful administrative assistants associated with Dan's group, for helping me go through the countless paper work. I also thank Eric Granlund, Hans Graetsch, and Dave Murai of the machine shop who turned my numerous draws into nicely finished parts.

A special thanks must go to my preliminary exam committee: Professor Yongqin Chen (Chair), Professor Paul Alivisatos, Professor William Lester and Professor Roger Falcone (Physics).

This work was supported by the National Science Foundation under Grant No. DMR-9521805, and in part by the Director, Office of Energy Research, Office of Basic Energy Sciences, Chemical Sciences Division of the U. S. Department of Energy under contract No. DE-AC03-76SF00098. I would also like to thank the Abraham and Lo Foundations for the fellowships.

I am truly blessed to have a wonderful and supportive family. Although thousands of miles have often separated us, they have been a constant source of love and encouragement. My deepest thanks to my parents and sister, who have inspired me throughout all my life. I also want to thank my cousin, Donna Kong, the only relative in the States. Finally, I wish to extend my heartfelt appreciation to Song, for her invaluable support and unending love.

1 Introduction

The electronic and vibrational spectroscopy of size-selected clusters has been an extremely active area in physical chemistry, as it offers an unprecedented opportunity to understand how the properties of matter evolve from the molecular to the bulk limits. This thesis describes the experiments aimed at probing the electronic and vibrational spectroscopy of carbon and semiconductor clusters as a function of their size. The experiments were carried out using negative ion photoelectron spectroscopy, which intrinsically offers mass-selectivity. The spectral resolution is about 60-80 cm^{-1}, which is sufficient to resolve vibrational structure of most of the species. Moreover, anion photoelectron spectroscopy allows us to observe optically dark states that are inaccessible by traditional absorption or emission experiments and vibrational frequencies in totally symmetric modes that are often complementary to the frequencies obtained by IR absorption spectroscopy. This technique has been applied successfully to obtain the electronic and vibrational structures of pure elemental semiconductor clusters of carbon[1-7], silicon[8-14], and germanium[10,15,16] clusters, as well as group III-V mixed clusters, such as gallium arsenide[17] and indium phosphide[18].

This thesis first describes the improvements of the experimental apparatus. The modifications increase our mass resolution by a factor of ten. The succeeding chapters will focus on the experiments of carbon, semiconductor, and related clusters using anion photoelectron spectroscopy. In Chapter 3, new anion photoelectron spectra of C_4^-, C_6^-,

and C_8^- will be presented. These better-resolved spectra provide a detailed picture of the low-lying excited electronic states of the neutral clusters. Chapter 4 represents an extension of our earlier work on the photoelectron spectroscopy of silicon cluster anions[8]. Vibrationally-resolved spectra of anion silicon clusters up to Si_7^- have been measured, yielding new information on the anion and neutral geometries as well as the excited state energies of the neutral clusters. Chapter 5 describes the study of small indium phosphide clusters using anion photoelectron spectroscopy. Electron affinities are determined from the photoelectron spectra. An electronic gap, typically quite close to the band gap of bulk crystalline indium phosphide, was observed in the spectra. The last two chapters will describe studies of other related clusters (silicon monohydrides and PO_2) using the same experimental technique.

Spectroscopy of carbon and semiconductor clusters

Carbon clusters have been the subject of experimental and theoretical research for many years. High resolution gas phase infrared and matrix isolation studies on the ground state of linear carbon clusters have provided rotational and some vibrational information for C_3-C_9 and C_{13} [19-25]. Anion photoelectron spectroscopy[1,4,5] and zero electron kinetic energy (ZEKE) spectroscopy[2,3,6] have been used to obtain vibrational frequencies of several totally symmetric modes. *Ab initio* calculations have predicted the existence of low-lying electronic states which are optically forbidden from the ground state of the neutral cluster[26-33], and are accessible via one-electron photodetachment from the anion

ground state. However, due to low resolution[4,5] or insufficient photon energy[1], only obscure information was extracted from the previous anion photoelectron spectra of these species.

Semiconductor clusters are of great interest from not only the perspective of fundamental chemistry and physics, but also the electronic industry. Small clusters have been found as reaction intermediates in the plasma processing of semiconductors,[34] and larger semiconductor clusters have shown promise for use in electronic devices.[35] In terms of their electronic structure, the small clusters are better viewed as large molecules. The large clusters which are composed of thousands of atoms, however, can be explained by quantum confinement. Characterization of the energetics and structure of these species are highly desirable.

Silicon clusters, for example, have been studied extensively because of their importance in astrophysics and chemical vapor deposition. These species are also of considerable interest from the perspective of spectroscopy. *Ab initio* calculations predict the structure of silicon clusters to change dramatically as the size of cluster increases and they are different from carbon clusters of the same number of atoms. However, experimental work on small silicon clusters is sparse. Smalley and coworkers[4,5] have obtained anion photoelectron spectra of Si_n^- ($n \leq 13$), showing a qualitative picture of the electronic states of the neutral clusters. Substantially higher resolution spectra of Si_2^-, Si_3^- and Si_4^- have been measured by Ellison[36] and our group[8,9,11-13] using anion photoelectron spectroscopy and threshold photodetachment spectroscopy. These spectra provide far more detailed insight into the electronic and vibrational structure of the low-lying excited

states. It has been difficult to obtain vibrationally-resolved photoelectron spectra of clusters larger than Si_4^-. Recently, Eberhardt and co-workers have obtained a spectrum of Si_7^- with sufficient resolution to observe a vibrational progression[37]. Matrix isolation spectroscopy of Si_n (n=3-4,6-7) complements the gas phase studies. Raman and infrared spectra of mass-selected clusters in matrices revealed vibrational frequencies for the ground electronic states of these species[38,39].

Mixed semiconductor clusters, such as GaAs, GaN, and InP, are more challenging to experimentalists and theoreticians. From a theoretical view of point, the number of possible isomers, particularly for clusters with heavy atoms, creates extra calculating complexity. From an experimental standpoint, better size-selectivity is required because of high-mass elements and isotope distribution, spectral resolution also becomes more critical in order to distinguish close-lying electronic states predicted by calculations. Mandich and co-workers[40,41] have performed a photodissociation spectroscopy study of small indium phosphide clusters and observed relatively sharp onsets in the photodissociation spectra corresponding to an energy gap between the ground and excited electronic states of the clusters. The energy gap in these very small clusters is quite close to the band gap in bulk indium phosphide, 1.34 eV, suggesting that these small clusters exhibit properties reminiscent of the bulk material. Smalley and co-workers[17,42-44] have performed photoionization and photodetachment experiments on gallium arsenide clusters, finding that clusters with an odd number of atoms consistently have lower ionization potentials and higher electron affinities than even clusters.

Principles of anion photoelectron spectroscopy

Figure 1 illustrates the fundamental principles of anion photoelectron spectroscopy. Briefly, a negative ion is photodetached and produces the corresponding neutral species, as shown by Equation (1):

$$M^- + h\nu \rightarrow M + e^-, \qquad (1)$$

where $h\nu$ is the photon energy[45,46]. The spectral features of a photoelectron spectrum correspond to the transitions between the anion electronic ground state and various neutral electronic states. For each peak, the electron kinetic energy (eKE) is given by:

$$eKE = h\nu - EA - T_o^{(o)} + T_o^{(-)} - E_v^{(o)} + E_v^{(-)}, \qquad (2)$$

where EA is the adiabatic electron affinity of the neutral species, $T_o^{(o)}$ and $T_o^{(-)}$ are the term values of the neutral and anion electronic states, and $E_v^{(o)}$ and $E_v^{(-)}$ are the neutral and anion vibrational energies, respectively, above the zero point energy.

Since anions are generated in a supersonic jet expansion, their internal energies are usually well defined, and a majority of them are in the ground electronic and vibrational state. In other words, $T_o^{(-)}$ and $E_v^{(-)}$ equal zero in most of the circumstances. Given a fixed photon energy $h\nu$, a measurement of the eKE's yields the internal energies of the neutral electronic and vibrational states. Higher eKE corresponds to a lower internal energy.

Besides energy information, one can obtain geometry information from the vibrational progression profiles, which are governed by Franck-Condon factor:

$$I \propto |\tau_e|^2 \bullet |\langle \Psi_{v''}(Q'') | \Psi_{v'}(Q') \rangle|^2, \qquad (3)$$

Anion Photoelectron Spectroscopy

$$M^- + h\nu \rightarrow M + e^-$$

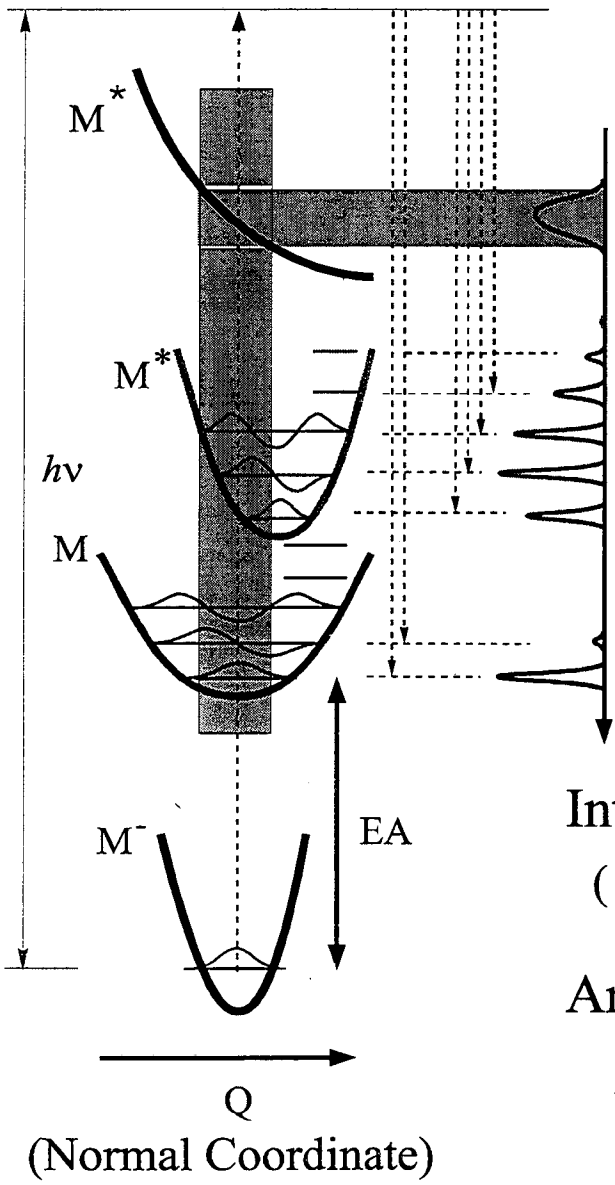

$eKE = h\nu - EA - E_{int}$

Higher electron kinetic energy (eKE) corresponds to lower internal energy of neutral molecule

eKE

$$\text{Intensity} \propto |\langle \Psi_{\upsilon''} | \Psi_{\upsilon'} \rangle|^2$$

(Franck-Condon Factor)

Angular distribution

$$\frac{d\sigma}{d\Omega} = \frac{\sigma_{total}}{4\pi}[1 + \beta(E)P_2(\cos\theta)]$$

FIG. 1. Principles of anion photoelectron spectroscopy.

where τ_e is the electronic transition dipole moment, $\Psi_{v"}(Q")$ and $\Psi_{v'}(Q')$ are the vibrational wave functions for the anion and neutral. We assume τ_e remain constant within an electronic transition. The relative peak intensities, therefore, provide the information on the geometry change between the anion and neutral. In general, larger normal coordinate displacement corresponds to a longer progression, which is demonstrated qualitatively in Figure 1. For instance, the transition from the anion ground state M^- to the neutral ground state M has a small value of displacement, resulting a very short vibrational progression. The transition to the neutral excited state M*, on the other hand, has a long vibrational progression because of the large ΔQ. The normal coordinate displacement is directly related to the difference in geometry. For a diatomic molecule, normal coordinate Q is the bond length. A non-zero ΔQ between two electronic states indicates they have different bond lengths.

In order to evaluate the integration in Equation (3) for polyatomic species, $\Psi_{v"}$ and $\Psi_{v'}$ must be expressed as functions of the same coordinates for both states. The transformation of the two normal coordinates is given by

$$Q" = J"Q' + K", \qquad (4)$$

where J" is the Duschinsky rotation matrix and K" is the normal coordinate displacements expressed in terms of the anion normal coordinates.[47-50] Under the parallel mode approximation, Duschinsky matrix J" equals E,[51,52] the unit matrix, and the integral in Equation (3) is separable into a product of integrals for each normal-coordinate modes:

$$\begin{aligned}\int \Psi_{v'}(Q')\Psi_{v"}(Q")dQ' &= \int \left[\Psi_{v_1'}\Psi_{v_2'}\ldots\Psi_{v_n'}\right]\bullet\left[\Psi_{v_1"}\Psi_{v_2"}\ldots\Psi_{v_n"}\right]\bullet dQ' \\ &= \left[\int \Psi_{v_1'}\Psi_{v_1"}dQ'\right]\bullet\left[\int \Psi_{v_2'}\Psi_{v_2"}dQ'\right]\bullet\ldots\bullet\left[\int \Psi_{v_n'}\Psi_{v_n"}dQ'\right]\end{aligned} \qquad (5)$$

One can obtain geometries and force constants of the anion and neutral from *ab initio* calculations. The geometry change between the anion and neutral is then converted to normal coordinate displacements using an in-house Fortran code (Appendix A). Given the normal coordinate displacements and apparatus resolution, a spectral simulation can be performed using an Franck-Condon integral analysis program that described in detail previously[53].

Besides *ab initio* calculations, photoelectron angular distribution is very useful in assigning overlapped transitions in photoelectron spectra, which is given by[54]

$$\frac{d\sigma}{d\Omega} = \frac{\sigma_{total}}{4\pi}\left[1 + \beta(E)P_2(\cos\theta)\right], \qquad (6)$$

where σ_{total} is the total photodetachment cross section and β(E) is the asymmetry parameter. β(E) varies from –1 to 2; these limits correspond to $\sin^2\theta$ and $\cos^2\theta$ distribution, respectively. One can determine β for each peak in the photoelectron spectrum through its intensity variation with laser polarization angle. The β parameter for each electronic band is then determined by averaging values of the constituent peaks. The β parameter is not expected to change significantly over a vibrational progression within the transition to a single electronic state of the neutral. Conversely, peaks with considerably different values of β should be associated with different electronic transitions. However, one cannot assume that peaks with the same value of β belong to the same electronic transition. Demonstrations of such determinations are given in Chapters 3-5.

References

[1] D. W. Arnold, S. E. Bradforth, T. N. Kitsopoulos, and D. M. Neumark, J. Chem. Phys. **95,** 8753 (1991).

[2] C. C. Arnold, Y. X. Zhao, T. N. Kitsopoulos, and D. M. Neumark, J. Chem. Phys. **97,** 6121 (1992).

[3] C. C. Arnold and D. M. Neumark, J. Chem. Phys. **99,** 1442 (1993).

[4] S. Yang, K. J. Taylor, M. J. Craycraft, J. Conceicao, C. L. Pettiette, O. Cheshnovsky, and R. E. Smalley, Chem. Phys. Lett. **144,** 431 (1988).

[5] S. H. Yang, C. L. Pettiette, J. Conceicao, O. Cheshnovsky, and R. E. Smalley, Chem. Phys. Lett. **139,** 233 (1987).

[6] T. N. Kitsopoulos, C. J. Chick, Y. Zhao, and D. M. Neumark, J. Chem. Phys. **95,** 5479 (1991).

[7] C. Xu, G. R. Burton, T. R. Taylor, and D. M. Neumark, J. Chem. Phys. **107,** 3428 (1997).

[8] T. N. Kitsopoulos, C. J. Chick, A. Weaver, and D. M. Neumark, J. Chem. Phys. **93,** 6108 (1990).

[9] T. N. Kitsopoulos, C. J. Chick, Y. Zhao, and D. M. Neumark, J. Chem. Phys. **95,** 1441 (1991).

[10] O. Cheshnovsky, S. H. Yang, C. L. Pettiette, M. J. Craycraft, Y. Liu, and R. E. Smalley, Chem. Phys. Lett. **138,** 119 (1987).

[11] C. C. Arnold, T. N. Kitsopoulos, and D. M. Neumark, J. Chem. Phys. **99,** 766 (1993).

[12] C. C. Arnold and D. M. Neumark, J. Chem. Phys. **99,** 3353 (1993).

[13] C. C. Arnold and D. M. Neumark, J. Chem. Phys. **100,** 1797 (1994).

[14] C. Xu, T. R. Taylor, G. R. Burton, and D. M. Neumark, J. Chem. Phys. , submitted (1997).

[15] G. R. Burton, C. Xu, C. C. Arnold, and D. M. Neumark, J. Chem. Phys. **104,** 2757 (1996).

[16] G. R. Burton, C. Xu, and D. M. Neumark, Surface Review and Letters **3,** 383 (1996).

[17] C. Jin, K. J. Taylor, J. Conceicao, and R. E. Smalley, Chem. Phys. Lett. **175,** 17 (1990).

[18] C. Xu, E. Debeer, D. W. Arnold, C. C. Arnold, and D. M. Neumark, J. Chem. Phys. **101,** 5406 (1994).

[19] N. Moazzen-Ahmadi, A. R. W. McKellar, and T. Amano, J. Chem. Phys. **91,** 2140 (1989).

[20] N. Moazzen-Ahmadi, A. R. W. McKellar, and T. Amano, Chem. Phys. Lett. **157,** 1 (1989).

[21] H. J. Hwang, A. Vanorden, K. Tanaka, E. W. Kuo, J. R. Heath, and R. J. Saykally, Mol. Phys. **79,** 769 (1993).

[22] J. R. Heath and R. J. Saykally, J. Chem. Phys. **94,** 3271 (1991).

[23] J. R. Heath and R. J. Saykally, in *On clusters and clustering, from atoms to fractals*, edited by P. J. Reynolds (Elsevier, Amsterdam, 1993), pp. 7-21.

[24] T. F. Giesen, A. Van Order, H. J. Hwang, R. S. Fellers, R. A. Provencal, and R. J. Saykally, Science **265,** 756 (1994).

[25] P. F. Bernath, K. H. Hinkle, and J. J. Keady, Science **244,** 562 (1989).

[26] L. Adamowicz, Chem. Phys. **156,** 387 (1991).

[27] L. Adamowicz, Chem. Phys. Lett. **182,** 45 (1991).

[28] L. Adamowicz, Chem. Phys. Lett. **180,** 466 (1991).

[29] C. Liang and H. F. Schaefer, III, Chem. Phys. Lett. **169,** 150 (1990).

[30] D. H. Magers, R. J. Harrison, and R. J. Bartlett, J. Chem. Phys. **84,** 3284 (1986).

[31] G. Pacchioni and J. Koutecký, J. Chem. Phys. **88,** 1066 (1988).

[32] V. Parasuk and J. Almlöf, J. Chem. Phys. **91,** 1137 (1989).

[33] V. Parasuk and J. Almlöf, J. Chem. Phys. **94,** 8172 (1991).

[34] A. Bouchoule, Physics World **6,** 47 (1993).

[35] V. L. Colvin, M. C. Schlamp, and A. P. Alivisatos, Nature **370,** 354 (1994).

[36] M. R. Nimlos and G. B. Ellison, J. Chem. Phys. **87,** 5116 (1987).

[37] G. S. Ickingkonert, H. Handschuh, P. S. Bechthold, G. Gantefor, B. Kessler, and W. Eberhardt, Surface Review and Letters **3,** 483 (1996).

[38] E. C. Honea, A. Ogura, C. A. Murray, K. Raghavachari, W. O. Sprenger, M. F. Jarrold, and W. L. Brown, Nature **366,** 42 (1993).

[39] S. Li, R. J. Vanzee, W. Weltner, and K. Raghavachari, Chem. Phys. Lett. **243,** 275 (1995).

[40] K. D. Rinnen, K. D. Kolenbrander, A. M. Desantolo, and M. L. Mandich, J. Chem. Phys. **96,** 4088 (1992).

[41] K. D. Kolenbrander and M. L. Mandich, J. Chem. Phys. **92,** 4759 (1990).

[42] S. C. O'Brien, Y. Liu, Q. Zhang, J. R. Heath, F. K. Tittel, R. F. Curl, and R. E. Smalley, J. Chem. Phys. **84,** 4074 (1986).

[43] L. Lou, L. Wang, L. P. F. Chibante, R. T. Laaksonen, P. Nordlander, and R. E. Smalley, J. Chem. Phys. **94,** 8015 (1991).

[44] L. Lou, P. Nordlander, and R. E. Smalley, J. Chem. Phys. **97,** 1858 (1992).

[45] J. Berkowitz, *Photoabsorption, Photoionization and Photoelectron Spectroscopy* (Academic Press, New York, 1979).

[46] J. W. Rabalais, *Principles of Ultraviolet Photoelectron Spectroscopy* (Wiley, New York, 1977).

[47] T. E. Sharp and H. M. Rosenstock, J. Chem. Phys. **41,** 3453 (1964).

[48] R. Botter, V. H. Dibeler, J. A. Walker, and H. M. Rosenstock, J. Chem. Phys. **44,** 1271 (1966).

[49] F. Duschinsky, Acta Physicochim. URSS **7** (1937).

[50] K. M. Ervin, J. Ho, and W. C. Lineberger, J. Phys. Chem. **92,** 5405 (1988).

[51] C. Eckart, Phys. Rev. **47,** 552 (1935).

[52] A. Warshel and M. Karplus, Chem. Phys. Lett. **17,** 7 (1972).

[53] D. W. Arnold, Ph. D. Dissertation, Univeristy of California, Berkeley, 1994.

[54] J. Cooper and R. N. Zare, in *Lectures in Theoretical Physics*, Vol. XI-C, edited by S. Geltman, K. T. Mahanthappa, and W. E. Brittin (Gordon and Breach, New York, 1969), pp. 317-337.

2 Experimental Improvements

The apparatus used in the experiments is a time-of-flight anion photoelectron spectrometer. The original version of this instrument has been described in detail previously[1-3]. Several modifications have been made to improve the overall performance. First, a modified laser ablation source has been developed for the use of disk-like target materials. In addition, a pulsed electrical discharge source has been employed to generate substantially "colder" ions. Detailed description of the free jet pulsed discharge source can be found in the dissertation of David Osborn[4]. The ion extraction electronic devices have been modified so that the ion source no longer needs to be floated at high voltage. Finally, a mass reflectron stage has been added to improve the resolution of the time-of-flight mass spectrometer. The entire modified apparatus is shown in Figure 1. Detailed descriptions are presented in the following sections.

I. Ion sources

Several ion sources have been used for making various negative ions. The previous semiconductor cluster experiments were carried out on a "rod" source described in the dissertation of Caroline Arnold[5]. However, the ion signal becomes unstable after a few runs due to the thinning of the rod and the required rod targets are difficult to pre-

pare. A modified version of the laser ablation source has been developed to allow the use of more easily obtained disk shape targets.

A schematic of the "disk" source is shown in Figure 2. Briefly, two mini motors are used to rotate and translate the disk target simultaneously. The second harmonic

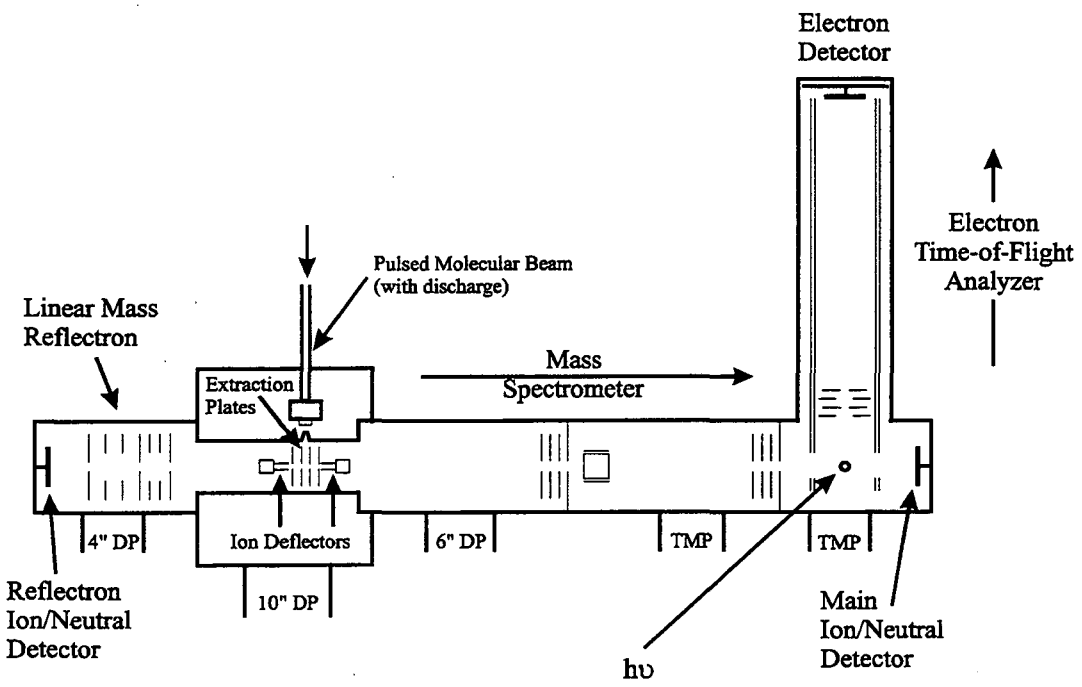

FIG. 1. Anion photoelectron spectrometer with linear mass reflectron.

532nm of a Nd: YAG laser is focused onto the fresh surface of the target. The laser operates at 20 Hz, and the power varies from 0.5 – 2.0 W. The resulting plasma is then entrained in a pulse of a rare gas and expends through the clustering channel. The distance between the ablated surface and the clustering channel wall can be easily adjusted, so that the thickness of the disk does not affect the ion stability. The speed and direction of the mini motors can be adjusted separately to obtain the best ion quality. Although the clus-

tering channel in the "disk" source is two inches long, about twice as long as the previous "rod" source, there is no significant decrease of the ion density.

The pulsed discharge source has proved to be a very stable and efficient alternative to generate cluster ions. Some previously hard-to-form ions are easy to obtain from the discharge source. For example, carbon hydrides $C_xH_y^-$ and silicon hydrides $Si_xH_y^-$ are generated by discharging rare-gas-buffered C_2H_2 and SiH_4, respectively. In addition, clusters formed by the discharge source seem to have a lower vibrational temperature which is demonstrated by the Si_4^- spectra in Chapter 4. The simple but significant improvement over the traditional ablation source facilitates the study of silicon clusters Si_n (n=3-7) in Chapter 4.

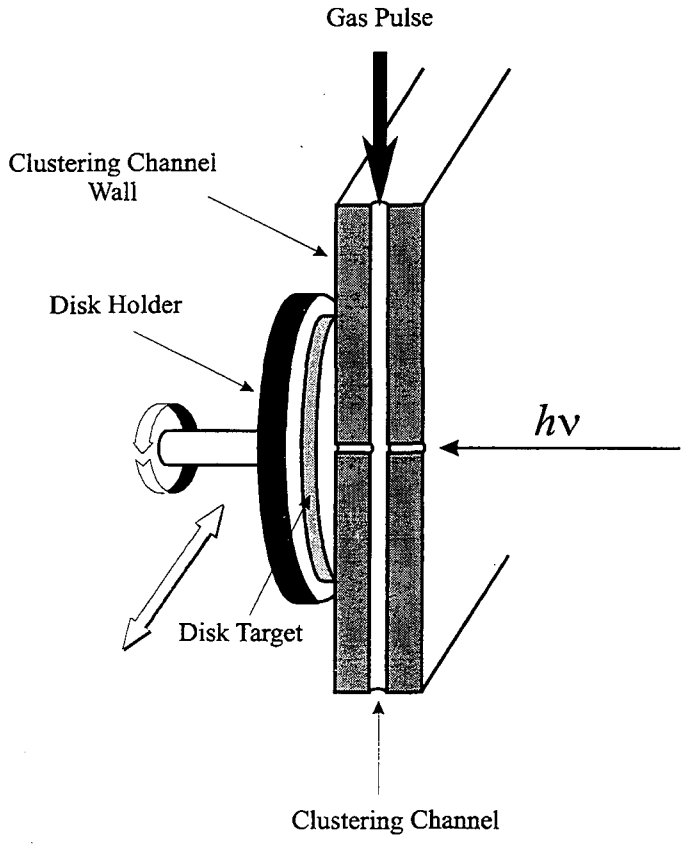

FIG. 2. Laser ablation source for disk targets.

II. Ion extraction

Previously, the entire source region was floated at -1000 V potential[1]. This floating design generates ions at –1 kV and accelerates them to the same ion beam energy after their leaving of the source region. However, it is not suitable for the use of higher beam energy. Moreover, the beam valve, the coupling ion generators, such as laser ablation or discharge sources, and their power supplies also need to be floated at the high voltage respect to ground. The cumbersome design creates potential safety hazards.

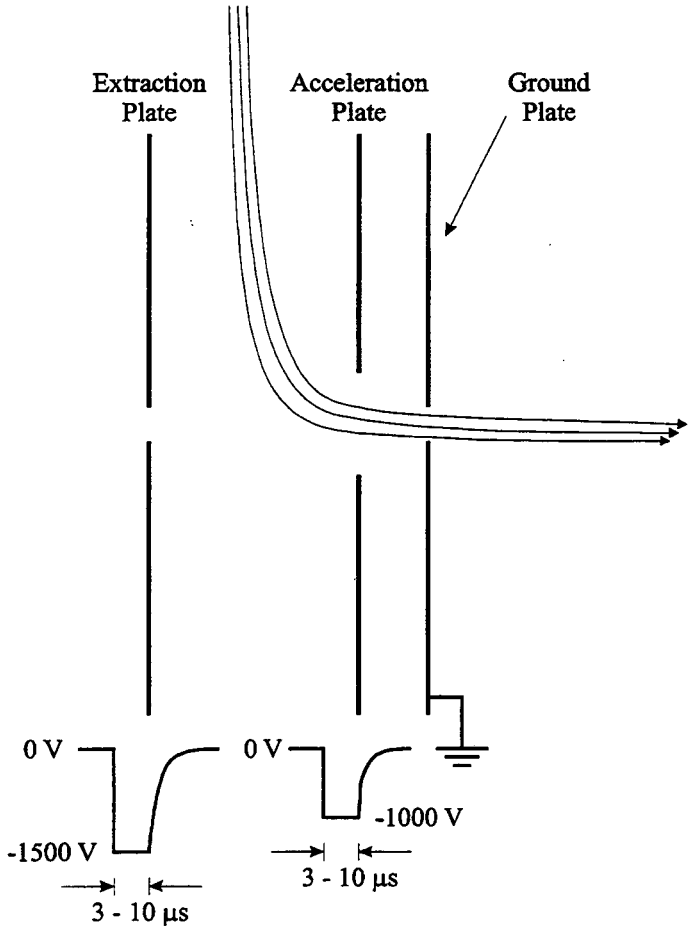

FIG. 3. Dual-pulse ion extraction scheme.

A double-pulse scheme shown in Figure 3 is used as a replacement of the floating design. Briefly, it is comprised of two major components: a set of three 1/16" thick stainless steel plates and a fast high voltage double-pulse generator. The three plates are labeled as extraction, acceleration, and ground plates, respectively. They are 4.5"x 4.5" square plates with apertures of ¼" diameter (for extraction and ground plates) or ½" diameter (for acceleration plate). The extraction region is defined by the extraction and acceleration plates separated by 3 cm, and the acceleration region is 1 cm wide, shown in Figure 3. The ions are extracted from the beam by applying a pulsed electric field across the extraction and acceleration plates; the ground plate is maintained at ground potential. Typically, pulses of –1500 V and –1000 V with less than 100 ns rise times from the double-pulse generator are applied to the extraction and acceleration plates, respectively, resulting in an extraction potential of 500 V and a nominal ion beam energy of 1250 eV. The pulse duration is around 3-10 μs, and the potentials of the extraction and acceleration plates are reset to ground by the time the ions return from the reflectron.

A stacked MOSFET design is employed in the fast double-pulse generator. This circuit was originally designed for the potential re-referencing cylinder in the Fast Molecular Beam Machine (FRBM), described in detail previously[4,6]. Slight modifications are made to generate two high-voltage negative pulses simultaneously. The circuit diagram is shown in Figure 4. Two parallel stacks of five and seven RFP4N100 MOSFET stages are driven by two separate TC4422CPA MOSFET drivers respectively. To ensure a simultaneous response, the two TC4422CPAs are triggered by the same TTL pulse. The pulse width is adjustable from 3 to 10 μs. The generator is capable of pulses up to 5

and 7 kV, respectively, corresponding to an ion beam energy of 6 kV. The switching time is less than 100 ns and the recovery time is about 5 μs.

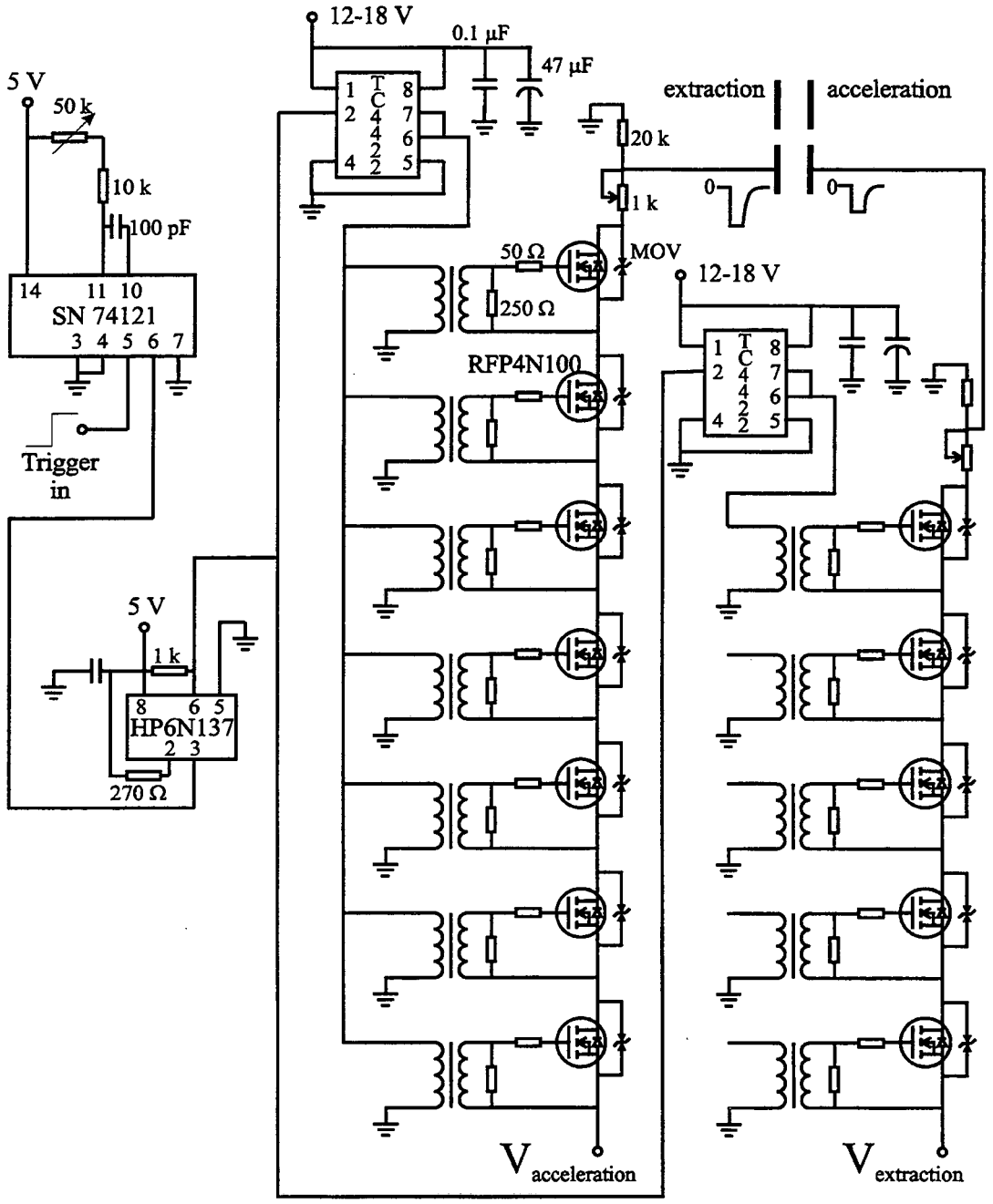

FIG. 4. Circuit diagram of dual-pulse generator.

III. Mass reflectron

The typical mass resolution M/ΔM of a Wiley-McLaren-type mass spectrometer[7] is about 300, which is suitable for low-mass ion separations. In the old design, negative ions are extracted from the source region to the acceleration region, in which a uniform electric field is applied to accelerate ions to a given energy. Ions then enter a field-free drift tube and separate by their mass to charge ratio. The first order space focus is obtained by

$$\left(\frac{dT}{ds}\right)_{s=s_0} = 0, \tag{1}$$

where T is the ions total flight time, and s_0 is the ion initial position as shown in Figure.5. The focal drift tube length is given by[7]

$$D = 2s_0 k_0^{\frac{3}{2}}\left(1 - \frac{1}{k_0 + \sqrt{k_0}}\frac{d}{s_0}\right), \tag{2}$$

where d is the length of the acceleration region and

$$k_0 = \frac{s_0 E_s + dE_d}{s_0 E_s}, \tag{3}$$

where E_s is the extraction field and E_d the acceleration field shown in Figure 5. The focal length can be adjusted by varying the electric fields. The second order space focus is also achievable, in which not only the linear but also the quadratic term, d^2T/ds^2, equals zero.[8,9] However, the position of the second order space focus is fixed, and determined by

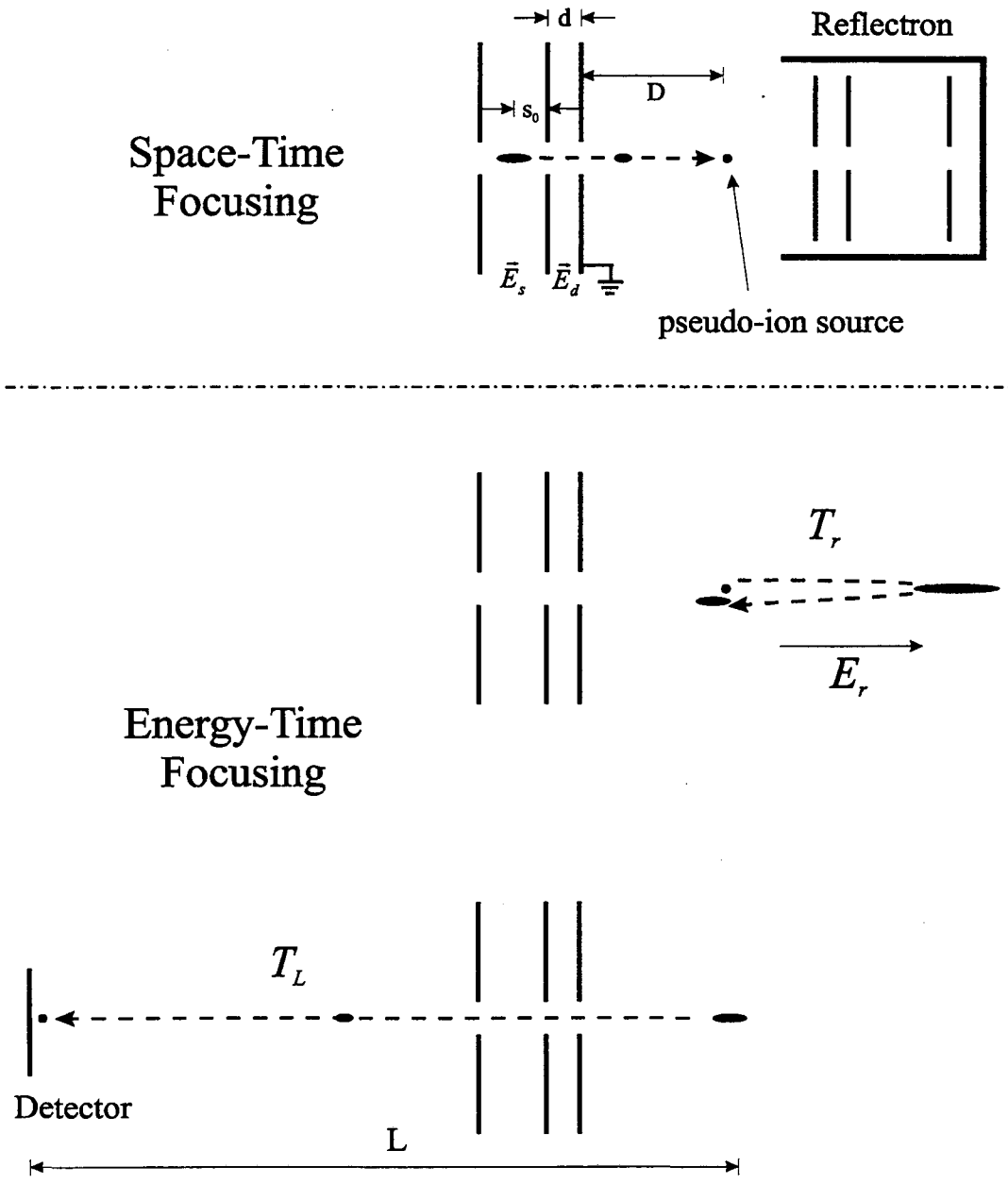

FIG. 5. Space-time focusing and Energy-time focusing in Time-of-flight mass spectroscopy.

$$s_0 = \frac{D-2d}{2(D+d)}\left[D\left(\frac{D-2d}{3d}\right)^{3/2} + d\right], \tag{4}$$

and

$$\frac{dE_d}{s_0 E_s + dE_d} = \frac{2(D+d)}{3D}. \tag{5}$$

One of the solutions to overcome this limit is the reflectron, in which the space focus of an ion source is used as pseudo-ion origin with minimized spatial distribution. Substantially higher resolution (over 1000) can be achieved by mass reflectrons. A linear double-field design[10] was chosen to increase the previous mass spectrometer resolution from 200 to about 2000.

The ions are first focused using Wiley-Mclaren mode of operation near the ion source. The first order space-focused ions packet serves as a pseudo-ion source with no spatial or temporal distribution, but with different kinetic energies. The energy-time focusing is then accomplished by the reflectron. To simplify the situation, a single field model is used for the following explanation. The total flight time T_2 from the pseudo-ion source to detector is given by:

$$T_2 = T_r + T_L, \tag{6}$$

$$T_r = \frac{\sqrt{8mU}}{qE_r}, \tag{7}$$

and

$$T_L = \sqrt{\frac{mL}{2U}}, \tag{8}$$

where T_r is the flight time in an ion reflecting system with a uniform electric field E_r, and T_L is the flight time in the drift space (L). With an appropriate choice of the parameters of the reflecting system, the time of movement of ions from the source to the detector can be made practically independent of their energy. The packets with a width close to the initial width of the packets in the space-time-focusing plane can be obtained at the detector plane. High mass resolution is achieved as a result of long flight time without flight-time broadening.

The double-field reflectron design shown in Figure 6 is more flexible to facilitate second order focus at various geometries. It consists three major components: a set of seven stainless steel plates, which form two uniform electric fields, a micro-channel plates ion/neutral detector, and a set of photodissociation windows.

The deceleration and reflection fields are defined by three plates, each with a 12.5 mm diameter aperture covered with a fine grid. The front plate (closest to the extraction region) is grounded, and progressively more negative DC voltages are applied to the middle and rear plates. The deceleration and reflection stages are 8 and 18 cm long, respectively. The other four plates have 25 cm diameter apertures without grids, and are connected by resistor chains order to maintain uniform electric field lines within each stage. Typical electric fields applied to a 1.25 keV ion beam are 125 Vcm^{-1} and 50 Vcm^{-1} in the deceleration and reflection stages, respectively. All the plates are held by four ¼" stainless steel rods and separated by spacers to maintain parallel positions between plates.

An ion/neutral detector with two 25 mm micro-channel plates (Galileo Electro-Optics Corp., Sturbridge, MA) is mounted behind the rear plate. The structure of the re-

flectron detector is identical to the ion/neutral detector near the photodetachment region. This detector can be used for initial ion optimization in the absence of the deceleration and reflection fields, as well as neutral detection during photodissociation study.

Two windows are mounted in front of the two stages to allow the photodissociation laser beam to cross the ion beam before it reaches the reflectron stages. Combined

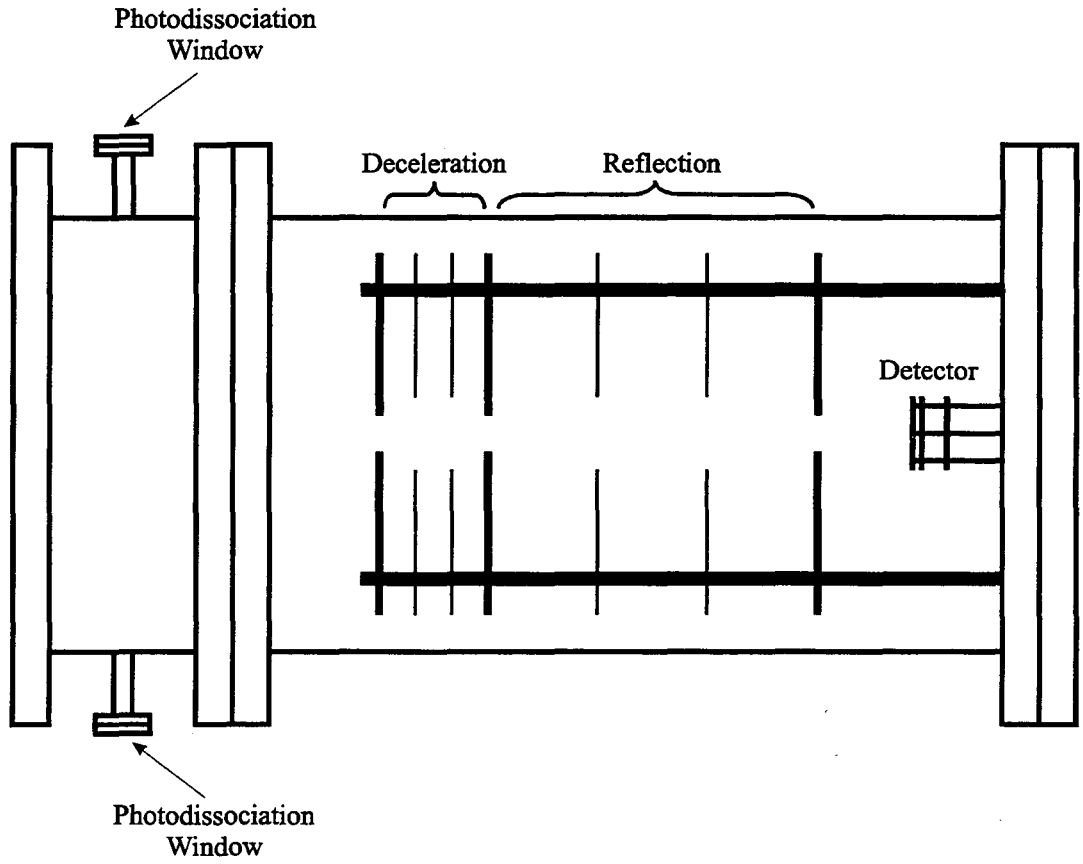

FIG. 6. Double-field linear mass reflectron.

with the reflectron detector, it is very convenient for future photodissociation and some two-photon process studies.

The reflectron, extraction, and the original first differential regions are separated from the source region by a 2 mm diameter skimmer located 1.5 cm down stream from the ion source nozzle. In order to maintain sufficient differential pumping, a 4" oil diffusion pump (Edwards, Diffstak 100) is also added to the reflectron region, sharing the same rotary pump (E2M18, 7 l/s) with the 6" diffusion pump at the original first differential region.

References

[1] A. Weaver, Ph. D. Dissertation, University of California, Berkeley, 1991.

[2] S. E. Bradforth, Ph. D. Dissertation, University of California, Berkeley, 1992.

[3] D. W. Arnold, Ph. D. Dissertation, Univeristy of California, Berkeley, 1994.

[4] D. L. Osborn, Ph. D. Dissertation, University of California, Berkeley, 1996.

[5] C. C. Arnold, Ph. D. Dissertation, Univerity of California, Berkeley, 1994.

[6] D. R. Cyr, Ph. D. Dissertation, University of California, Berkeley, 1993.

[7] W. C. Wiley and I. H. McLaren, Rev. Sci. Instrum. **26,** 1150 (1955).

[8] R. Weinkauf, K. Walter, C. Weickhardt, U. Boesl, and E. W. Schlag, Zeitschrift fur Naturforschung, Teil A (Physik, Physikalische Chemie, Kosmophysik) **44A,** 1219 (1989).

[9] U. Boesl, R. Weinkauf, and E. W. Schlag, Inter. J. Mass. Spec. and Ion. Proc. **112,** 121 (1992).

[10] B. A. Mamyrin and D. V. Shmikk, Zh. Eksp. Teor. Fiz. **76,** 1500 (1979).

3 Photoelectron Spectroscopy of C_4^-, C_6^-, and C_8^-

Abstract

Photoelectron spectra of C_4^-, C_6^-, and C_8^- were obtained at two photodetachment wavelengths, 266 nm (4.657 eV) and 213 nm (5.822 eV). The spectra reveal considerably more electronic and vibrational structure than was seen in previous studies of these species [D. W. Arnold *et al.*, J. Chem. Phys. **95**, 8753 (1991)]. Term values for several low-lying excited electronic states of the neutral carbon clusters have been obtained, as well as new vibrational frequencies for the ground and some of the excited electronic states of the neutral clusters. The assignments of excited electronic states were aided by measurements of the photoelectron angular distributions. A new assignment of the vibrational frequencies for C_6 is in considerably better agreement with *ab initio* results than our original assignment.

I. Introduction

Small polyatomic carbon clusters have been of considerable interest to experimentalists and theoreticians for many years. Up until 1989, the spectroscopy of carbon clusters consisted primarily of matrix isolation studies; these are summarized in the excellent review of Weltner and van Zee.[1] Since then, high-resolution gas-phase infrared spectra have been measured for the linear carbon clusters C_3-C_9 and C_{13}, yielding rotational constants and some vibrational frequencies for the ground electronic states of these species.[2-8] Vibrational frequencies for several totally symmetric (and IR inactive) modes have been determined for several clusters using anion photoelectron spectroscopy and zero electron kinetic energy (ZEKE) spectroscopy.[9-11] Thus, the ground-state spectroscopy of linear carbon clusters is reasonably well characterized.

The low-lying excited electronic states of carbon clusters have received far less attention, even though electronic transitions in these species are of considerable interest as possible candidates for the diffuse interstellar bands.[4,12] This possibility has motivated studies by Maier and co-workers[13-15] in which visible and ultraviolet absorption spectra were obtained for a series of mass-selected anion and neutral carbon clusters in cryogenic matrices. However, *ab initio* calculations[16-21] predict the existence of additional lower-lying electronic states in linear carbon clusters, particularly for the open-shell species C_4, C_6, and C_8. Many of these states are optically inaccessible from the ground state of the neutral cluster, but they can be reached by photodetachment of the corresponding anion if the photon energy is sufficient. The anion photoelectron spectra measured by Yang *et al.*

were obtained at a sufficiently high photon energy to access excited states lying within 2-4 eV of the ground state, but due to the low resolution of these spectra no assignments were attempted.[22,23] In the higher-resolution anion photoelectron spectra obtained by Arnold *et al.*[9] several transitions were tentatively assigned to excited electronic states. However, the term values implied by these assignments were often comparable to vibrational frequencies of the cluster, making it difficult to distinguish transitions to excited electronic states from transitions to excited vibrational levels of the ground electronic state.

In this study, we report anion photoelectron spectra of C_4^-, C_6^-, and C_8^- at photodetachment wavelengths of 266 nm (4.657 eV) and 213 nm (5.822 eV). The lower-photon energy was also used in our earlier study, but several modifications to the apparatus (see below) have resulted in higher quality spectra. The new spectra resolve some of the questions raised in *ab initio* calculations by Liu[24] and Botschwina[25] regarding our original assignments of vibrational frequencies in C_6 photoelectron spectrum. The spectra at 213 nm show a wealth of new transitions to excited vibrational levels and electronic states of the neutral clusters that are inaccessible at 266 nm. By combining the larger number of observed transitions with measurements of the photoelectron angular distributions, we can sort out most of the overlapped vibrational and electronic transitions seen in these spectra, thereby obtaining a detailed picture of the low-lying electronic states of the neutral clusters.

II. Experiment

The experiments were carried out on a time-of-flight negative ion photoelectron spectrometer. The original version of this instrument has been described in detail previously.[26] However, several modifications have been made since our previous study on carbon clusters.[9] The ion source was changed from a laser ablation/pulsed molecular beam source to a pulsed electrical discharge source.[27] The ion extraction electronics were

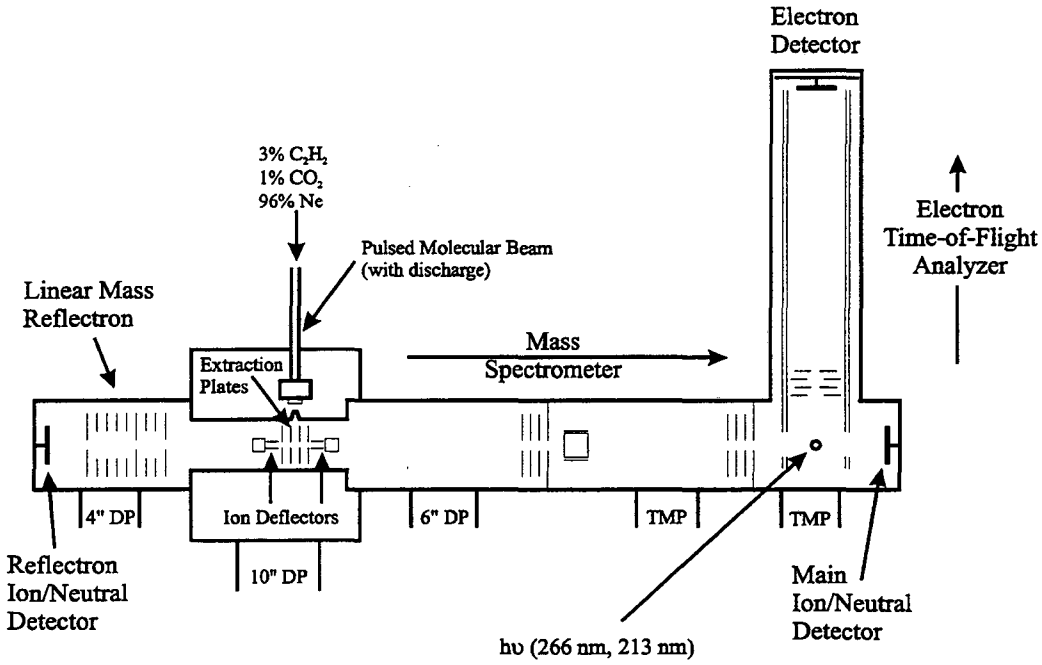

FIG. 1. Anion photoelectron spectrometer with linear mass reflectron.

modified so that the ion source no longer needs to be floated at high voltage. Finally, a reflectron stage has been added to improve the resolution of the time-of-flight mass spec-

trometer. The modified instrument is shown in Fig. 1 and the new features are described below.

The construction of the free jet pulsed discharge source is discussed elsewhere[27]. To make carbon cluster anions, a burst of a gas mixture (3% C_2H_2, 1% CO_2 and 96% Ne) from a piezo electric valve passes through two stainless steel plates between which a high voltage (about 600 V) pulse is applied and expands into a vacuum chamber. The resulting free jet is collimated by a 2 mm diam skimmer located 1.5 cm downstream from the nozzle and then enters a differentially pumped region. Here, the ions are extracted from the beam by applying a pulsed electric field across the two central plates shown in Fig. 1; the two outer plates are maintained at ground potential. Typically, voltages of -1500 V and -1000 V with less than 100 ns rise time[28] are applied to the right and left central plates, respectively, resulting in a nominal ion beam energy of 1250 eV. Since both plates are pulsed simultaneously, it is no longer necessary to float the ion source at the nominal ion beam energy.

The extracted ions are mass-selected using a time-of-flight mass spectrometer with a newly added linear reflectron stage. A similar setup has been reported by Cheshnovsky and co-workers.[29] Although not necessary for this experiment, the reflectron stage increases our mass resolution from 150 to about 2000 by so-called "second order focusing"[30,31], which corrects the energy spread left over by the traditional Wiley-McLaren-type mass spectrometer[32]. A two-stage reflectron design[33] is used, consisting of seven stainless steel plates which form two uniform electric fields; these deceleration and reflection fields are defined by three plates, each with a 12.5 mm diam aperture covered with a fine

grid. The front plate (closest to the extraction region) is grounded, and progressively more negative dc voltages are applied to the middle and rear plates. The deceleration and reflection stages are 8 and 18 cm long, respectively. The other four plates have 25 cm diameter apertures without grids, and are connected by resistor chains in order to maintain uniform electric field lines within each stage. Typical electric fields applied to a 1.25 keV ion beam are 125 and 50 V cm^{-1} in the deceleration and reflection stages, respectively.

The potentials of the extraction plates are reset to ground before the reflected ions pass through the second time, on their way to the laser interaction region. The accelerated ions separate in time and space according to their mass to charge ratios, and are selectively detached by a pulsed Nd:YAG laser.

Two different wavelengths, the fourth and fifth harmonics (266 nm, 4.657 eV and 213 nm, 5.822 eV, respectively) from a pulsed Nd:YAG laser are used in these experiments. The photoelectron kinetic energy is measured by time-of-flight. The instrumental resolution is 8 - 10 meV for an electron kinetic energy (eKE) of 0.65 eV and degrades as $(eKE)^{3/2}$. The polarization angle θ between the laser polarization and the direction of electron collection can be varied using a half-wave plate. The variation of peak intensities with θ is used to separate the contributions of different electronic states to the photoelectron spectra.

Secondary electrons resulting from scattered photons create enough noise to necessitate background subtraction in the 213 nm spectra. This problem also exists to a considerably lesser extent in the 266 nm data.

III. Results

The photoelectron spectra of C_4^-, C_6^-, and C_8^-, obtained at a photodetachment wavelength of 266 nm (4.657 eV) are presented in Figs 2-4. The 213 nm (5.822 eV) spectra are shown in Fig. 5. Data were taken at laser polarization angles of 0°, 54.7° (magic angle) and 90° for all three clusters at both wavelengths. The spectral features correspond to the transitions between the anion electronic ground state and various neutral electronic states. For each peak, the electron kinetic energy (eKE) is given by

$$eKE = h\nu - EA - T_o^{(o)} + T_o^{(-)} - E_v^{(o)} + E_v^{(-)},$$

where hν is the laser photon energy, EA is the adiabatic electron affinity of the neutral species, $T_o^{(o)}$ and $T_o^{(-)}$ are the term values of the neutral and anion electronic states, and $E_v^{(o)}$ and $E_v^{(-)}$ are the neutral and anion vibrational energies, respectively, above the zero-point energy. The peak positions at both photodetachment energies are listed in Table I.

From the changes in peak intensity with laser polarization angle, one obtains information on the photoelectron angular distribution associated with each peak. This is given by[34]

$$\frac{d\sigma}{d\Omega} = \frac{\sigma_{total}}{4\pi}[1 + \beta(E)P_2(\cos\theta)],$$

where σ_{total} is the total photodetachment cross section and β(E) is the asymmetry parameter. β(E) varies between -1 and 2; these limits correspond to $\sin^2\theta$ and $\cos^2\theta$ distri-

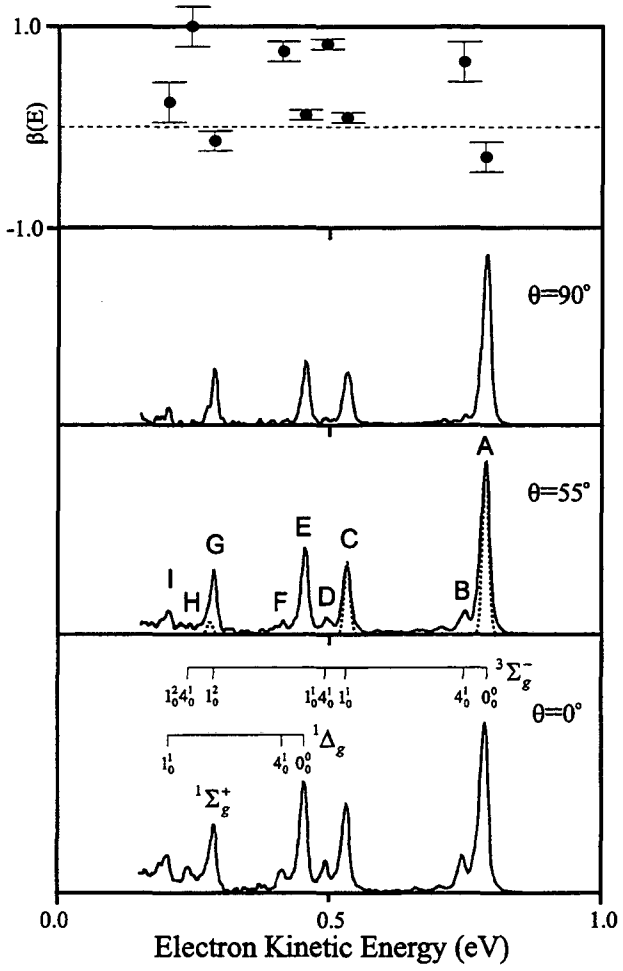

FIG. 2. Photoelectron spectra of C_4^- taken at photodetachment wavelength of 266 nm (4.657 eV). Laser polarization angles are θ = 90°, 55°, and 0° with respect to direction of electron collection. Top panel shows anisotropy parameters β(E) for several peaks in the spectra, plotted from -1 to 1 for greater clarity (β_{max} = 2). The dotted line in the third panel shows a Franck-Condon simulation. Assignments are indicated in the bottom panel

butions, respectively. One can therefore determine β for each peak in the photoelectron

spectrum. The results are shown in Table I with the peak positions, and plotted in the top panels (for the major peaks) of Fig. 2 – Fig. 5.

Table I. Peak positions and assignments for the C_4^-, C_6^-, and C_8^- photoelectron spectra.

Mole-cule	Peak	Position (eV) 266 nm	Position (eV) 213 nm	β(E) 266 nm	β(E) 213 nm	Assignments
C_4	A	0.787	1.960	-0.30 ± 0.15	-0.57 ± 0.10	$^3\Sigma_g^-$ Origin
	B	0.747	1.882	0.65 ± 0.20		4_0^1 ($^3\Sigma_g^-$)
	C	0.532	1.700	0.09 ± 0.05	-0.64 ± 0.10	1_0^1 ($^3\Sigma_g^-$)
	D	0.495		0.83 ± 0.05		$1_0^1 4_0^1$ ($^3\Sigma_g^-$)
	E	0.455	1.621	0.12 ± 0.05	-0.54 ± 0.10	$^1\Delta_g$ Origin
	F	0.414		0.76 ± 0.10		4_0^1 ($^1\Delta_g$)
	G	0.286	1.454	-0.14 ± 0.10	-0.66 ± 0.10	1_0^2 ($^3\Sigma_g^-$), $^1\Sigma_g^+$ Origin
	H	0.243		1.00 ± 0.20		$1_0^2 4_0^1$ ($^3\Sigma_g^-$)
	I	0.203	1.370	0.25 ± 0.20	-0.51 ± 0.20	1_0^1 ($^1\Delta_g$)
	J		1.140		0.81 ± 0.15	$^3\Pi_g$ Origin
	K		1.032		-0.17 ± 0.20	$^3\Pi_u$ Origin
	L		0.800		-0.32 ± 0.10	1_0^1 ($^3\Pi_u$), $^1\Pi_u$ Origin
	M		0.548		0.66 ± 0.10	$^1\Pi_g$ Origin
C_6	A	0.479	1.645	0.07 ± 0.05	-0.15 ± 0.10	$^3\Sigma_g^-$ Origin
	B	0.457				9_0^2 ($^3\Sigma_g^-$)
	C	0.435				9_0^4 ($^3\Sigma_g^-$)
	D	0.418		-0.12 ± 0.05		7_0^2 ($^3\Sigma_g^-$)
	E	0.400				3_0^1 ($^3\Sigma_g^-$)
	F	0.313	1.475	-0.16 ± 0.10	-0.06 ± 0.10	$^1\Delta_g$ Origin
	G	0.269	1.433	0.29 ± 0.20	-0.05 ± 0.20	2_0^1 ($^3\Sigma_g^-$)
	H	0.220	1.384	-0.10 ± 0.10	-0.03 ± 0.10	1_0^1 ($^3\Sigma_g^-$)
	I		1.266		-0.26 ± 0.10	2_0^1 ($^1\Delta_g$)
	J		1.225		-0.08 ± 0.10	1_0^1 ($^1\Delta_g$)
	K		1.174		-0.02 ± 0.05	$1_0^1 2_0^1$ ($^3\Sigma_g^-$)

	L		1.132		-0.12 ± 0.10	1_0^2 ($^3\Sigma_g^-$)
	M		0.796		0.03 ± 0.20	$^3\Sigma_u^+$ Origin
	N		0.547		-0.29 ± 0.10	$^3\Pi_u$ Origin
	O		0.467		-0.22 ± 0.10	3_0^1 ($^3\Pi_u$)
C_8	A	0.280	1.450	-0.40 ± 0.20	-0.18 ± 0.05	$^3\Sigma_g^-$ Origin
	B	0.205	1.379	-0.37 ± 0.20	-0.13 ± 0.05	$^1\Delta_g$ Origin
	C	0.165	1.341	-0.32 ± 0.20	-0.06 ± 0.10	$^1\Sigma_g^+$ Origin
	D		1.281		-0.03 ± 0.10	3_0^1 ($^3\Sigma_g^-$)
	E		1.211		-0.13 ± 0.10	1_0^1 ($^3\Sigma_g^-$) and 3_0^1 ($^1\Delta_g$)
	F		1.143		-0.02 ± 0.05	1_0^1 ($^1\Delta_g$)
	G		0.667		0.94 ± 0.10	$^3\Sigma_u^+$ Origin
	H		0.423		0.77 ± 0.10	$^3\Pi_g$ Origin

We first consider the photoelectron spectra. In all of the 266 nm spectra, the largest peak occurs at the highest electron energy. This is the vibrational origin transition between the electronic ground states of the anion and neutral, and from this one obtains the adiabatic electron affinity. The electron affinities from the new spectra are unchanged from our previous work.[9,10] In comparison to our previous results[9] at 266 nm, several of the peaks are better resolved in the current work, and more features are seen at low eKE. In the C_4^- spectra, peaks F, G, H, and I are new features which were not observed previously. In the earlier C_6^- spectra, peak A had a wide shoulder towards lower electron energy. This is now resolved as a series of peaks (B - E). Peaks F and G (formerly D and E) are better resolved, and peak H is a new feature. In the C_8^- spectra, peak C is a new feature.

The 213 nm spectra show many more peaks than the 266 nm spectra, corresponding to higher energy levels of the neutral species. For peaks appearing in both

spectra, however, the energy resolution is poorer at 213 nm because the electron kinetic energy is higher. The most noticeable difference in the 213 nm spectra is that a new peak at lower eKE is the largest feature for all three species. This is peak J in the C_4^- spectra, peak M in the C_6^- spectra, and peak G in the C_8^- spectra. Although some peaks at low eKE are not very well resolved due to the low signal-to-noise ratio, we are still able to identify most of them by comparing the three spectra at different polarization angles.

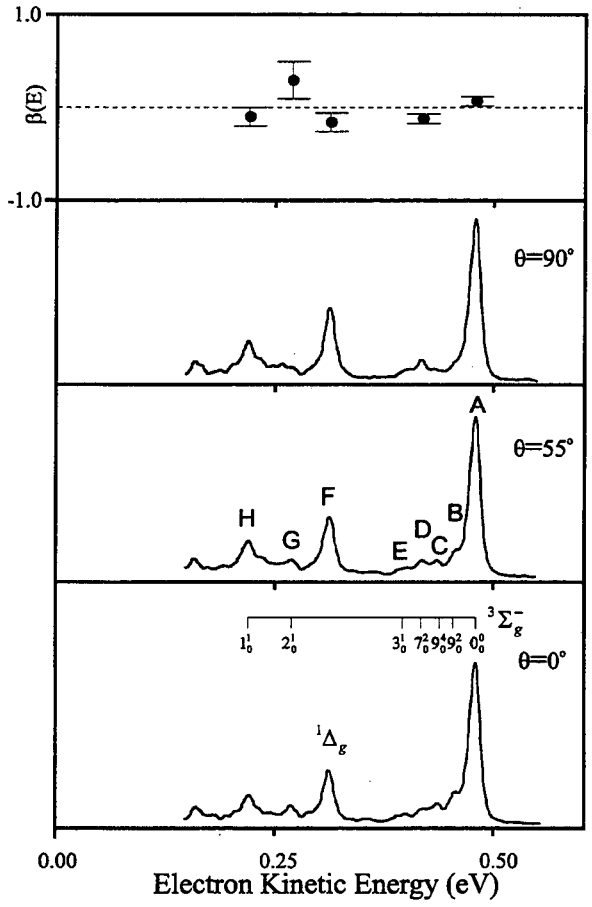

FIG. 3. Photoelectron spectra of C_6^- taken at 266 nm. Laser polarization angles are θ = 90°, 55°, and 0° with respect to direction of electron collection. Top panel shows β(E) parameters.

The laser polarization results for C_4^- show substantial variation in the photoelectron angular distribution among the peaks. At 266 nm, we find $\beta \approx 0$ for the major peaks (A,C, E, G, I), but the photoelectron angular distributions for several of the smaller peaks (B,D, F, H) are

considerably more anisotropic with $\beta \approx 1$. At 213 nm, the anisotropy parameters cluster about three values. We find β has dropped from 0 to -0.6 for peaks A,C,E,G, and I, $\beta \approx$ -0.25 for peaks K and L, and $\beta \approx 0.75$ for peaks J and M. There is considerably less variation among the β values for the peaks in the C_6^- spectra. At 266 nm, all the features are essentially isotropic with $\beta \approx 0$. The same is true at 213 nm, except for peaks N and O for which $\beta \approx$ -0.25. The results at 213 nm for C_8^- show that β lies between -0.03 and -0.18 for peaks A - F, but that peaks G and H have considerably more anisotropic distributions with β = 0.94 and 0.77, respectively.

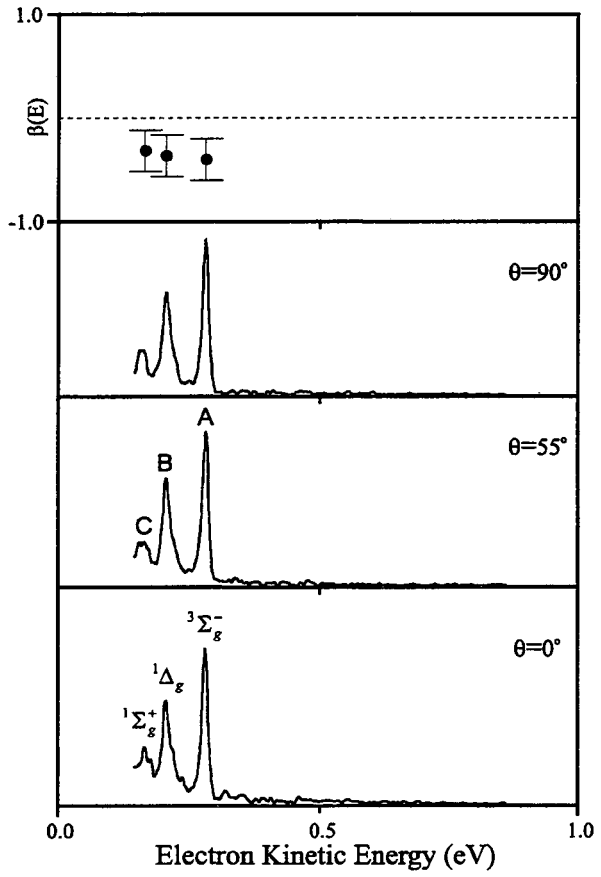

FIG. 4. Photoelectron spectra of C_8^- taken at 266 nm. Laser polarization angles are θ = 90°, 55°, and 0° with respect to direction of electron collection. Top panel shows β(E) parameters.

The polarization dependence results clearly show that transitions to multiple electronic states contribute to the photoelectron spectra. In order to help assign these transitions, we performed geometry optimization and frequency

calculations on various electronic states at the HF/6-31G* and MP2/6-31G* levels of theory, using the Gaussian 92 package[35]. Franck-Condon simulations can be performed using the geometries and force constants obtained from the calculation. The adiabatic excitation energies from our calculations and results from previous *ab initio* studies are summarized in Table II - Table IV. Note that the $^3\Sigma_u^+$ state that we have calculated is a cumulenic state in which all the carbon atoms are connected by double bonds, in contrast to the low-lying polyacetylenic $^3\Sigma_u^+$ state predicted in some of the calculations.[17,21]

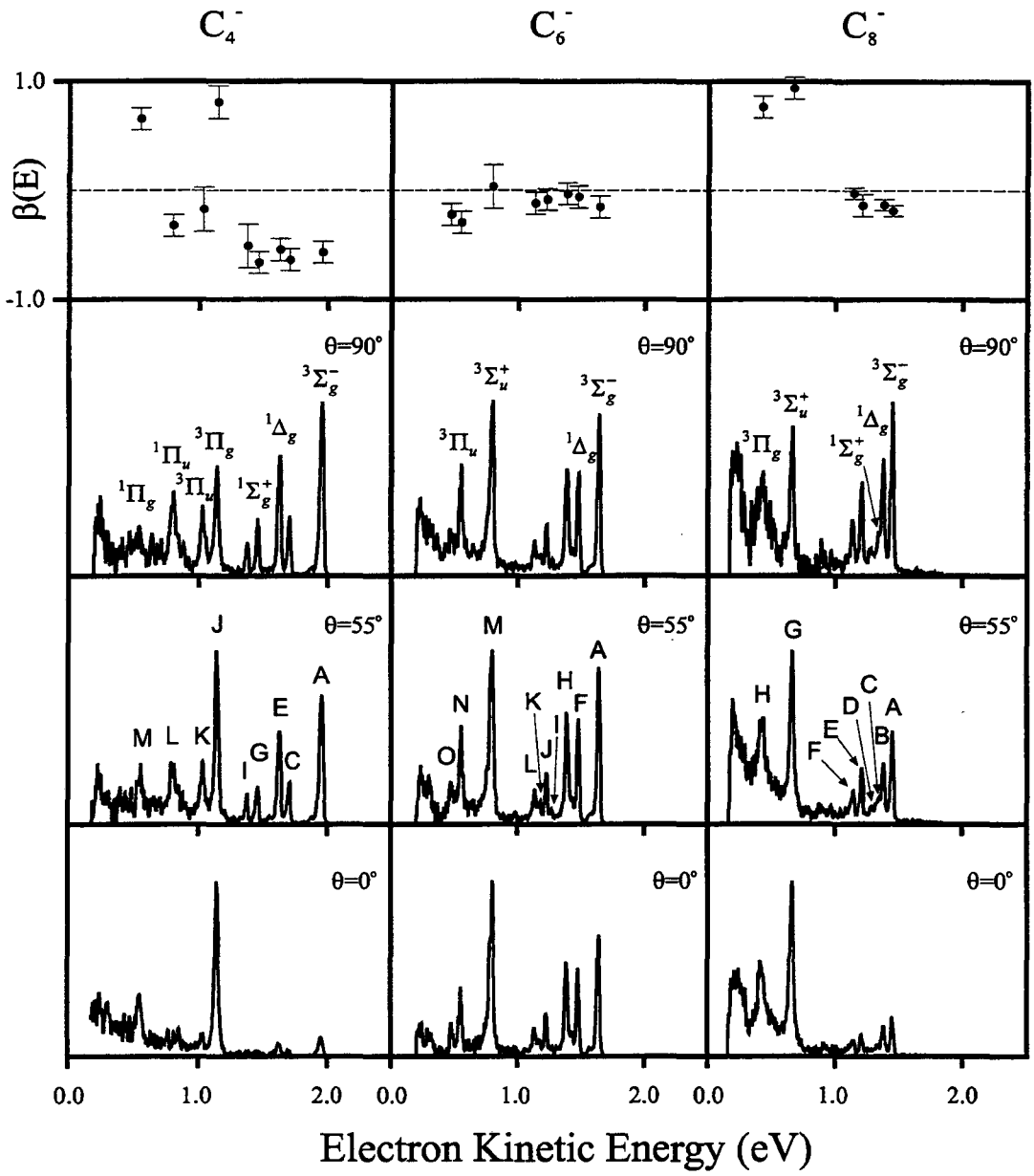

FIG. 5. Photoelectron spectra of C_4^-, C_6^-, and C_8^- taken at photodetachment wavelength of 213 nm (5.822 eV) Laser polarization angles are $\theta = 90°$, 55°, and 0° with respect to direction of electron collection. Top panel shows β(E) parameters for several peaks. Low-lying electronic state assignments are indicated in the second panel.

IV. Analysis and Discussion

A. General

In this section we review the electronic structure of C_4, C_6, C_8, and their anion counterparts. We then discuss strategies for assigning the various electronic transitions that comprise the photoelectron spectra.

Table II. Calculated and experimental energies[a] of C_4 low-lying electronic states (eV).

Method/Basis set	$^3\Sigma_g^-$	$^1\Delta_g$	$^1\Sigma_g^+$	$^3\Pi_g$	$^1\Pi_g$	$^3\Pi_u$	$^1\Pi_u$
MBPT(4) / DZP [b]	0.0	0.25	0.256	0.84		1.15	
CC / DZP [b]	0.0			0.97		1.30	
MRD CI/DZP [c]	0.0	0.41	0.68	1.00	1.73	1.54	2.05
CISD with Davidson's correction [d]	0.0	0.33	0.40 [e]				
UHF / FOCO / CC [f]	0.0	0.40		0.96		1.26	
10-CAS / G[4421] [g]	0.0	0.30	0.42				
10-MRCI / G[4421] [g]	0.0	0.35					
MP2 / 6-31G* [h]	0.0			0.46	0.71	0.75	1.06
UV – PES [h]	0.0	0.332	0.50	0.82	1.41	0.93	1.16

[a] Vertical excitation energies except for the present work which indicates adiabatic energies.

[b] Reference 16.

[c] Reference 19.

[d] Reference 17.

[e] A mixture of the $^1\Sigma_g^+$ and $^1\Delta_g$ singlet states.

[f] Reference 20.

[g] Reference 18.

[h] Present work. Error bars from photoelectron spectra assignments are ± 0.02 eV except for the $^1\Delta_g$ state of ± 0.015 eV.

The ground-state molecular orbital configurations for the three anions are: $...(1\pi_u)^4(4\sigma_u)^2(5\sigma_g)^2(1\pi_g)^3$ for C_4^-,[36] $...(1\pi_u)^4(6\sigma_u)^2(7\sigma_g)^2(1\pi_g)^4(2\pi_u)^3$ for C_6^-,[37] and $...(8\sigma_u)^2(9\sigma_g)^2(2\pi_u)^4(2\pi_g)^3$ for C_8^-,[38] yielding $^2\Pi_g$ ground states for C_4^- and C_8^- and a $^2\Pi_u$ ground state for C_6^-. In each case, removal of an electron from the highest occupied molecular orbital (HOMO) leaves a neutral cluster with a π^2 configuration, resulting in a $^3\Sigma_g^-$ ground state and the low-lying $^1\Delta_g$ and $^1\Sigma_g^+$ excited states. Thus, all three states are accessible via one-electron photodetachment transitions from the anions. Higher lying excited states can be formed by removal of electrons from orbitals other than the HOMO, yielding, for example, triplet and singlet Π_g and Π_u states of C_4, and $^3\Sigma_u^+$ state for C_6 and C_8. According to the *ab initio* results listed in Table II - Table IV, many of these states will be accessible by photodetachment at 213 nm. In order to assign the observed transitions, we use the anisotropy parameters β described in the previous section and *ab initio* vibrational frequencies and term values.

The photoelectron angular distributions are determined by the distribution of partial waves contributing to each peak. The relevant selection rules for these near threshold are straightforward; for a linear, centrosymmetric molecule, *s*-wave (l = 0) detachment can occur from orbitals of *u* symmetry, but *p*-wave (l = 1) detachment is the lowest allowed partial wave from orbitals of *g* symmetry.[39] Pure *s*-wave detachment yields an isotropic ($\beta = 0$) angular distribution, whereas pure *p*-wave detachment leads to a $\cos^2\theta$ distribution with $\beta = 2$.[40] As examples, C_6^- can undergo *s*-wave detachment near the threshold whereas C_4^- and C_8^- cannot. The situation is more complicated in photoelectron

spectroscopy, however, because one is typically well above the detachment threshold for a particular neutral←anion transition, so that many partial waves typically contribute to the signal. One still has the restrictions that only even partial waves result from a *u* orbital, and only odd partial waves from a *g* orbital, but it is difficult to predict in advance the value of β for a photodetachment transition.

Table III. Calculated and experimental energies[a] of C_6 low-lying electronic states (eV).

Method/Basis set	$^3\Sigma_g^-$	$^1\Delta_g$	$^1\Sigma_g^+$	$^3\Sigma_u^+$	$^3\Pi_u$
10-CAS [b]	0.0	0.30	0.53		
10-MCRI [b]	0.0	0.15	0.28		
CISD with Davidson's correction [c]	0.0	0.19	0.16 [d]		
MP2 / 6-31G* [e]	0.0			1.00	1.20
UV – PES [e]	0.0	0.166		0.85	1.10

[a] Vertical excitation energies except for the present work which indicates adiabatic energies.

[b] Reference 21.

[c] Reference 17.

[d] A mixture of the $^1\Sigma_g^+$ and $^1\Delta_g$ singlet states.

[e] Present work. Error bars from photoelectron spectra assignments are ± 0.02 eV except for the $^1\Delta_g$ state of ± 0.015 eV.

Nonetheless, one does expect relatively small variations in β for photodetachment transitions within an electronic manifold, or for transitions between states with the same orbital configurations, because detachment from the same orbital in the anion is occurring. Thus, for example, transitions involving removal of an electron from the anion HOMO to yield the $^3\Sigma_g^-$ ground state $^1\Delta_g$ and $^1\Sigma_g^+$ excited states should have approximately the same values of β. This is in fact observed in the photoelectron spectrum of O_2^- ,[41] where the symmetries of the states involved are the same as for carbon clusters: O_2^- has

a $^2\Pi_g$ ground state, and O_2 has a $^3\Sigma_g^-$ ground state and $^1\Delta_g$ and $^1\Sigma_g^+$ excited states. Conversely, peaks with significantly different values of β should be associated with different electronic transitions. This is a useful diagnostic for distinguishing transitions between different electronic states from those involving vibrational transitions within the same electronic manifold, and it can also indicate the presence of vibronic coupling between electronic states of different symmetry (see below). However, one cannot assume that peaks with the same value of β belong to the same electronic transition, or even to transitions involving detachment from orbitals of the same symmetry. The photoelectron angular distributions are therefore useful in assigning the photoelectron spectra, but are by no means unambiguous. We therefore tend to minimize the number of electronic states needed to describe the spectrum so long as this does not lead to unreasonable vibrational frequencies. The term values obtained from our assignments of the photoelectron spectra are summarized in Table V.

Table IV. Calculated and experimental energies[a] of C_8 low-lying electronic states (eV).

Method/Basis set	$^3\Sigma_g^-$	$^1\Delta_g$	$^1\Sigma_g^+$	$^3\Sigma_u^+$	$^3\Pi_u$
CISD with Davidson's correction [b]	0.0	0.14	0.01 [c]		
MP2 / 6-31G* [d]	0.0			1.45	1.53
UV – PES [d]	0.0	0.071	0.115	0.78	1.03

[a] Vertical excitation energies except for the present work which indicates adiabatic energies.

[b] Reference 17.

[c] A mixture of the $^1\Sigma_g^+$ and $^1\Delta_g$ singlet states.

[d] Present work. Error bars from photoelectron spectra assignments are ± 0.015 eV for the $^1\Delta_g$ and $^1\Sigma_g^+$ states and ± 0.02 eV for the others.

Table V. Adiabatic excitation energies (eV) of C_4, C_6, and C_8 low-lying states from present work.

	$T_o(^1\Delta_g)$	$T_o(^1\Sigma_g^+)$	$T_o(^3\Sigma_u^+)$	$T_o(^3\Pi_g)$	$T_o(^3\Pi_u)$	$T_o(^1\Pi_u)$	$T_o(^1\Pi_g)$
C_4	0.332	0.93		0.82	0.93	1.16	1.41
C_6	0.166		0.85		1.10		
C_8	0.071	0.115	0.78	1.03			

B. C_4

C_4 has two totally symmetric stretching modes (ν_1 and ν_2), one σ_u antisymmetric stretch (ν_3), and two degenerate bending modes of π_g and π_u symmetry (ν_4 and ν_5, respectively). In our previous study of C_4^-, peaks A - D were assigned to the $^3\Sigma_g^-$ ground-state vibrational origin, 4_0^1, 1_0^1, and $1_0^1 4_0^1$ transitions.[9] These assignments were aided by vibrational frequencies from *ab initio* calculations[42-44]. The ν_4 (π_g) mode is not totally symmetric, so the 4_0^1 and $1_0^1 4_0^1$ transitions are Franck-Condon forbidden. However, the 4_0^1 transition can occur in the case of vibronic coupling to a nearby Π_g electronic state; this is discussed further below. Peak E was assigned as the origin of the first excited state $^1\Delta_g$ because the splitting between peaks A and E, 2680 cm^{-1}, is too large for a vibrational frequency of C_4.

While these assignments are still valid, the new spectra give slightly different vibrational frequencies: $\nu_1 = 2057 \pm 50$ cm^{-1} and $\nu_4 = 323 \pm 50$ cm^{-1}. The new term value of $T_o(^1\Delta_g) = 0.332 \pm 0.015$ eV is in good agreement with the calculated values of 0.346 eV

and 0.331 eV by Almlöf[18] and Schaefer,[17] respectively (see Table II). Based on these ν_1 and ν_4 frequencies, the new features, peak G and H, are assigned to the 1_0^2 and $1_0^2 4_0^1$ transitions of the $^3\Sigma_g^-$ ground state. Peaks F and I are assigned to the 4_0^1 and 1_0^1 transitions of the $^1\Delta_g$ state respectively. This yields a symmetric stretch frequency of $\nu_1 = 2032 \pm 50$ cm^{-1} and a bending frequency of $\nu_4 = 331 \pm 50$ cm^{-1} for the $^1\Delta_g$ state, which are very close to those of the ground state. Peak I is quite weak in the 266 nm spectrum due to the low-energy cutoff of the spectrometer.

Peak G lies at the energy expected for the 1_0^2 transition to the $^3\Sigma_g^-$ state, but its intensity is anomalously high. This is demonstrated in the third panel of Fig. 2, which shows a Franck-Condon simulation of the C_4^- photoelectron spectrum. The neutral geometry is adopted from the CCSD(T)/PVTZ calculation by Watts and Bartlett[45], and the anion geometry is from the RCCSD(T) calculation by Schmatz and Botschwina.[46] The force constants from our MP2/6-31G* calculation have been applied to obtain the normal coordinate change between the anion and neutral. Since the 4_0^1 transition is not Franck-Condon allowed, only excitation of the ν_1 mode appears in the simulation, which shows that that the actual intensity of peak G is about 5 times higher than predicted in the simulation. It is possible that the anomalous intensity of peak G arises because it is in part due to the transition to the $^1\Sigma_g^+$ state. As shown in Table II, calculations by Koutecký[19] and Almlöf[18] predict vertical excitation energies of 0.68 eV and 0.42 eV, respectively, for this state; these values bracket the experimental spacing of 0.50 eV between peaks A and G.

We therefore tentatively assign peak G to a combination of the $^1\Sigma_g^+$ state origin and the 1_0^2 transition from the ground state, yielding a term energy of T_o ($^1\Sigma_g^+$) = 0.50 ± 0.02 eV.

All of the major peaks discussed thus far have approximately the same anisotropy parameter. Peak J in the 213 nm spectrum is the first large peak that shows a significantly different polarization dependence. We assign it to the lowest electronic state of C_4 which can be accessed by removing an electron from an orbital other than the HOMO. From Table II, theoretical calculations have predicted this to be the $^3\Pi_g$ state with a term value between 0.8 to 1 eV;[16,19] the photodetachment transition involves removal of a $5\sigma_g$ electron. Assigning peak J to this state yields a term energy of T_o ($^3\Pi_g$) = 0.82 ± 0.02 eV. Peak J has the same polarization dependence as peaks B, D, F, and H, which supports the earlier claim that these latter peaks occur due to vibronic coupling between the $^3\Sigma_g^-$ and $^1\Delta_g$ states via the ν_4 mode to a nearby $^3\Pi_g$ state.

Based on their anisotropies, peaks K and L clearly are associated with a different electronic transition than peak J. We therefore assign peak K to the transition to the $^3\Pi_u$ state of C_4 in which a $4\sigma_u$ electron is removed from the anion; this should be the next excited electronic state with a molecular orbital configuration that differs from the $^3\Pi_g$ state. Our assignment yields a term energy of $T_o(^3\Pi_u)$ = 0.93 eV for this state, a somewhat lower value than the previously calculated vertical excitation energies of 1.15 eV and 1.54 eV by Bartlett[16] and Koutecký, [19] respectively. Peak L is more problematic. It can be assigned as the 1_0^1 transition within the $^3\Pi_u$ manifold, yielding a symmetric stretch fre-

quency of ν_1 = 1871 ± 50 cm^{-1} for the $^3\Pi_u$ state. While this is a reasonable vibrational frequency, peaks K and L have the same intensity, which implies a significant normal coordinate change of the ν_1 mode upon photodetachment to this state. This disagrees with the trend followed by every other photodetachment transition in linear carbon clusters in which the 0_0^0 transition is the most intense. Alternatively, peak L could be the transition to the $^1\Pi_u$ state, as this should have approximately the same intensity and polarization dependence as the transition to the $^3\Pi_u$ state. This assignment implies T_o ($^1\Pi_u$) = 1.16 ± 0.02 eV and a singlet-triplet splitting of 0.23 eV. This splitting is somewhat smaller than the value of 0.50 eV calculated by Koutecký,[19] but agrees well with our MP2/6-31G* calculations which predict a singlet-triplet splitting of 0.31 eV. In any case, the assignment of peak L to the $^1\Pi_u$ state is certainly reasonable, but somewhat tentative.

Although peak M is not well resolved due to low signal-to-noise, it is the only other peak in the 213 nm spectrum with a similar anisotropy parameter as peak J. Since the splitting between peaks M and J is too large to assign peak M to a vibrational transition, we assign peak M to the transition to the $^1\Pi_g$ state in which, as with peak J, a $4\sigma_g$ electron is detached. This yields a singlet-triplet splitting of 0.59 eV and term energy of T_o ($^1\Pi_g$) = 1.41 ± 0.02 eV, slightly smaller than the vertical term energy of 1.73 eV predicted by Pacchioni and Koutecký[19].

C. C_6

We have previously studied C_6^- using photoelectron spectroscopy[9] and a combination of autodetachment and zero electron kinetic energy (ZEKE) spectroscopy.[11] In this earlier work, the peaks now labeled A, F, and G were assigned to the vibrational origin, 3_0^1, and 2_0^1 photodetachment transitions of the $^3\Sigma_g^-$ ground state of C_6. The latter two assignments yielded vibrational frequencies of 492 and 1339 cm^{-1} for the ν_3 and ν_2 symmetric stretches, respectively. Both values are substantially lower than *ab initio* harmonic frequencies[24,25,47] which, for example, are calculated by Botschwina[25] to be 653 and 1697 cm^{-1}. The new features observed in the current work now lead to an assignment more in line with the *ab initio* values.

Peak H in the 266 nm spectrum at eKE 0.22 eV is 2089 ± 50 cm^{-1} from the origin. We assign it to the 1_0^1 transition of the $^3\Sigma_g^-$ ground state, in good agreement with the *ab initio* value[25] of ν_1 = 2142 ± 50 cm^{-1} and the previously observed peak in the ZEKE spectrum[11] at 2061 ± 10 cm^{-1}. Peak E, which was not observed previously, and peak G, which is considerably better-resolved than in our previous photoelectron spectrum, lie 637 ± 50 cm^{-1} and 1694 ± 50 cm^{-1}, respectively, from the origin, and assigning these to the 3_0^1 and 2_0^1 transitions yields vibrational frequencies in much better agreement with the *ab initio* values. Moreover, the relative intensities of peaks E, G, and H are in qualitative accord with the Franck-Condon simulation calculated by Botschwina.[25] Based on these new as-

signments, peaks K and L in the 213 nm spectrum are assigned to the $1_0^1 2_0^1$ and 1_0^2 transitions of the C_6 $^3\Sigma_g^-$ state.

The smaller peaks B, C and D near the origin could be from even $\Delta\upsilon$ transitions involving the low-frequency π bending modes or from sequence bands, with the latter being less likely due to the absence of hot band transitions at higher eKE than the origin. Even $\Delta\upsilon$ transitions in nontotally symmetric vibrations can be observed if the change in frequency between the anion and neutral is large. Our MP2/6-31G* calculation yields ν_7 (π_g) and ν_9 (π_u) frequencies of 124 and 278 cm^{-1} for the anion, and 197 and 105 cm^{-1} for the neutral. Based on these large frequency changes, peaks B and C are assigned to the 9_0^2 and the 9_0^4 transitions, respectively, and peak D is assigned to the 7_0^2 transition. The resulting vibrational frequencies, $\nu_7 = 246 \pm 50$ cm^{-1} and $\nu_9 = 90 \pm 50$ cm^{-1}, are in reasonable agreement with our *ab initio* values as well as those of a previous calculation.[48] Note that three peaks analogous to peaks B, C, and D were seen in the autodetachment spectrum[11] of C_6^-; these were labeled b_o, c_o, and d_o, and should be reassigned to the 9_0^2, 9_0^4, and 7_0^2 autodetachment transitions, respectively.

The second largest feature in the 266 nm spectrum is peak F, which was assigned to the 2_0^1 transition in our previous study. Given our new assignment of peak G to this transition, peak F is assigned to the origin of the $^1\Delta_g$ excited state, and peaks I and J in the 213 nm spectrum to the corresponding 2_0^1 and 1_0^1 transitions. The resulting term energy T_o ($^1\Delta_g$) = 0.166 ± 0.015 eV is in good agreement with the *ab initio* values of 0.15 eV and

0.19 eV calculated by Almlöf [21] and Schaefer,[17] respectively. This assignment provides two symmetric stretch frequencies of the $^1\Delta_g$ state, $\nu_1 = 2016 \pm 50$ cm^{-1} and $\nu_2 = 1686 \pm 50$ cm^{-1}, which are very close to their $^3\Sigma_g^-$ state counterparts.

We next consider the remaining peaks M, N, and O. These clearly correspond to transitions to one or more excited states of C_6, but since the anisotropy parameters are approximately the same (≈ 0) for all the C_6^- transitions, the excited state assignments are more ambiguous than for C_4^-. Peak M, which lies 0.849 eV from peak A, is the most intense feature in the spectra and is readily assigned to the origin of an excited state. This could be the $^1\Sigma_g^+$ state which has the same $...(1\pi_g)^4(2\pi_u)^2$ configuration as the $^3\Sigma_g^-$ and $^1\Delta_g$ states, or the $^3\Sigma_u^+$ state resulting from the $...(1\pi_g)^3(2\pi_u)^3$ configuration. The term energy for the $^1\Sigma_g^+$ state has been calculated at the MRCI level by Almlöf[21] and found to be 0.28 eV, a considerably lower value than the experimental A - M spacing. The term energy for the $^3\Sigma_u^+$ state from our MP2/6-31G* level calculation is 1.20 eV. Furthermore, peak M has a somewhat different polarization dependence from peaks associated with the $^3\Sigma_g^-$ and $^1\Delta_g$ states; peak M is clearly more intense than peak A at $\theta = 0°$ but has the same intensity at the other two angles. We therefore assign peak M to the $^3\Sigma_u^+$ state.

Peaks N and O are separated by 640 ± 50 cm^{-1}. They have the same polarization dependence but differ sufficiently from peak M to warrant their assignment to transitions to a different electronic state. The $^3\Pi_u$ state is the next triplet state expected above the $^3\Sigma_u^+$ state. Assigning peak N to the origin of this state yields T_o ($^3\Pi_u$) = 1.10 ± 0.02 eV,

very close to our MP2/6-31G* value of 1.20 eV. This calculation also yields ν_3 (σ_g) = 642 cm^{-1}, so we assign peak O to the 3_0^1 transition of the $^3\Pi_u$ state manifold.

The $^1\Sigma_g^+$ manifold has not been identified in the above assignments. There are several small unassigned peaks in the 266 nm spectrum near eKE = 0.25 eV. This is the energy range where transitions to the $^1\Sigma_g^+$ state are expected,[21] and these small peaks may be due to this state. If so, it remains an open question as to why the cross section for photodetachment to the $^1\Sigma_g^+$ state is considerably smaller than for the $^3\Sigma_g^-$ and $^1\Delta_g$ states.

D. C_8

In our previous study[9] of C_8^-, the high electron affinity of C_8 (4.379 ± 0.006 eV) limited the amount of information obtained at 266 nm, and only peaks A and B were observed. Peak A was assigned to the origin of the $^3\Sigma_g^-$ ground state, where peak B was tentatively assigned to the 4_0^1 transition. The possible assignment of peak B to the $^1\Delta_g$ state was also proposed. The new results at 266 and 213 nm provide a considerably more complete assignment of the electronic and vibrational states of C_8. These assignments are aided by a recent high level calculation by Schmatz and Botschwina[49] in which vibrational term energies (including anharmonicities) for levels involving the four totally symmetric stretches were calculated for the anion and the neutral ground state. A Franck-Condon simulation of the anion photoelectron spectrum was also carried out in that paper.

The assignment of peak A is unchanged. According to Botschwina's simulation, the strongest vibrational transition other than the origin should be the 1_0^1 (2053 cm^{-1}/24%) transition, followed by the 3_0^1 (1357 cm^{-1}/13%) transition. Peaks D and E lie 1361 and 1928 cm^{-1} from the origin, respectively. Peak D is therefore assigned to the 3_0^1 transition. While the A - E spacing is actually closer to the calculated energy of the ν_2 level (1977 cm^{-1}), the intensity of the 2_0^1 transition in the simulated photoelectron spectrum is negligible, and we assign peak E to the 1_0^1 transition.

The assignment of peak B to the 4_0^1 transition yields ν_4 = 605 cm^{-1}, which is significantly larger than the calculated value of 500 cm^{-1}.[49] In addition, the 4_0^1 transition is calculated to have only 2% of the intensity of the origin, whereas peak B is about 70% as intense as peak A. We therefore assign peak B to the $^1\Delta_g$ excited electronic state, yielding a term energy of T_o ($^1\Delta_g$) = 0.071 ± 0.015 eV. This is somewhat smaller than the value of 0.141 eV calculated by Schaefer,[17] but the deviation is only slightly larger than for C_6. The decreasing $^3\Sigma_g^-$ - $^1\Delta_g$ splitting as the number of carbon atoms increases (Table V) is also consistent with the trend seen in Schaefer's calculation.[17] Peak F lies 0.236 eV from peak B, close to the spacing between peaks A and E(0.239 eV), and is assigned to the 1_0^1 transition of the $^1\Delta_g$ excited state, yielding ν_1 = 1903 ± 50 cm^{-1} for the $^1\Delta_g$ state. The splitting between peaks B and E is 1355 cm^{-1}, virtually identical to the ν_3 frequency in the $^3\Sigma_g^-$ state. It is therefore likely that the 3_0^1 transition in the $^1\Delta_g$ state manifold contributes to the intensity of peak E.

Peak C is 0.115 eV (927 cm^{-1}) from the $^3\Sigma_g^-$ state origin, and only 0.040 eV (322 cm^{-1}) from the $^1\Delta_g$ state origin. Within the ground-state manifold, the closest calculated vibrational energy level involving totally symmetric modes only is the $2\nu_4$ level (999 cm^{-1}), but the intensity of the 4_0^2 transition should be negligible. The splitting between peaks B and C is too small for peak C to be a transition to a symmetric stretch level of the $^1\Delta_g$ state. We therefore assign peak C to the origin of the $^1\Sigma_g^+$ state, yielding a term energy of $T_o\ (^1\Sigma_g^+) = 0.115 \pm 0.015$ eV.

The two peaks at lowest eKE, peaks G and H, have anisotropy parameters close to 1, in contrast to the nearly isotropic angular distributions at 213 nm for the other peaks. The first excited state with a different molecular orbital configuration from the ground state should be the $^3\Sigma_u^+$ cumulenic state, which can be accessed by detachment of a $2\pi_u$ electron from C_8^-, and the next triplet state should be the $^3\Pi_g$ state, accessible by detachment of a $9\sigma_g$ electron. Our MP2/6-31G* level calculations yield term energies of 1.45 and 1.53 eV for the $^3\Sigma_u^+$ and $^3\Pi_g$ states, respectively. We assign peak G to the $^3\Sigma_u^+$ state origin, yielding $T_o\ (^3\Sigma_u^+) = 0.78 \pm 0.02$ eV. Peak H lies 0.244 eV (1970 cm^{-1}) from peak G, and could be assigned to the 1_0^1 transition of the $^3\Sigma_u^+$ state, or the origin of the $^3\Pi_g$ state. The latter assignment is favored due to the small but significant difference in the anisotropy parameters for peaks G and H, yielding $T_o\ (^3\Pi_g) = 1.03 \pm 0.02$ eV.

V. Conclusions

From the photoelectron spectra of C_4^-, C_6^-, and C_8^- and measurements of the photoelectron angular distributions, we have mapped out many of the low-lying electronic states of C_4, C_6, and C_8 and have obtained new vibrational frequencies for some of these states. These assignments are facilitated by comparisons with *ab initio* calculations. The electronic states we have observed include the $^1\Delta_g$ and $^1\Sigma_g^+$ states, which are derived from the same molecular orbital configuration as the $^3\Sigma_g^-$ ground state, as well as several additional triplet and singlet states lying less than 1.5 eV above the electronic ground state of the neutral clusters. The spectra show that the $^3\Sigma_g^- - {}^1\Delta_g$ splitting becomes smaller as the chain length increases. Also, each of the transitions to the various neutral electronic states is dominated by the vibrational origin, indicating relatively small geometry changes upon photodetachment. On the basis of the new spectra, our original assignment of the vibrational frequencies of the C_6 ground state have been modified and are now in much better agreement with *ab initio* values.

All of the excited states seen in this study occur at lower excitation energies than the optical transitions seen by Maier and co-workers.[13,15] In addition, most of the states seen here are optically inaccessible from the $^3\Sigma_g^-$ ground states. However, transitions to the $^3\Pi_u$ excited states in C_4 and C_6, with assigned term values of 0.93 and 1.10 eV, respectively, are optically allowed. It will therefore be of interest to see if these transitions can be located in gas phase or matrix isolation spectroscopy studies of these clusters.

Acknowledgment

This work is supported by the National Science Foundation under Grant No. DMR-9521805.

References

[1] W. Weltner and R. J. Van Zee, Chem. Rev. **89,** 1713 (1989).

[2] N. Moazzen-Ahmadi, A. R. W. McKellar, and T. Amano, Chem. Phys. Lett. **157,** 1 (1989).

[3] N. Moazzen-Ahmadi, A. R. W. McKellar, and T. Amano, J. Chem. Phys. **91,** 2140 (1989).

[4] P. F. Bernath, K. H. Hinkle, and J. J. Keady, Science **244,** 562 (1989).

[5] J. R. Heath and R. J. Saykally, J. Chem. Phys. **94,** 3271 (1991).

[6] H. J. Hwang, A. Vanorden, K. Tanaka, E. W. Kuo, J. R. Heath, and R. J. Saykally, Mol. Phys. **79,** 769 (1993).

[7] J. R. Heath and R. J. Saykally, in *On clusters and clustering, from atoms to fractals*, edited by P. J. Reynolds (Elsevier, Amsterdam, 1993), pp. 7-21.

[8] T. F. Giesen, A. Van Order, H. J. Hwang, R. S. Fellers, R. A. Provencal, and R. J. Saykally, Science **265,** 756 (1994).

[9] D. W. Arnold, S. E. Bradforth, T. N. Kitsopoulos, and D. M. Neumark, J. Chem. Phys. **95,** 8753 (1991).

[10] C. C. Arnold, Y. X. Zhao, T. N. Kitsopoulos, and D. M. Neumark, J. Chem. Phys. **97,** 6121 (1992).

[11] C. C. Arnold and D. M. Neumark, J. Chem. Phys. **99,** 1442 (1993).

[12] A. E. Douglas, Nature **269,** 130 (1977).

[13] D. Forney, J. Fulara, P. Freivogel, M. Jakobi, D. Lessen, and J. P. Maier, J. Chem. Phys. **103,** 48 (1995).

[14] D. Forney, P. Freivogel, M. Grutter, and J. P. Maier, J. Chem. Phys. **104,** 4954 (1996).

[15] P. Freivogel, J. Fulara, M. Jakobi, D. Forney, and J. P. Maier, J. Chem. Phys. **103,** 54 (1995).

[16] D. H. Magers, R. J. Harrison, and R. J. Bartlett, J. Chem. Phys. **84,** 3284 (1986).

[17] C. Liang and H. F. Schaefer, III, Chem. Phys. Lett. **169,** 150 (1990).

[18] V. Parasuk and J. Almlöf, J. Chem. Phys. **94,** 8172 (1991).

[19] G. Pacchioni and J. Koutecký, J. Chem. Phys. **88,** 1066 (1988).

[20] L. Adamowicz, Chem. Phys. **156,** 387 (1991).

[21] V. Parasuk and J. Almlöf, J. Chem. Phys. **91,** 1137 (1989).

[22] S. H. Yang, C. L. Pettiette, J. Conceicao, O. Cheshnovsky, and R. E. Smalley, Chem. Phys. Lett. **139,** 233 (1987).

[23] S. Yang, K. J. Taylor, M. J. Craycraft, J. Conceicao, C. L. Pettiette, O. Cheshnovsky, and R. E. Smalley, Chem. Phys. Lett. **144,** 431 (1988).

[24] R. F. Liu and X. F. Zhou, J. Chem. Phys. **99,** 1440 (1993).

[25] S. Schmatz and P. Botschwina, Chem. Phys. Lett. **235,** 5 (1995).

[26] R. B. Metz, A. Weaver, S. E. Bradforth, T. N. Kitsopoulos, and D. M. Neumark, J. Phys. Chem. **94,** 1377 (1990).

[27] D. L. Osborn, D. J. Leahy, D. R. Cyr, and D. M. Neumark, J. Chem. Phys. **104,** 5026 (1996).

[28] R. E. Continetti, D. R. Cyr, and D. M. Neumark, Rev. Sci. Instrum. **63,** 1840 (1992).

[29] G. Markovich, R. Giniger, M. Levin, and O. Cheshnovsky, J. Chem. Phys. **95,** 9416 (1991).

[30] V. I. Karataev, B. A. Mamirin, and D. V. Shmikk, Zh. Tekh. Fiz. **41,** 1498 (1971).

[31] B. A. Mamyrin, V. I. Karataev, D. V. Shmikk, and V. A. Zagulin, Zh. Eksp. Teor. Fiz. **64,** 82 (1973).

[32] W. C. Wiley and I. H. McLaren, Rev. Sci. Instrum. **26,** 1150 (1955).

[33] B. A. Mamyrin and D. V. Shmikk, Zh. Eksp. Teor. Fiz. **76,** 1500 (1979).

[34] J. Cooper and R. N. Zare, in *Lectures in Theoretical Physics*, Vol. XI-C, edited by S. Geltman, K. T. Mahanthappa, and W. E. Brittin (Gordon and Breach, New York, 1969), pp. 317-337.

[35] GAUSSIAN 92, M. J. Frisch, G. W. Trucks, M. Head-Gordon, P. M. W. Gill, M. W. Wong, J. B. Foresman, B. G. Johnson, H. B. Schlegel, M. A. Robb, E. S. Replogle, R. Gomperts, J. L. Andres, K. Raghavachari, J. S. Binkley, C. Gonzalez, R. L. Martin, D. J. Fox, D. J. Defrees, J. Baker, J. J. P. Stewart, and J. A. Pople (Gaussian, Inc., Pittsburgh, 1992).

[36] J. D. Watts, I. Cernusak, and R. J. Bartlett, Chem. Phys. Lett. **178,** 259 (1991).

[37] L. Adamowicz, Chem. Phys. Lett. **182,** 45 (1991).

[38] J. D. Watts and R. J. Bartlett, J. Chem. Phys. **97,** 3445 (1992).

[39] K. J. Reed, A. H. Zimmerman, H. C. Anderson, and J. I. Brauman, J. Chem. Phys. **64,** 1368 (1976).

[40] J. Cooper and R. N. Zare, J. Chem. Phys. **48,** 942 (1968).

[41] C. Xu, T. R. Taylor, and D. M. Neumark, (unpublished results).

[42] J. Kurtz and L. Adamowicz, Astrophys. J. **370,** 784 (1991).

[43] J. M. L. Martin, J. P. Francois, and R. Gijbels, J. Comp. Chem. **12,** 52 (1991).

[44] J. M. L. Martin, J. P. Francois, and R. Gijbels, J. Chem. Phys. **94,** 3753 (1991).

[45] J. D. Watts and R. J. Bartlett, J. Chem. Phys. **101,** 409 (1994).

[46] S. Schmatz and P. Botschwina, Inter. J. Mass. Spec. and Ion. Proc. **150,** 621 (1995).

[47] J. M. L. Martin, J. P. Francois, and R. Gijbels, J. Chem. Phys. **93,** 8850 (1990).

[48] J. Hutter, H. P. Luthi, and F. Diederich, J. Am. Chem. Soc. **116,** 750 (1994).

[49] S. Schmatz and P. Botschwina, Chem. Phys. Lett. **245,** 136 (1995).

4 Vibrationally-resolved Photoelectron Spectroscopy of Silicon Cluster Anions Si_n^- (n=3-7)

Abstract

Photoelectron spectra of Si_n^- (n=3-7) have been measured at several photodetachment energies. The anions were created using a pulsed discharge source, resulting in considerably colder clusters than in earlier work. As a result, vibrationally-resolved spectra were obtained for larger clusters and more electronic states than in previous studies of these species, leading to more accurate electron affinities, term energies, and vibrational frequencies for the ground and excited electronic states of the neutral clusters. The assignments of excited states were aided by *ab initio* calculations and photoelectron angular distributions.

I. Introduction

Small silicon clusters have been the subject of a series of experimental and theoretical studies during the last ten years. This work has been in part motivated by the

important role that silicon plays in the electronics industry, since studies of silicon clusters can provide insight into how the optical and electronic properties of semiconductors evolve from the molecular to macroscopic size regimes. Silicon clusters are also of considerable interest from the perspective of fundamental chemistry. Silicon lies directly below carbon in the periodic table, but *ab initio* calculations predict that the structures of silicon clusters differ substantially from carbon clusters in the same size range. While small carbon clusters form linear chains and rings, silicon clusters are predicted to form more compact three-dimensional structures. This difference is attributed to the much weaker π-bonding in Si clusters, thereby favoring structures with more single bonds. Thus, for example, the ground state of C_5 is linear, whereas calculations indicate the ground state of Si_5 to be a trigonal bipyramid. The remarkable differences between the structures for silicon and carbon clusters have motivated the experiments described in this paper, in which anion photoelectron spectroscopy is used to probe the vibrational frequencies and low-lying electronic states of Si_n (n=3-7) clusters.

The experimental investigation of silicon clusters in this size range has proved to be a challenge, but there has been considerable progress in recent years. Cheshnovsky *et al.* measured anion photoelectron spectra of Si_n^- ($n \leq 13$) clusters, yielding electron affinities and a qualitative picture of the electronic states of the neutral clusters.[1] The experimental resolution was insufficient to observe any vibrational structure, and no assignments of the electronic states were attempted. Neumark and co-workers later obtained vibrationally resolved anion photoelectron spectra[2] and zero electron kinetic energy (ZEKE) spectra of Si_3^- and Si_4^-.[3,4] These spectra showed well-resolved vibrational

progressions for several electronic bands, yielding vibrational frequencies and electronic term values for some of the low-lying electronic states of Si_3 and Si_4. Eberhardt and co-workers have recently measured the photoelectron spectrum of Si_7^- with sufficient resolution to observe a vibrational progression.[5] These gas phase studies have been complemented by matrix isolation spectroscopy. Jarrold and co-workers have measured Raman spectra of mass-selected clusters in matrices, yielding some vibrational frequencies for the ground electronic states of silicon clusters up to Si_7 (excluding Si_5).[6] Infrared spectra of silicon clusters in matrices were also obtained recently and assigned to Si_3,Si_4, Si_6, and Si_7 by Li *et al.*[7]

Ab initio calculations of the properties of silicon clusters have been carried out by several investigators.[8-22] These calculations have proved invaluable in understanding the various experiments carried out on Si clusters. For example, the geometries and vibrational frequencies of neutral silicon clusters up to Si_{10} were calculated by Raghavachari[9] before any of the above experiments were carried out. This work was followed by calculations by Raghavachari and Rohlfing on the negative ion geometries and frequencies as well as the low-lying excited states for several of the neutral clusters,[15-17] work which greatly aided in interpreting the photodetachment spectra of Si_3^- and Si_4^-.

This paper represents an extension of our earlier work on the photoelectron spectroscopy of silicon cluster anions.[2] Our original attempts to measure vibrationally-resolved photoelectron spectra of clusters larger than Si_4^- were unsuccessful. The laser ablation source originally used to produce the anions has been replaced by a new method

which produces substantially colder ions, resulting in less spectral congestion from "hot bands". As a result, we have obtained improved spectra for Si_3^- and Si_4^-, as well as vibrationally-resolved spectra of Si_5^- - Si_7^-. The new spectra for Si_3^- and Si_4^- provide more accurate electron affinities and vibrational frequencies, along with a clearer picture of the low-lying electronic states of the neutral clusters. The spectra of the three larger clusters provide new information on the anion and neutral geometries as well as the excited state energies of the neutral clusters.

II. Experiment

The experiments were carried out on a time-of-flight negative ion photoelectron spectrometer. The instrument has been described in detail previously[23]; recent modifications have resulted in considerably improved mass resolution.[24] Silicon cluster anions are generated by expanding a dilute mixture of SiH_4 (5% SiH_4, 95% He) through a pulsed piezoelectric valve/pulsed electrical discharge source.[25] In this source, the gas pulse from the beam valve passes through two stainless steel plates between which a high voltage (about 600 V) pulse is applied. The pulse then expands into a vacuum chamber. The resulting free jet is collimated by a 2 mm diameter skimmer located 1.5 cm downstream from the ion source and then enters a differentially pumped region. Here, the ions are extracted from the beam and enter a time-of-flight mass spectrometer with a linear reflectron stage. The accelerated ions separate in time and space according to their mass to charge ratios, and are selectively detached by a pulsed Nd:YAG laser.

Four different wavelengths, the third and fourth harmonics (355 nm, 3.493 eV and 266 nm, 4.657 eV, respectively) from a pulsed Nd:YAG laser and the first Stokes Raman lines (416nm, 2.977 eV and 299 nm, 4.141 eV) of these wavelengths generated in a high pressure H_2 cell are used in these experiments. The photoelectron kinetic energy is measured by time-of-flight in a field-free flight tube 100 cm in length. The instrumental resolution is 8 - 10 meV for an electron kinetic energy (eKE) of 0.65 eV and degrades as $(eKE)^{3/2}$. The polarization angle θ between the laser polarization and the direction of electron collection can be varied using a polarization compensator (New Focus, Model 5540). The variation of peak intensities with θ is used to separate the contributions of different electronic states to the photoelectron spectra. Secondary electrons resulting from scattered photons necessitated background subtraction in the 266 nm spectra.

III. Results

Fig. 1 shows the anion mass spectrum obtained from the discharge source. Bare silicon clusters as well as partially hydrogenated species $Si_xH_y^-$ are observed. Fig. 2 compares the photoelectron spectra of Si_4^- at a photodetachment wavelength of 355 nm (3.493 eV) using the pulsed discharge and laser ablation ion sources. It is clear upon inspection that the former spectrum shows considerably better-resolved vibrational structure, which we attribute to a lower vibrational temperature and therefore less spectral congestion from "hot band" transitions originating from vibrationally excited anions.

The photoelectron spectra for Si_3^- - Si_7^- at a variety of wavelengths are presented in Fig. 3 - 8. Spectra were taken at laser polarization angles of 90°, 54.7° (magic angle),

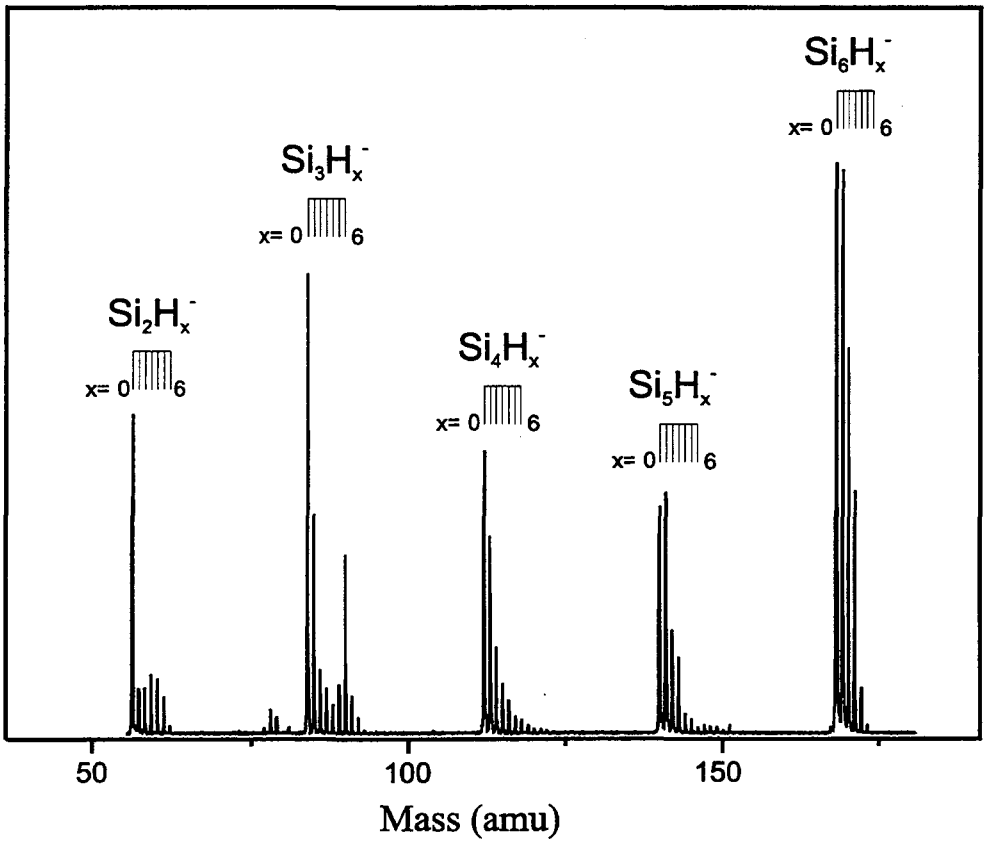

FIG. 1. Mass spectrum of bare silicon anion clusters and corresponding silicon hydride anions generated from the discharge ion source.

and 0° for each anion at least one photodetachment wavelength. The spectra consist of bands corresponding to transitions from the anion to various neutral electronic states. Vibrational structure is resolved in many of these bands. For each peak, the electron kinetic energy (eKE) is given by:

$$eKE = h\nu - EA - T_o^{(o)} + T_o^{(-)} - E_v^{(o)} + E_v^{(-)}, \qquad (1)$$

where hν is the laser photon energy, EA is the adiabatic electron affinity of the neutral species, $T_o^{(o)}$ and $T_o^{(-)}$ are the term values of the neutral and anion electronic states, and $E_v^{(o)}$ and $E_v^{(-)}$ are the neutral and anion vibrational energies, respectively, above the zero point energy. The photoelectron angular distribution is given by[26]

$$\frac{d\sigma}{d\Omega} = \frac{\sigma_{total}}{4\pi}[1 + \beta(E)P_2(\cos\theta)], \qquad (2)$$

where σ_{total} is the total photodetachment cross section and β(E) is the asymmetry parameter, varying from –1 to 2. One can determine β for each peak in the photoelectron spectrum through its intensity variation with laser polarization angle. The β parameter for each electronic band is then determined by averaging values of the constituent peaks.

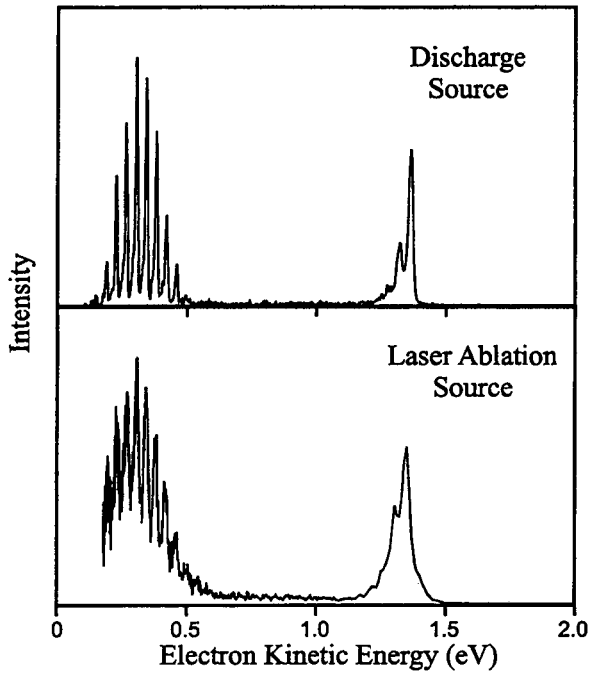

FIG. 2. Si_4^- photoelectron spectra at 355 nm using different ion sources. The discharge source generates substantially colder ions than the traditional laser ablation source.

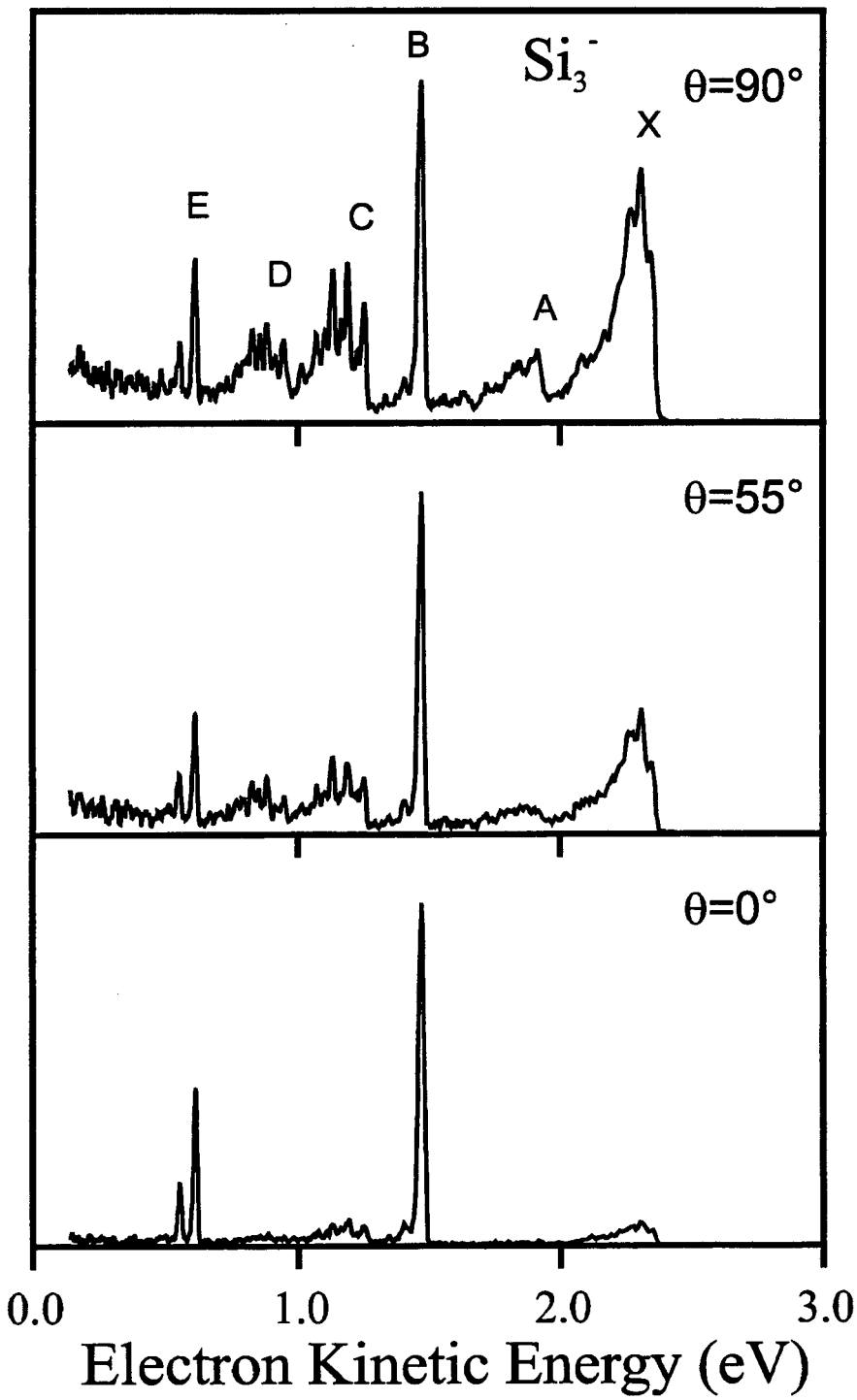

FIG. 3. Photoelectron spectra of Si_3^- taken at 266 nm. Laser polarization angles are θ = 90°, 55°, and 0° with respect to direction of electron collection.

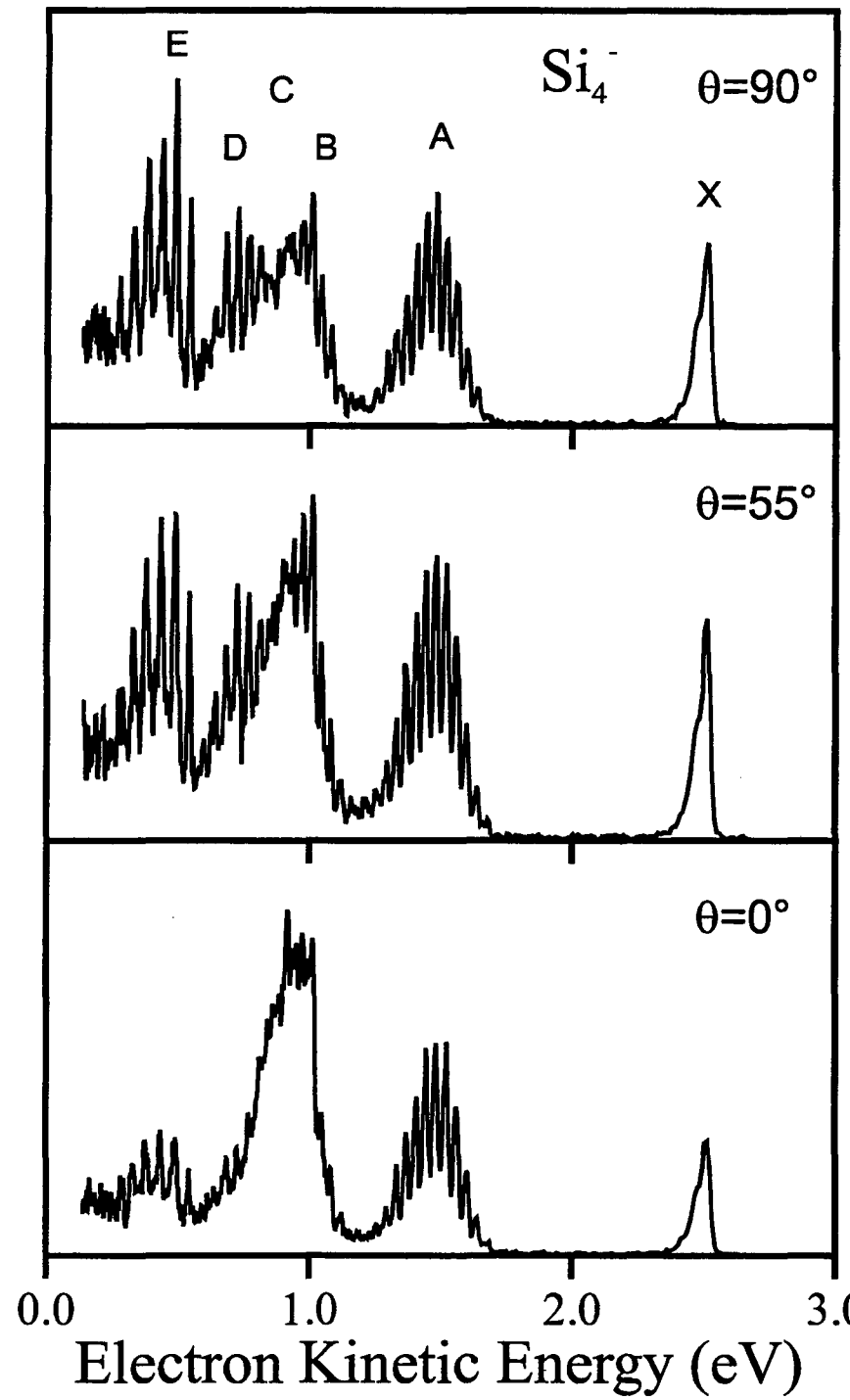

FIG. 4. Photoelectron spectra of Si_4^- taken at 266 nm. Laser polarization angles are θ = 90°, 55°, and 0° with respect to direction of electron collection.

The Si_3^- spectrum at 266 nm, Fig. 3, shows six distinct bands labeled X, and A - E. Bands X and A at high electron energy are essentially the same as in our previous spectrum at this wavelength,[2] with each showing some vibrational structure superimposed on a broad background. Band B consists of a very short progression of three peaks, dominated by the most intense peak of the spectrum at eKE = 1.463 eV. The peak spacing of band B is 500 ± 20 cm^{-1}. The band that was labeled as band C in our earlier study is better resolved here and clearly consists of two bands, labeled as bands C and D in Fig. 3. Both show regular progressions. Band C consists of five main peaks with an average spacing of 480 ± 20 cm^{-1}. There is a set of less intense peaks with the same peak spacing shifted 260 cm^{-1} towards lower eKE from the main progression. A similar pattern is observed in band D. The intensity profile of band E resembles that of band B, with a single intense peak and a rapid drop of intensity towards lower eKE. The peak spacing in band E is 480 ± 20 cm^{-1}. Bands B and E have β parameters of 1.9 and 1.5, respectively, both showing high intensity at $\theta = 0°$. These values are considerably large than those for bands X, A, C, and D, for which $\beta = -0.2$, -0.5, 0.2, and 0, respectively.

The Si_4^- photoelectron spectra at 266 nm in Fig. 4 are substantially improved over our previous spectra at this wavelength.[2] The vibrational progression of 310 ± 20 cm^{-1} comprising band A is now clearly resolved, and in fact resembles our earlier photoelectron spectrum at 355 nm (Fig. 2) where the energy resolution is higher because the electrons are slower. At lower electron kinetic energies, we now observe three distinct bands labeled B, C, and D, which appeared in our earlier spectrum to be a single structures band (previously labeled band B). Bands B and D show regularly spaced

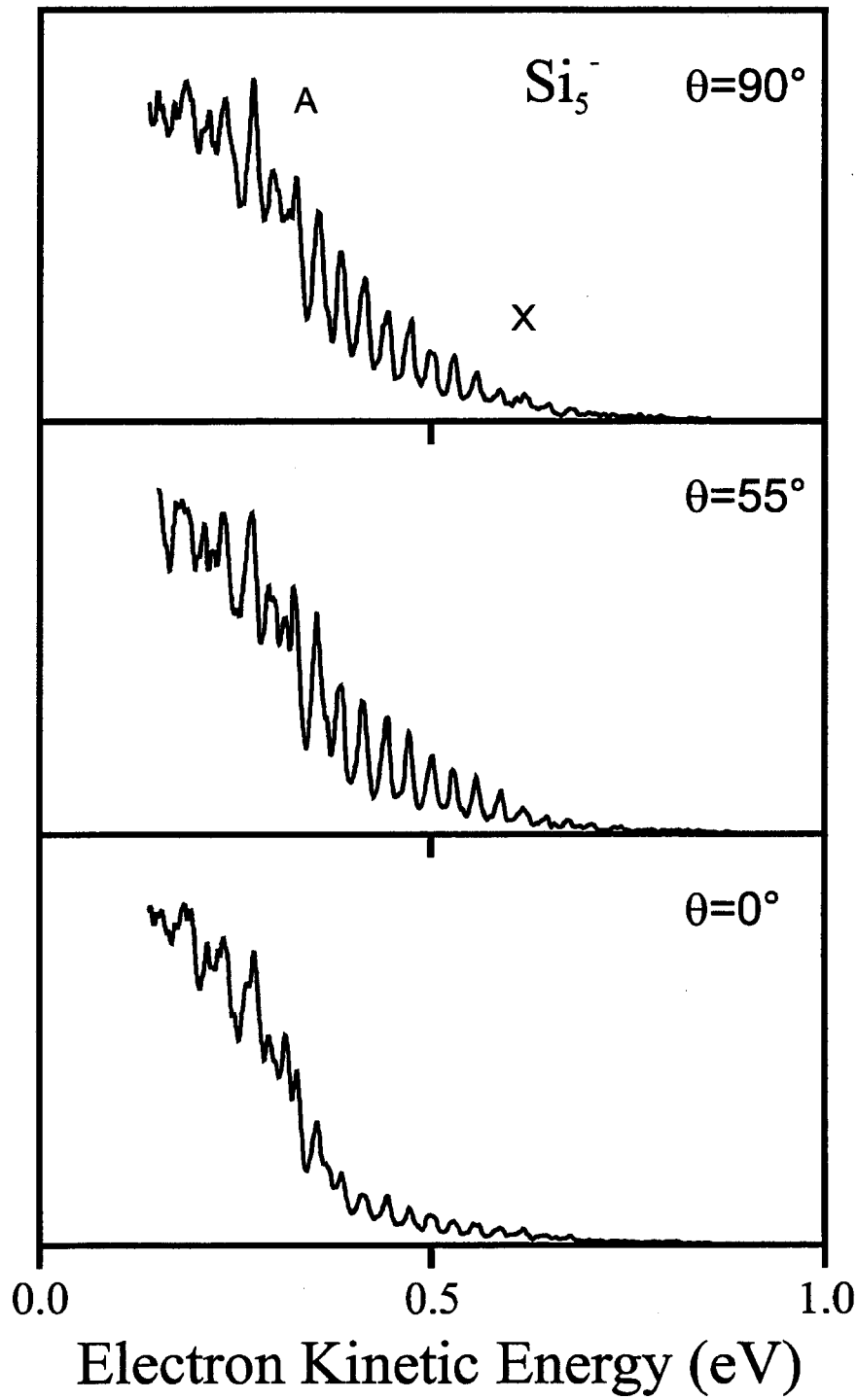

FIG. 5. Photoelectron spectra of Si_5^- taken at 355 nm. Laser polarization angles are θ = 90°, 55°, and 0° with respect to direction of electron collection.

vibrational transitions, while band C does not. At low eKE, band B is not resolved due to overlap with band C. Seven peaks spaced by 290 ± 20 cm^{-1} are apparent in band B starting at eKE = 1.160 eV; the peak spacing and intensity profile are similar to the first several peaks of band A. Band D, on the other hand, consists of six peaks with an average spacing of 355 ± 20 cm^{-1}. Band E shows a well-resolved progression of six

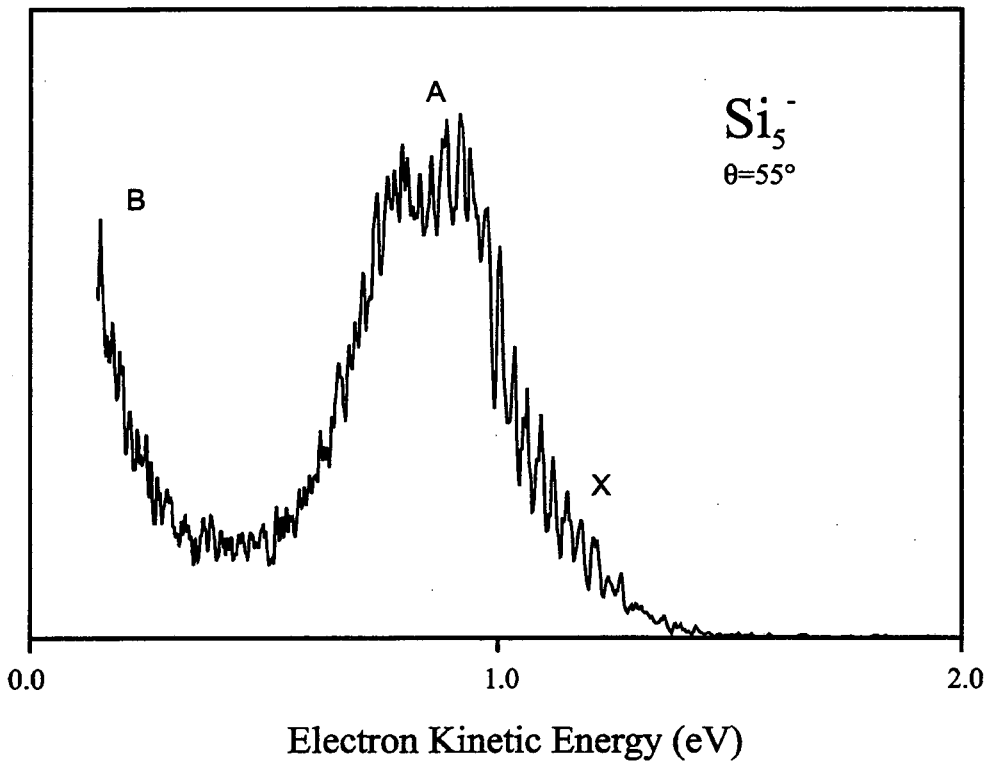

FIG. 6. Photoelectron spectra of Si_5^- taken at 299 nm. Laser polarization angle is θ = 55° (magic angle) with respect to direction of electron collection.

peaks spaced by 450 ± 20 cm^{-1}. The polarization studies indicate band C is the most intense band at $\theta = 0°$ with $\beta = 0.8$, whereas band E is the largest band at $\theta = 90°$ with $\beta = -0.1$. For bands X, A, B, and D, $\beta = 0.2$, 0.5, 0.3, and 0, respectively.

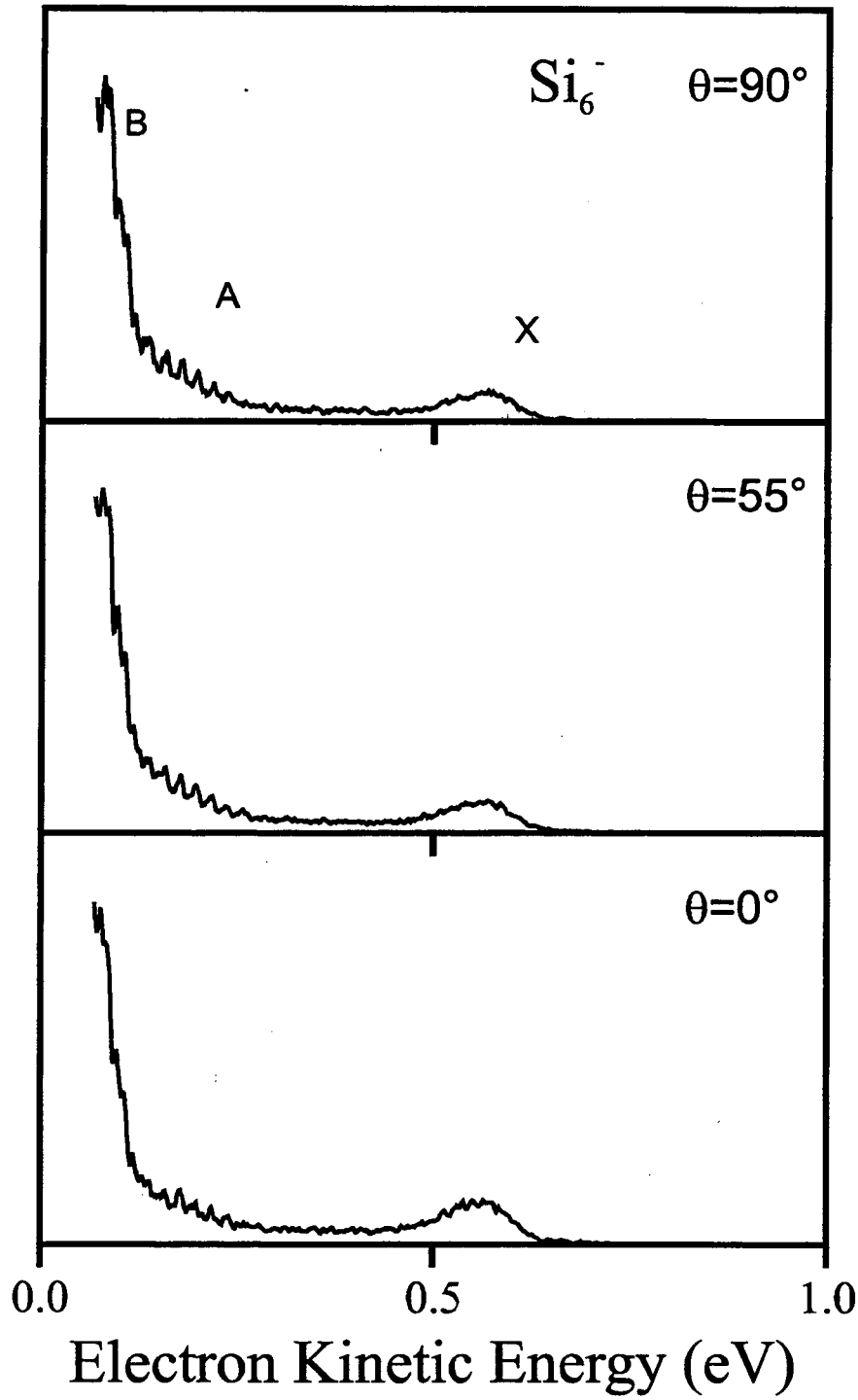

FIG. 7. Photoelectron spectra of Si_6^- taken at 355 nm. Laser polarization angles are θ = 90°, 55°, and 0° with respect to direction of electron collection.

The polarization dependence of the spectra of Si_5^- at 355 nm (Fig. 5) clearly shows that two electronic bands, labeled X and A, contribute to the spectra. Band X consists of a regular, well-resolved progression of at least fifteen peaks with an average spacing of 233 ± 20 cm^{-1}. The apparent origin of this transition is at 0.735 eV, although this is very approximate due to extended nature of the progression. Band A is most

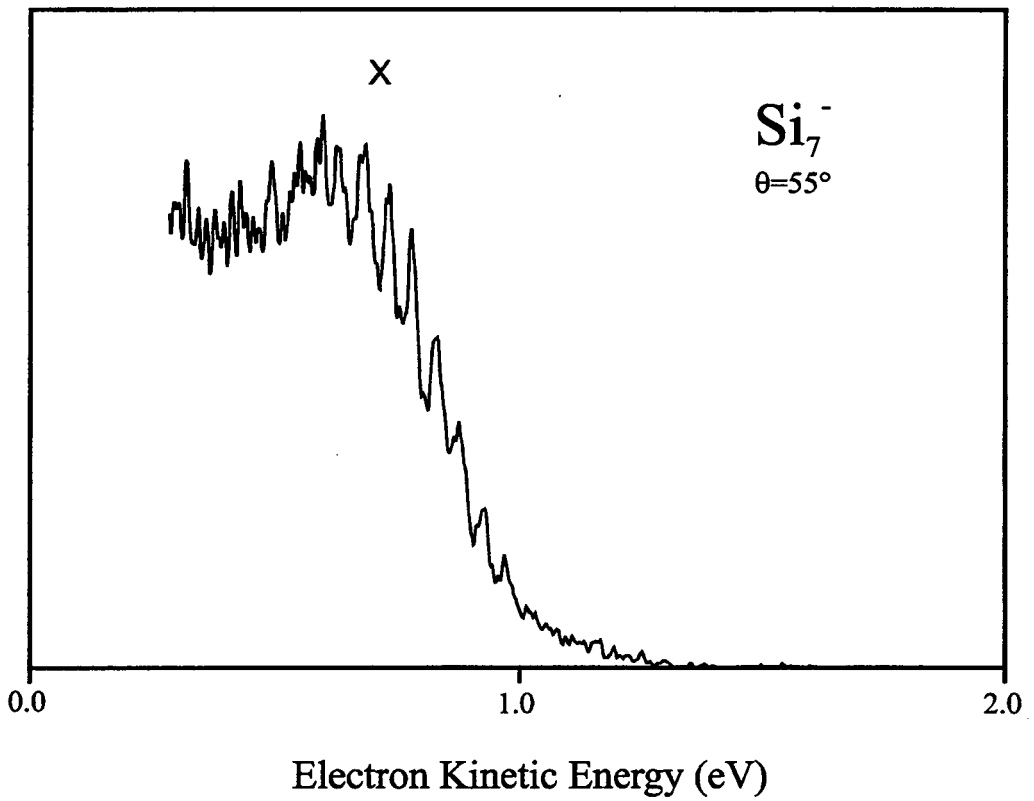

FIG. 8. Photoelectron spectrum of Si_7^- taken at 416 nm. Laser polarization angles are θ = 55° (magic angle) with respect to direction of electron collection.

apparent at $\theta = 0°$. It corresponds to the transition to a low-lying excited state of Si_5. While band A is structured, it does not show a regular progression as was seen in band X. Only part of band A is seen at 355 nm. The photoelectron spectrum of Si_5^- was also measured at a higher detachment energy of 4.141 eV (299 nm), shown in Fig. 6. Band A

can be seen here in its entirety, although there is still no obvious pattern to the vibrational structure.

The photoelectron spectra of Si_6^- at 355 nm, shown in Fig. 7, is comprised of three bands labeled X, A, and B. Band X is a weak unstructured, transition that reaches a maximum at eKE = 1.13 eV; its apparent onset occurs at eKE =1.28 eV. Attempts to observe vibrational structure in band X by measuring its photoelectron spectrum at 416 nm were unsuccessful. Band A, representing a transition to an excited state of Si_6, consists of seven resolved peaks starting at eKE = 0.476 eV with an average spacing of 323 ± 20 cm^{-1}. Band B at low eKE is the most intense transition. It corresponds to another low-lying electronic state and only the onset of this band was observed at 355 nm. Band X is isotropic with $\beta = 0$. Bands A and B have negative β parameters of –0.3 and –0.2, respectively.

The Si_7^- spectra at 416 nm and 355 nm in Fig. 8 and 9, respectively, show evidence for two bands, labeled X and A. Band X shows a progression of ten peaks spaced by 385 ± 20 cm^{-1}; this progression is slightly better resolved at 416 nm. At the higher wavelength, the onset of band X occurs at eKE ≅ 1.0 eV. At 355 nm, band A dominates the spectrum at low electron kinetic energies, with a β parameter of –0.3. As shown in the top panel of Fig. 9, β for band X varies from –0.5 to 0.5 as the electron energy decreases.

Assignment of the electronic and vibrational features in the experimental spectra is greatly facilitated by *ab initio* calculations of the geometries, vibrational frequencies, force constants, and state energies. From these, one obtains normal coordinate

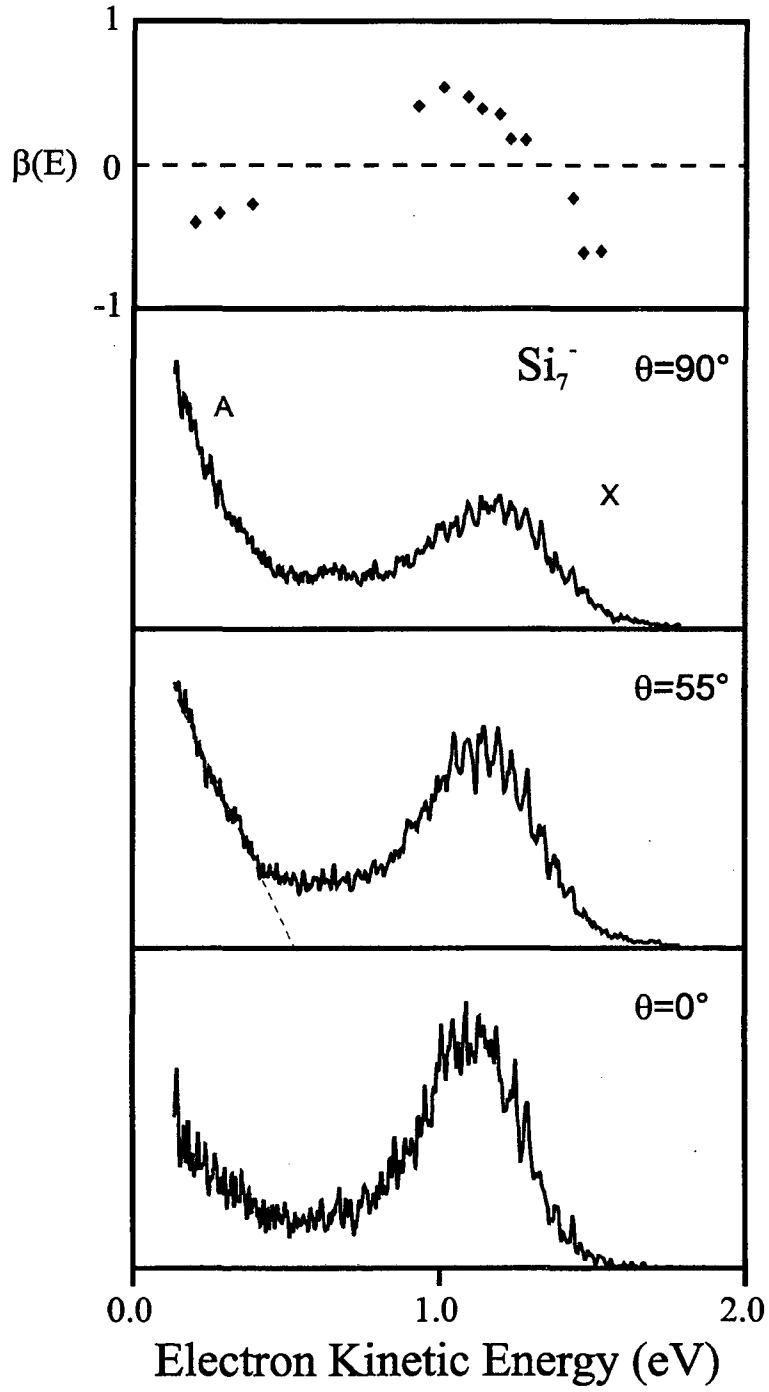

FIG. 9. Photoelectron spectra of Si_7^- taken at 355 nm. Laser polarization angles are θ = 90°, 55°, and 0° with respect to direction of electron collection. Top panel shows β(E) parameters.

displacements for photodetachment to each neutral state. The displacements are calculated within the parallel mode approximation, in which the force constants for the neutral state are assumed for both the anion and neutral. One can then perform Franck-Condon simulations of the spectrum based on the *ab initio* calculations and compare with experiment.

Tables I-II summarize the *ab initio* results for Si_3^-/Si_3 and Si_4^-/Si_4. Most of these are from published and unpublished calculations at the MP2 and QCISD(T) levels

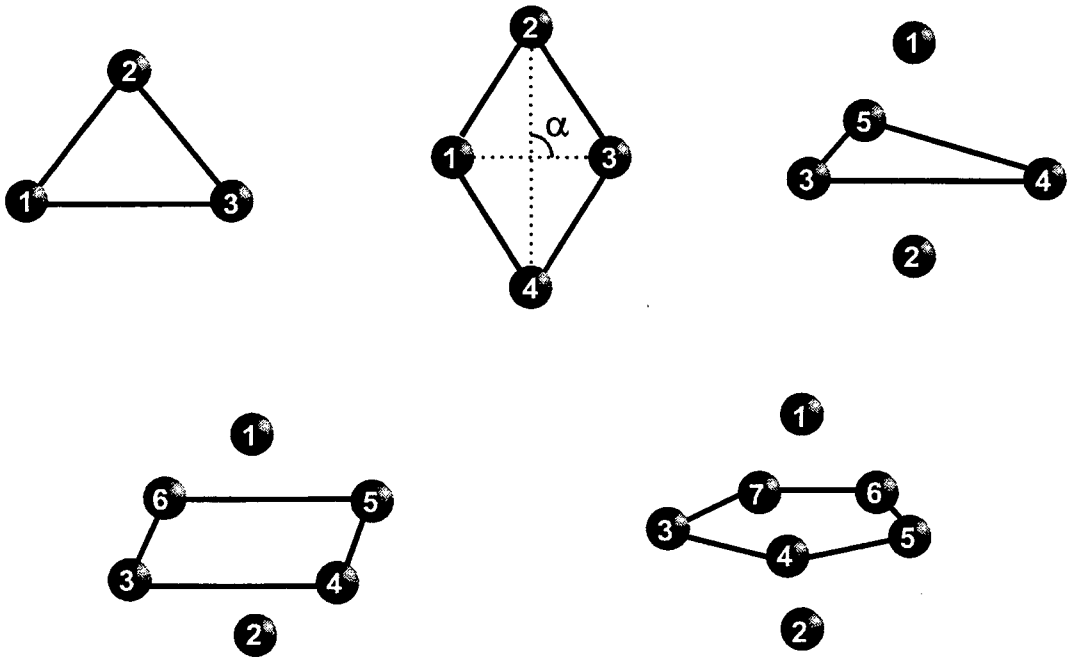

FIG. 10. Geometries of the silicon clusters studied in the current work.

performed by Rohlfing;[17,27] the MP2 frequencies for the $^3B_{3u}$, $^3B_{1g}$, and $^3B_{1u}$ states of Si_4 are from our calculations using Gaussian 92,[28] as are the normal coordinate displacements for all the Si_4 states in Table II. In these tables, geometries were optimized and

frequencies and force constants are calculated at the QCISD(T)/6-31G* level for Si_3^-/Si_3 and at the MP2/6-31G* level for Si_4^-/Si_4. Electronic state energies are then calculated at the QCISD(T) level using the larger 6-311+G(3DF) basis. We also calculated eometries, frequencies, and force constants for various electronic states of Si_5, Si_6, and Si_7 at the MP2/6-31G* level of theory; these along with previous calculations by Honea *et al.* [6] are summarized in Tables III-V. Note that low-lying, open shell singlet states are expected for many of these clusters but cannot be calculated with the methods used here. The geometries of the silicon clusters used in these Tables are shown in Fig. 10.

Table I. QCISD(T)/6-31G* optimized geometries, frequencies, and normal coordinate displacements for Si_3 [a]

	States	QCISD(T) / 6-311+G(3DF) Energy (Hartrees)	T_e (eV)	R(1-2) (Å)	R(1-3) (Å)	Angle (1-2-3)	Frequencies (cm^{-1}) / ΔQ (Å•$amu^{1/2}$)
Si_3^-	$^2A_1$ (C_{2v})	-867.12532	-2.21	2.261	2.437	65.2°	297(a_1), 370(b_2), 533(a_1)
Si_3	$^1A_1$ (C_{2v})	-867.04393	0.0	2.191	2.806	79.6°	148(a_1), 525(b_2), 551(a_1)
	$^3A_2$' (D_{3h})	-867.04330	0.02	2.290	2.290	60.0°	285(e), 522(a_1)
	$^3A_1$ (C_{2v})	-867.01028	0.92	2.281	2.436	64.6°	325(a_1) / 0.05, 405(b_2), 523(a_1) / 0.09
	$^3B_1$ (C_{2v})	-867.00287	1.12	2.333	2.579	67.1°	247(a_1) / 0.38, 321(b_2), 481(a_1) / 0.41

[a] Reference 27.

Table II. MP2/6-31G* optimized geometries, frequencies, and normal coordinate displacements for Si_4 [a]

	States	QCISD(T) / 6-311+G(3DF) Energy (Hartrees)	T_e (eV)	R(1-2) (Å)	R(1-3) (Å)	α	Frequencies (cm^{-1}) / ΔQ (Å•$amu^{1/2}$) [b]
Si_4^-	$^2B_{2g}$ (D_{2h})	-1156.20909	-2.06	2.303	2.352	90.0°	361(a_g), 485(a_g)
Si_4	^1A_g (D_{2h})	-1156.13324	0.0	2.312	2.413	90.0°	332(a_g) / 0.19, 463(a_g) / 0.15
	$^3B_{3u}$ (D_{2h})	-1156.10185	0.85	2.265	2.544	90.0°	330(a_g) / 1.07, 480(a_g) / 0.04 [c]
	^3B_g (C_{2h})	-1156.07806	1.50	2.285 2.383	2.219	87.3°	148(a_g) / 0.38, 372(a_g) / 1.36, 529(a_g) / 0.36
	$^3B_{1g}$ (D_{2h})	-1156.07041	1.71	2.352	2.280	90.0°	353(a_g) / 0.64, 491(a_g) / 0.08
	$^3B_{1u}$ (D_{2h})	-1156.06020	1.99	2.378	2.443	90.0°	329(a_g) / 0.22, 440(a_g) / 0.52

[a] MP2 frequencies are scaled by 0.95.[6] Reference. 27.

[b] Only totally symmetric modes (a_g) are listed.

[c] QCISD/6-31G* frequencies from Ref. 27; normal coordinate displacements based on QCISD/6-31G* geometries and force constants.

IV. Analysis and Discussion

A. General

In this section, the photoelectron spectra will be analyzed and assignments of the various bands made, when possible. The assignments are facilitated by comparison with

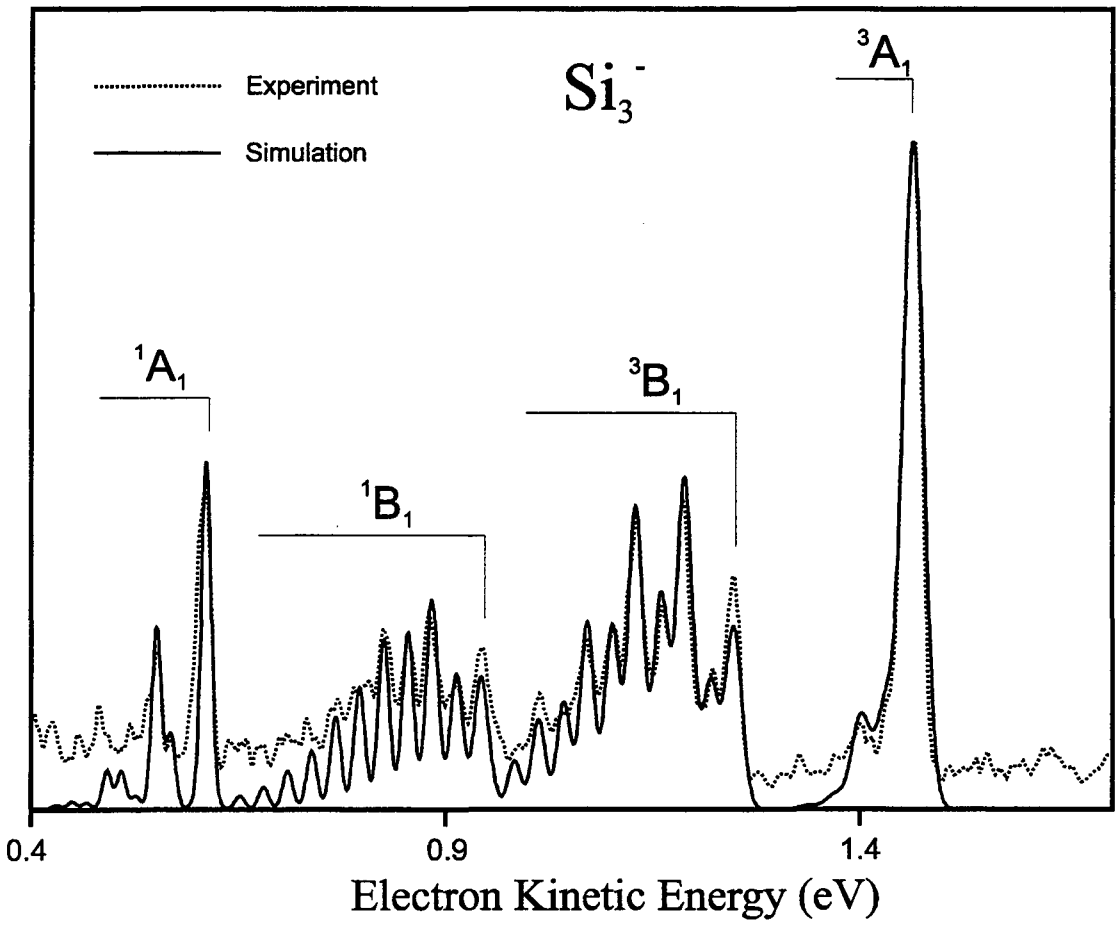

FIG. 11. Franck-Condon simulation of the Si_3^- spectrum. Parameters given in Table VI.

previous *ab initio* studies as well as calculations performed as part of this investigation. Spectral simulations of the vibrational profiles based on the Franck-Condon

approximation are also very useful in assigning the bands, as are the photoelectron angular distributions. In the case of Si_3^- and Si_4^-, where there has already been considerable discussion of the anions and the ground and lowest excited states of the neutrals, the discussion below focuses more on the higher-lying states that are better characterized experimentally in the spectra presented here. The larger clusters have received less attention so all aspects of their photoelectron spectra are considered below.

B. Si_3^-

Several *ab initio* calculations have been performed on Si_3^- and the low-lying states of Si_3.[8-11,16-19,29,30] The ground state of the anion is predicted to have C_{2v} symmetry with the valence electron configuration ... $(10a_1)^2(3b_1)^2(7b_2)^2(11a_1)^1$, resulting a $^2A_1$ state. The neutral $^1A_1$ ground state is formed by photodetaching an electron from the highest occupied molecular orbital (HOMO), the $11a_1$ orbital, of the anion. The low-lying electronic states accessible via anion photoelectron spectroscopy are the singlet and triplet pairs of the B_2, B_1, and A_1 states, corresponding to removal of an electron from the $7b_2$, $3b_1$, and $10a_1$ orbitals, respectively. The $^3B_2$ state collapses to a D_{3h} $^3A_2$' state, 0.02 eV above the ground state. *Ab initio* results at the QCISD(T) level [17,27] for the anion and neutral ground states and several triplet states of Si_3 are listed in Table I.

In our previous photoelectron spectrum of Si_3^-, five bands (C and D in Fig. 3 were labeled as a single band C) were observed at 266 nm.[2] Band X was also investigated by ZEKE spectroscopy of Si_3^-.[4] Based on the experimental and theoretical results, band X was assigned to overlapped transitions to the $^1A_1$ ground state and the low-lying $^3A_2$'

state. Rohlfing and Raghavachari assigned bands A, B, C, and D to the $^1B_2$, $^3A_1$, $^3B_1$, and $^1B_1$ states, respectively, based on their calculations at the QCISD(T) level for the triplet states and at the single excitation CI level (CIS) for the open shell singlets.[17] Since band C is now resolved to be two distinct bands (C and D in Fig. 3) some new assignments are required.

The assignments of bands X, A, and B are unchanged. To aid in assigning the higher energy bands, we obtained the normal coordinate displacements from the anion ground state to the neutral states, using the geometries and force constants from the QCISD(T)/6-31G* calculations for the excited triplet states[17]. These displacements are obtained within the parallel mode approximation in which the force constants for the relevant neutral electronic state are used for both the neutral and the anion. Given these displacements, one can simulate the photoelectron spectrum within the Franck-Condon approximation. For some bands, the normal coordinate displacements were adjusted to obtain a better fit to the experimental spectrum. Simulations of bands B-E are shown in Fig. 11 superimposed on the experimental data; the parameters used in the simulations are listed in Table VI.

The appearance of band B indicates that the molecular geometries of the anion and neutral electronic states are very similar, consistent with the *ab initio* results. To simulate the spectrum of band B in Fig. 11, we used symmetric stretch and bend frequencies ν_1 = 500 cm^{-1} and ν_2 = 250 cm^{-1}, respectively, and normal mode displacements ΔQ_1 = 0.13 Å•$amu^{1/2}$ and ΔQ_2 = 0.19 Å•$amu^{1/2}$. These values agrees reasonably well with the QCISD(T) values of ν_1 = 523 cm^{-1} and ΔQ_1 = 0.09 Å•$amu^{1/2}$,

and ν_2 = 325 cm^{-1} and ΔQ_2 = 0.05 Å•$amu^{1/2}$. We also obtain a new term energy of T_o ($^3A_1$) = 0.90 ± 0.02 eV from our simulation given the electron affinity of 2.29 ± 0.02 eV, in good agreement with the QCISD(T) value of 0.92 eV[17].

Bands C and D have approximately equal β parameters of 0.2 and 0, respectively. The similarity of the vibrational progressions shows that the two neutral states have similar geometries and frequencies. These two observations indicate that the neutral states probably have the same molecular orbital configuration. We therefore assign bands C and D to the $^3B_1$ and $^1B_1$ states, respectively. This yields a term value for the $^3B_1$ state, 1.12 ± 0.02 eV, which is in excellent agreement with the previously calculated term value of 1.12 eV.[17] The resulting singlet-triplet splitting of 0.31 ± 0.01 eV based on the apparent band origins is somewhat lower than the calculated value of 0.41 eV by Sabin *et al,*[10] but is clearly in the right range. The QCISD(T)/6-31G* calculation[17] for the $^3B_1$ state gives ΔQ_1 = 0.41 Å•$amu^{1/2}$ and ΔQ_2 = 0.38 Å•$amu^{1/2}$. Similar normal coordinate displacements are expected for the $^1B_1$ state, so both the symmetric stretch (ν_1) and bend (ν_2) modes should be active in the $^3B_1$ and $^1B_1$ states. The Franck-Condon simulations of these two transitions are shown in Fig. 11. The parameters used in the simulations, listed in Table VI, show that the vibrational frequencies and normal coordinate displacements for the two neutral states are quite similar to one another and in good agreement with the calculated values for the $^3B_1$ state in Table I.

Band E was originally assigned to the $^1B_1$ state. Given our new assignment of band D to this state, we assign band E to the open-shell $^1A_1$ state, the singlet counterpart of the $^3A_1$ state (band B), corresponding to removal of an electron from the $10a_1$ orbital.

Our assignment is supported by the polarization results, which show bands B and E have similar β parameters, and by the similar vibrational progressions in the two bands. Since the ground state is also a $^1A_1$ state, we were not able to perform an SCF calculation on this higher energy $^1A_1$ state. The simulation shown in Fig. 11 was obtained using the parameters $\nu_1 = 480$ cm^{-1}, $\Delta Q_1 = 0.23$ Å•amu$^{1/2}$, and $\nu_2 = 340$ cm^{-1}, $\Delta Q_2 = 0.20$ Å•amu$^{1/2}$. These frequencies and normal coordinate displacements are similar to those for photodetachment to the $^3A_1$ state, supporting our singlet-triplet pair assignment.

C. Si_4^-

Ab initio calculations show that the ground state of Si_4^- is a rhombus with D_{2h} symmetry. The valence orbital configuration is $...(b_{3u})^2(a_g)^2(b_{1u})^2(b_{2g})^1$ yielding a $^2B_{2g}$ electronic state.[17] Photodetachment from the b_{2g} HOMO yields the ^1A_g neutral ground state which is also a rhombus.[13] Removal of electrons from other orbitals yields low-lying excited states that are accessible via anion photoelectron spectroscopy. From the *ab initio* calculations[17,27] in Table II, the low-lying triplet states in order of increasing energy are the $^3B_{3u}$, ^3B_g, $^3B_{1g}$, and $^3B_{1u}$ state; all have D_{2h} symmetry except the ^3B_g state with C_{2h} symmetry which results from slight geometric distortion of a $^3B_{2g}$ (D_{2h}) state. Calculated energies, geometries, frequencies, and normal coordinate displacements are also shown in Table II. Each triplet excited state has a corresponding open-shell singlet state which has not been calculated here. A simulation of the Si_4^- photoelectron spectrum resulting from photodetachment to several of these excited states is shown in Fig. 12. The simulation parameters are shown in Table VI.

The ground state, band X, is best seen in the 355 nm photoelectron spectrum (Fig. 2). The electron affinity was measured to be 2.15 eV from our earlier photoelectron

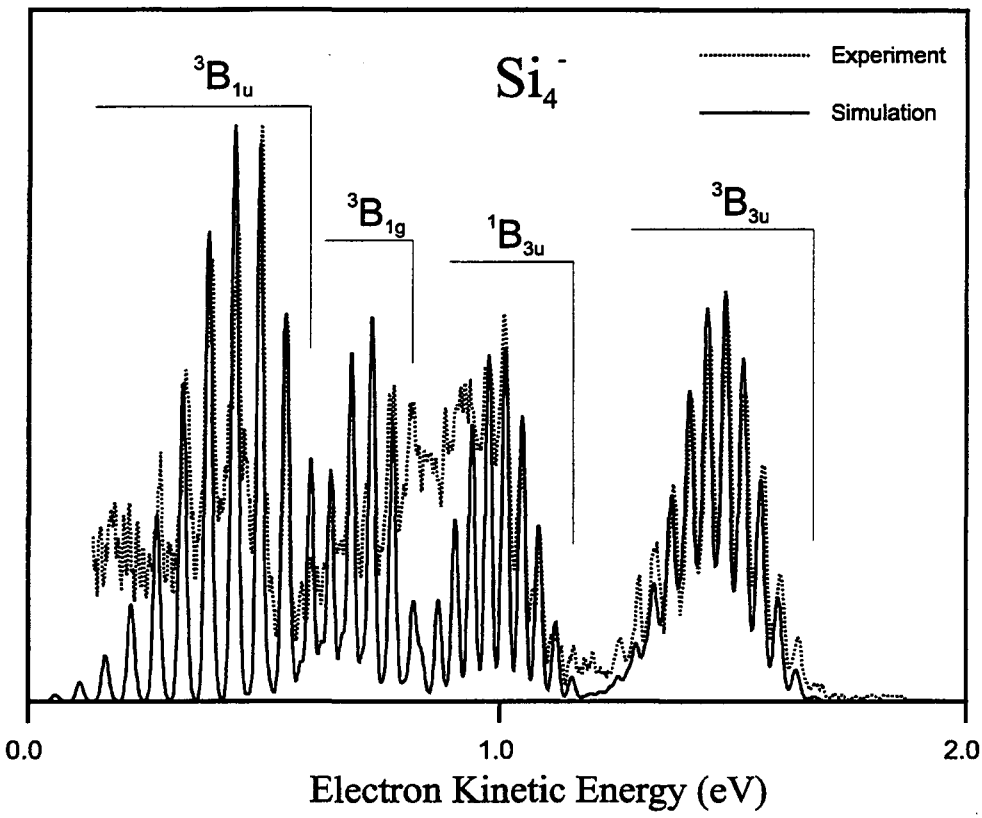

FIG. 12. Franck-Condon simulation of the Si_4^- spectrum. Parameters given in Table VI.

spectrum.[2] The new spectrum is slightly better calibrated through comparison with the ZEKE spectrum of Si_4^-.[3] The spectrum in Fig. 2 shows a progression of three peaks spaced by 380 ± 20 cm^{-1} in band X, corresponding to photodetachment to the ^1A_g ground state. The band is dominated by the vibrational origin at eKE=1.365 eV, yielding a new Si_4 electron affinity of 2.13 ± 0.01 eV.

Band A was studied by ZEKE spectroscopy[3] in some detail, and a comparison with theory confirmed that this band corresponds to the transition to the $^3B_{3u}$ state, resulting from photodetachment from the b_{1u} orbital.[17] Several vibrational frequencies were obtained. The $^3B_{3u}$ state has two totally symmetric vibrational modes, the ν_1 overall stretch and ν_2 symmetric distortion modes. In addition there are three asymmetric stretching modes (ν_3, ν_4, and ν_5), and a bending mode of b_{3u} symmetry (ν_6). The ν_2 mode has the largest displacement upon photodetachment, resulting in the main progression of 310 ± 20 cm^{-1} in the 266 nm spectrum. This is in good agreement with the ZEKE spectrum which yielded a frequency of $\nu_2 = 312$ cm^{-1}.

Band B appeared as a very short progression in the ZEKE spectrum and was assigned to the $^1B_{3u}$ state. In Fig. 4, band B consists of a longer progression of peaks spaced by 290 ± 20 cm^{-1}, in good agreement with the ZEKE value of 300 cm^{-1} and close to the ν_2 frequency in the $^3B_{3u}$ state. Bands A and B exhibit similar peak spacings and intensity profiles. Moreover, the anisotropy parameters are similar: β=0.3 for band B and 0.5 for band A. These observations support the previous assignment of band B to the $^1B_{3u}$ state, which has the same molecular orbital configuration as the $^3B_{3u}$ state. Band B can be simulated using almost the same normal coordinate displacements as band A. The simulation of band B shown in Fig. 12 yields a term energy of 1.34 ± 0.02 eV for the $^1B_{3u}$ state, and a $^1B_{3u}$-$^3B_{3u}$ singlet-triplet splitting of 0.49 ± 0.02 eV.

Band C does not show a regular progression, and it has the most positive β parameter (0.8) of all the bands. The QCISD(T) energy calculations predict the term

value of the ^3B_g state to be 1.50 eV. The corresponding electron kinetic energy of 1.04 eV is just where band C is found. Moreover, the ^3B_g state is a lower symmetry, Jahn-Teller distorted state, so an additional low-frequency bending vibration (156 cm^{-1} in Table II) is totally symmetric. This mode should also active (ΔQ_3 = 0.38 Å•$amu^{1/2}$ in Table II) due to the symmetry change upon photodetachment along with other two modes. One therefore expects a higher density of vibrational transitions which, given the resolution of our spectrometer, might well result in the absence of a clear vibrational progression. We therefore assign band C to the ^3B_g state.

Band D shows a single progression of 355 ± 20 cm^{-1}. From Table II, the $^3B_{1g}$ state of Si_4 is predicted to lie in this energy range, and the calculated normal coordinate displacements for photodetachment to this state are significant only for a single vibrational mode with frequency 353 cm^{-1}. Band D is therefore assigned to the $^3B_{1g}$ state. The simulation of photodetachment to the $^3B_{1g}$ state is shown in Fig. 12. Due to overlap with band C, the band origin is difficult to locate. Fig. 12 shows the best fit to the experimental vibrational profile. The resulting term energy of T_o ($^3B_{1g}$) = 1.71 ± 0.02 eV is in excellent agreement with the calculated value in Table II, and the normal coordinate displacements used in the simulations are in reasonable agreement with the calculated displacements, further supporting this assignment.

Band E stands alone with well-resolved vibrational structure. It lies about 2 eV above the ground state and the peak spacing is 451 ± 20 cm^{-1}. The *ab initio* calculation predicts a term energy of 1.99 eV for the $^3B_{1u}$ state, and a large displacement of ΔQ_1=0.52 Å•$amu^{1/2}$ along the ν_1 mode for which the frequency is 440 cm^{-1}. Although the

calculated ΔQ_2 = 0.22 Å•amu$^{1/2}$, the resulting Franck-Condon profile in this mode is much shorter than for the ν_1 mode because of the smaller frequency of 346 cm^{-1}. We therefore assign band E to the $^3B_{1u}$ state, which is the only state in Table II for which ΔQ is largest for the ν_1 mode. A term energy of T_o ($^3B_{1u}$) = 1.93 ± 0.02 eV is obtained from the simulation shown in Fig. 12, slightly lower than the *ab initio* term value. Agreement between the simulated and *ab initio* normal coordinate displacements is satisfactory.

One might argue that either band D or E is due to the $^1B_{2g}$ state, the singlet counterpart of the ^3B_g state responsible for band C. Although the vibrational profile of band C is quite different from the other two, the $^1B_{2g}$ state is not expected to undergo geometric distortion from C_{2v} symmetry,[17] so this alone does not rule out an alternate assignment. However, the anisotropy parameter $\beta = 0.8$ for band C, while $\beta = 0$ and –0.1 for bands D and E, respectively. Thus, it is unlikely that either band is from the $^1B_{2g}$ state. The question remains as the location of the $^1B_{2g}$ state. Rohlfing predicts a singlet-triplet splitting of only 0.17 eV for the $^1B_{2g}$ and ^3B_g states. Either this value is too low, or the transition to the $^1B_{2g}$ state overlaps with band C. The latter is certainly possible given the broad, unstructured appearance of band C. This issue can be addressed by higher level *ab initio* calculations.

D. Si_5^-

Little is known about the ground and excited states of Si_5 from previous experimental studies. The concentration of Si_5 was presumably too low to be observed in

earlier matrix spectroscopy studies.[6,7] The photoelectron spectra of Si_5^- obtained by Cheshnovsky *et al.*[1] did not have sufficient resolution to map out any vibrational structure.

More information is available from the *ab initio* calculations by Raghavachari and Rohlfing, which predicted that Si_5 and Si_5^- have compressed trigonal bipyrimidal ground states with D_{3h} symmetry.[9,15] The molecular orbital configuration for Si_5^- is $\ldots(e'')^4(a_1')^2(e')^4(a_2'')^1$, yielding a $^2A_2''$ ground state. Removal of an electron from the HOMO leaves a closed-shell neutral $^1A_1'$ ground state. Si_5 was also predicted to have a low-lying $^3B_1$ triplet state with a Jahn-Teller distorted C_{2v} structure. The molecular orbital configuration of this state is $\ldots(a_1)^2(a_2)^2(b_1)^2(b_2)^2(b_1)^1(a_1)^1$ which correlates with the $\ldots(e'')^4(a_1')^2(e')^3(a_2'')^1$ state of the trigonal bipyramid. The $^3B_1$ state is accessible by removal of an electron from the e' orbital in the anion. Calculations at the MP4/6-31G* level indicate that the $^3B_1$ state lies about 0.5 eV above the ground state.[15] *Ab initio* results for Si_5^- and Si_5 are summarized in Table III.

Table III. MP2/6-31G* optimized geometries, frequencies, and normal coordinate displacements[a] for Si_5

	States	T_e (eV)	R(1-2) (Å)	R(1-3) (Å)	R(1-4) (Å)	R(3-4) (Å)	Angle (4-3-5)	Frequencies (cm^{-1}) / ΔQ (Å•$amu^{1/2}$) [b]
Si_5^-	$^2A_2$" (D_{3h})	-2.14	3.468	2.326	2.326	2.685	60.0°	473(a_1'), 309(a_1')
Si_5	$^1A_1$' (D_{3h})	0	3.057	2.296	2.296	2.967	60.0°	476(a_1') / 0.21, 247(a_1') / 2.12
	$^3B_1$ (C_{2v})	0.5	3.575	2.294	2.361	2.483	69.8°	494(a_1) / 0.70, 373(a_1) / 0.48, 364(a_2) / 0.71, 320(a_1) / 0.29, 159(a_1) / 0.99

[a] MP2 frequencies are scaled by 0.95.[6]

[b] Only totally symmetric modes (a_1') are listed.

In the Si_5^- spectrum taken at 355 nm (Fig. 5), band X consists of an extended progression with a peak spacing of 233 ± 10 cm^{-1} beginning around eKE=0.75 eV. This long progression indicates a large geometry change between the anion the neutral

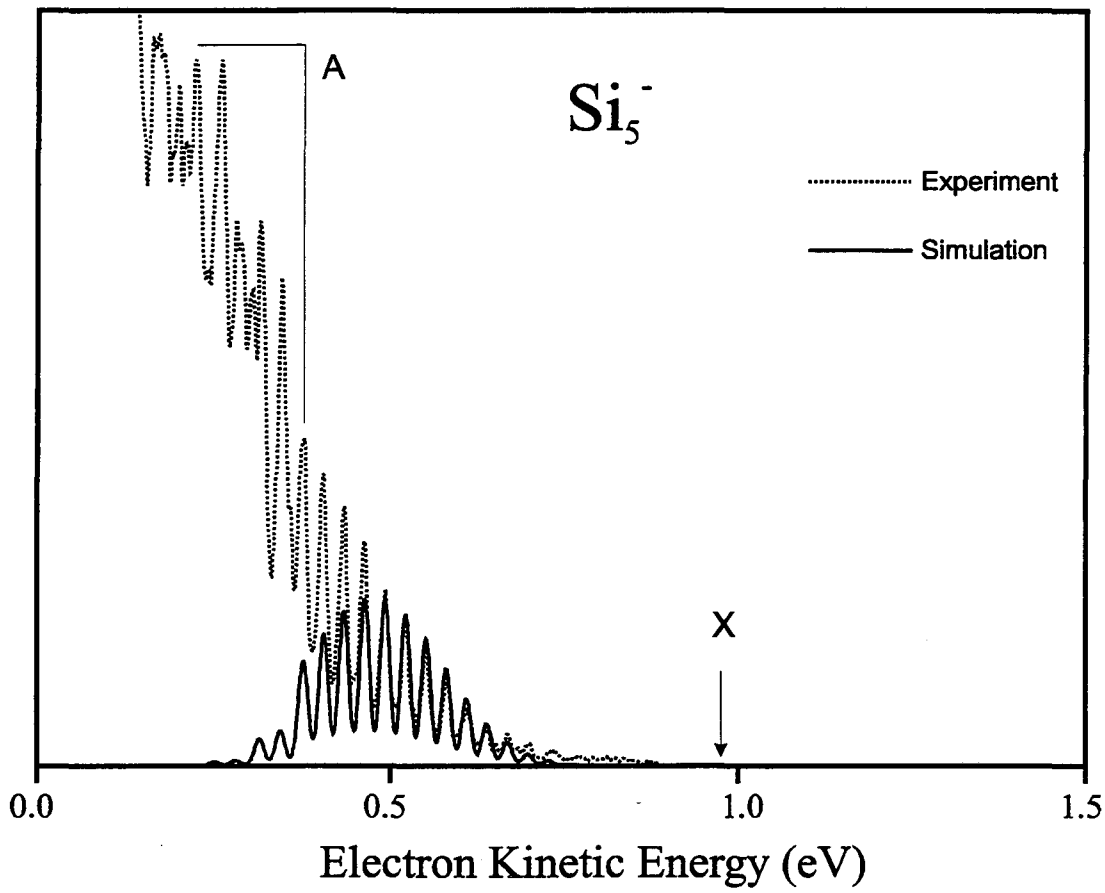

FIG. 13. Franck-Condon simulation of the Si_5^- spectrum. Parameters given in Table VI.

electronic ground states. The $^1A_1$' ground state is formed by photodetaching an electron from the a_2" orbital which is anti-bonding between the two apex atoms. The *ab initio* calculations indicate that photodetachment to the $^1A_1$' state results in a significant reduction of the distance between the apical atoms, leading to a large displacement along

the totally symmetric ν_2 normal coordinate mode. The observed peak spacing is in good agreement with our MP2/6-31G* value of $\nu_2 = 247$ cm^{-1} shown in Table III.

The anion, neutral geometries and force constants from our MP2/6-31G* calculations have been applied to obtain the normal coordinate change between the anion and neutral. The Franck-Condon simulation of band X is shown in Fig. 13. The experimental ν_2 frequency was used, but the other parameters were taken directly from the MP2/6-31G* calculation: $\Delta Q_1 = 0.21$ Å•amu$^{1/2}$, $\Delta Q_2 = 2.12$ Å•amu$^{1/2}$, and $\nu_1 = 501$ cm^{-1}. The extraordinarily large normal coordinate displacement for ΔQ_2 results in poor overlap with the vibrational origin; this transition has no intensity in the simulated spectrum. To obtain the best fit, we chose the vibrational origin at 0.935 eV electron energy, yielding an electron affinity of 2.59 ± 0.02 eV for Si_5. Although one could obtain a satisfactory fit assuming the vibrational origin shifted by a vibrational quantum in either direction, this required using normal coordinate displacements that differed more from the *ab initio* values. The adiabatic electron affinity from our assignment is 0.5 eV less than the vertical detachment energy of 3.10 eV calculated by Adamowicz.[31] This discrepancy is due at least in part to the large geometry change between the anion and neutral ground state. Raghavachari and Rohlfing[16] reported an adiabatic electron affinity of 2.26 eV at the QCISD(T) / 6-31+G* level, in reasonable agreement with our experimental value.

The $^3B_1$ state excited state is a Jahn-Teller distorted C_{2v} state with four totally symmetric vibrational modes. One therefore expects a congested photoelectron spectrum to result from photodetachment to this state. The irregular vibrational structure of band

A therefore suggests that we assign it as the transition to the $^3B_1$ state. From the spectrum at $\theta = 0°$ in which the ground state has little intensity, we estimate the $^3B_1$ state origin to be at eKE= 0.36 ± 0.05 eV, 0.58 eV above the $^1A_1$' ground state. This is in agreement with the calculated term value of 0.5 eV, further supporting our assignment.

Besides the X and A bands, a new band B shows up at low eKE in the 299 nm spectrum (Fig. 6). We estimate the origin of this band to occur at eKE=0.39 eV, yielding a term energy of 1.16 ± 0.05 eV for this neutral excited state.

E. Si_6^-

Ab initio calculations predict Si_6^- to have a $^2A_{2u}$ ground state with D_{4h} symmetry, corresponding to a tetragonal bipyramidal structure, with valence orbital configuration $...(e_g)^4(a_{1g})^2(b_{2g})^2(e_u)^4(a_{2u})^1$.[16] Calculations also predict that neutral Si_6 has three nearly isoenergetic structures: a tetragonal bipyramid ($^1A_{1g}$, D_{4h}) and two in which this structure is distorted ($^1A_1$, C_{2v}). The $^1A_{1g}$ state corresponds to removal an electron from the a_{2u} HOMO. At the HF/6-31G* level, Raghavachari found the two C_{2v} structures are separated by 0.04 eV while the D_{4h} structure is about 0.4 eV higher in energy.[9] Fournier *et al.* reported similar results using density functional theory,[19] with the three structures lying within 0.2 eV of one another. At the MP2/6-31G* level, the $^1A_{1g}$ state with D_{4h} symmetry is more favored. The assignment of this structure as the ground state is consistent with the experimental vibrational frequencies from matrix Raman spectroscopy.[6] *Ab initio* results for the ground and excited states at the MP2/6-31G* level are summarized in Table IV.

In the 355 nm photoelectron spectrum, Fig. 7, the transition to the Si_6 ground state (band X) appears as a weak, unstructured band. For a D_{4h} tetragonal bipyramidal molecule, there are two totally symmetric modes ν_1 and ν_2. A Franck-Condon simulation using the frequencies and normal coordinate displacements in Table IV for photodetachment to the $^1A_{1g}$ state shows extended progressions in both modes, and this along with incomplete vibrational cooling may explain the absence of structure in band X. We note that this simulation (not shown) is considerably broader than the experimental band, indicating that the calculated normal coordinate displacements and/or vibrational frequencies need to be adjusted.

Table IV. MP2/6-31G* optimized geometries, frequencies,[a] and normal coordinate displacements for Si_6

	States	T_e (eV)	R(1-2) (Å)	R(1-3) (Å)	R(3-4) (Å)	Frequencies (cm^{-1}) / ΔQ (Å•amu$^{1/2}$) [b]
Si_6^-	$^2A_{2u}$ (D_{4h})	-1.45	3.114	2.397	2.577	444(a_{1g}), 306(a_{1g})
Si_6	$^1A_{1g}$ (D_{4h})	0	2.694	2.356	2.734	447(a_{1g}) / 0.49, 298(a_{1g}) / 1.90
	^3E_g (D_{4h})	1.26	3.282	2.413	2.501	
	$^3B_{1u}$ (D_{4h})	3.44	3.156	2.441	2.632	

[a] MP2 frequencies are scaled by 0.95. Geometries and frequencies are same as Reference 6.

[b] Only totally symmetric modes (a_{1g}) are listed.

In contrast to band X, band A in Fig. 7 shows a progression of 323 ± 20 cm^{-1} between 0.25 to 0.50 eV. The presence of a single progression indicates that the neutral is at least as symmetric as the anion; if the anion has D_{4h} symmetry, band A should

correspond to the transition to a state with D_{4h} or O_h symmetry. Although a low-lying triplet state with O_h symmetry was investigated in the calculation by Fournier *et al.*, it was predicted to have two imaginary frequencies.[19] We performed *ab initio* calculations on two low-lying states restricted to D_{4h} symmetry. At the MP2/6-31G* level, a ^3E_g state was found to lie 1.26 eV above the ground state, corresponding removal of an e_u electron from the anion $^2A_{2u}$ state. However, one imaginary frequency was also found at the HF/6-31G* level. Photodetaching a b_{2g} electron from the anion ground state results a $^3B_{1u}$ state which is 3.44 eV less stable than the neutral $^1A_{1g}$ ground state. Neither state appears to be a likely candidate for band A. Alternatively, if the anion ground state had C_{2v} symmetry, then band A could be explained as a transition to the low-lying C_{2v} structures of Si_6 predicted by Raghavachari[9]. In any case, further theoretical work on the low-lying states of both Si_6 and Si_6^- appears needed to explain this band and the intense, unstructured band B at lower eKE.

F. Si_7^-

Si_7^- is predicted to have a pentagonal bipyramidal D_{5h} ground state geometry.[15] The valence electron configuration is $\ldots(e_1")^4(a_1)^2(e_1')^4(e_2')^4(a_2")^1$, resulting a $^2A_2"$ state. Photodetaching an electron from the HOMO orbital yields the $^1A_1'$ ground state of the neutral species, which also has D_{5h} symmetry. As the $a_2"$ orbital is antibonding between the apex atoms, detachment to the $^1A_1'$ state results a more compact structure along the apex, just as for Si_5^-. The $^1A_1'$ state has two totally symmetric stretch modes (ν_1 and ν_2). The optimized geometries, frequencies and resulting normal mode displacements at the MP2/6-31G* level are shown in Table V. Raghavachari and Rohlfing studied other two

isomers, a tricapped trigonal pyramid and a capped octahedral structure, both of C_{3v} symmetry. They were found to be 0.95 and 2.08 eV less stable than the $^1A_1$' state at the MP4/6-31G* level, respectively.[15]

Table V. MP2/6-31G* optimized geometries, frequencies,[a] and normal coordinate displacements for Si_7

	States	T_e (eV)	R(1-2) (Å)	R(1-3) (Å)	R(3-4) (Å)	Frequencies (cm^{-1}) / ΔQ (Å•amu$^{1/2}$) [b]
Si_7^-	$^2A_2$" (D_{5h})	-1.25	2.837	2.507	2.431	407(a_1'), 295(a_1')
Si_7	$^1A_1$' (D_{5h})	0	2.512	2.457	2.483	440(a_1') / 0.67, 352(a_1') / 1.15

[a] MP2 frequencies are scaled by 0.95. Geometries and frequencies are same as Reference 6.

[b] Only totally symmetric modes (a_1') are listed.

In the Si_7^- photoelectron spectrum at 416 nm (Fig. 8), band X shows a resolved vibrational progression with a peak spacing of 385 ± 20 cm^{-1}. Comparison to Table V shows that this frequency lies between the calculated values for the two totally symmetric modes of the $^1A_1$' state. However, the experimental value is closer to the calculated ν_2 frequency (352 cm^{-1}), and the calculated normal coordinate displacement is considerably larger for the ν_2 mode. We therefore assign the observed progression to this mode. Fig. 14 shows a simulated spectrum in which only the ν_2 frequency is changed from the *ab initio* values. Note that although the ν_2 progression dominates, the ν_1 mode is also active, resulting in only partial resolution of the ν_2 progression in the simulation and, presumably, the experiment. The vibrational origin at eKE=1.12 eV yields an electron

affinity of 1.85 ± 0.02 eV for Si_7. While acceptable simulations at different origins can be achieved by changing the normal mode displacements, best results are obtained with the values reported here. Raghavachari and Rohlfing reported an electron affinity of 1.7 eV

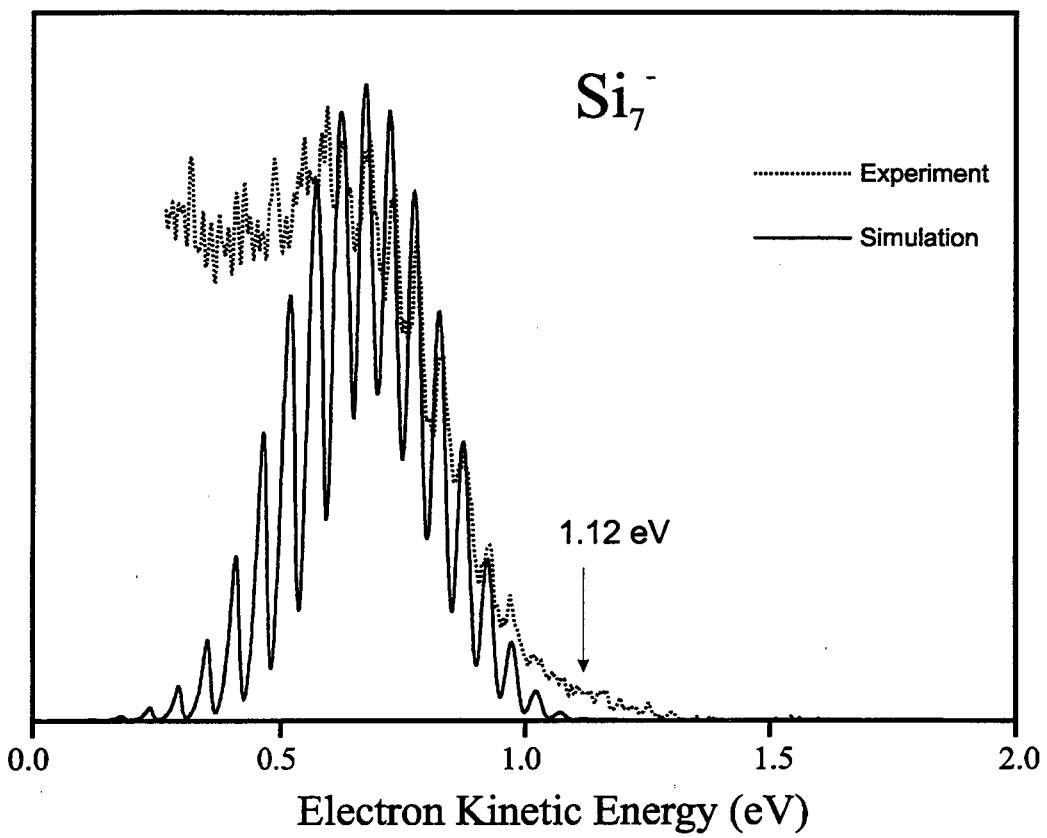

FIG. 14. Franck-Condon simulation of the Si_7^- spectrum. Parameters given in Table VI.

at the MP2/6-31G* level.[16]

Recently, Eberhardt reported the vibrationally resolved photoelectron spectrum of annealed Si_7^- at a photon energy of 2.897 eV photon energy.[5] They measured a frequency of 380 ± 20 cm^{-1} for Si_7. This is very close to our value, but both gas phase values are

slightly less than the vibrational frequency of 435 cm^{-1} seen in the matrix Raman experiment.[6] This discrepancy may be due to matrix effects.

The photoelectron spectrum at 355 nm (Fig. 9) shows band X in its entirety and the onset of a second band labeled band A at low eKE. The origin of band A was estimated as the intercept resulting from an extrapolation of the linear portion of this band in the photoelectron spectrum to the energy axis. The best estimate of 0.50 eV electron energy corresponds to a term energy of 1.14 ± 0.05 eV. Raghavachari and Rohlfing found a C_{3v} tricapped tetrahedron isomer of a $^1A_1$ state which lies 0.95 eV above the $^1A_1$' ground state the MP4/6-31G* level.[15] We therefore assign band A to this excited state.

The anisotropy parameter β for band X varies significantly with electron energy, as shown in the top panel of Fig. 9. This could signify that transitions to two neutral electronic states with different polarization dependence contribute to band X. However, this would require an open-shell excited state of Si_7 with nearly the same energy as the $^1A_1$' state. The low electron affinity of Si_7 suggests that the $^1A_1$' state is particularly stable, so this is an unlikely scenario. Moreover, no variation of β occurs in the photoelectron spectrum at 416 nm in Fig. 8. An alternative explanation is that there is an excited electronic state of Si_7^- near 355 nm, and that autodetachment from this state contributes to the photoelectron spectrum along with direct detachment.

Table VI. Term energies, frequencies, and normal coordinate displacements used in the simulations.

			Frequencies (cm^{-1}) / ΔQ (Å•$amu^{1/2}$)			
	States	T_o (eV) [a]	ν_1	ΔQ_1	ν_2	ΔQ_2
Si_3	$^3A_1$ (C_{2v})	0.90	500	0.13	250	0.19
EA = 2.29 ± 0.02 eV	$^3B_1$ (C_{2v})	1.12	480, x_1=0.5 [b]	0.46	225	0.40
	$^1B_1$ (C_{2v})	1.43	475, x_1=1.0 [b]	0.40	235	0.50
	$^1A_1$ (C_{2v})	1.76	480	0.23	340	0.20
Si_4	$^3B_{3u}$ (D_{2h})	0.85	450	0.18	308	1.14
EA = 2.13 ± 0.01 eV	$^1B_{3u}$ (D_{2h})	1.34	490	0.05	290	1.15
	$^3B_{1g}$ (D_{2h})	1.71	517	0.15	355	0.727
	$^3B_{1u}$ (D_{2h})	1.93	448	0.65	346	0.22
Si_5	$^1A_1$' (D_{3h})	0.0	501	0.21	233	2.12
EA = 2.59 ± 0.02 eV	$^3B_1$ (C_{2v})	1.16 ± 0.05				
Si_7	$^1A_1$' (D_{5h})	0.0	463	0.67	385	1.15
EA = 1.85 ± 0.02 eV	$^1A_1$ (C_{3v})	1.14 ± 0.05				

[a] The error bars are ± 0.02 eV, except noticed.

[b] x_1 is the anharmonicity used in the simulations.

V. Conclusions

The anion photoelectron spectra presented here provide new information on the ground and low-lying electronic states of silicon clusters. Several new assignments of the excited state bands are based on the vibrational structure that is resolved in many of these spectra, the angular distribution of the photoelectrons, and comparison with *ab initio* calculations. For Si_3 and Si_4, all excited states accessible via photodetachment with $T_o <$ 2.5 eV have been assigned. Vibrational frequencies are obtained for the ground states of Si_5 and Si_7. In both cases, an extended progression is observed for a single, totally symmetric vibrational mode, indicating a substantial geometry change but no change in symmetry upon photodetachment. This progression corresponds to excitation in the ν_2 symmetric distortion mode of the neutral cluster, resulting from a considerable reduction in the spacing between the apical Si atoms upon photodetachment. In the Si_6^- spectra, vibrational structure was resolved for a low-lying excited state, the identity of which still needs to be determined.

Acknowledgments

This work is supported by the National Science Foundation under Grant No. DMR-9521805. Support from the National Energy Research Scientific Computing Center (NERSC) is gratefully acknowledged. We thank C. M. Rohlfing for communicating results from calculations and for helpful discussions and comments regarding the manuscript.

References

[1] O. Cheshnovsky, S. H. Yang, C. L. Pettiette, M. J. Craycraft, Y. Liu, and R. E. Smalley, Chem. Phys. Lett. **138,** 119 (1987).

[2] T. N. Kitsopoulos, C. J. Chick, A. Weaver, and D. M. Neumark, J. Chem. Phys. **93,** 6108 (1990).

[3] C. C. Arnold and D. M. Neumark, J. Chem. Phys. **99,** 3353 (1993).

[4] C. C. Arnold and D. M. Neumark, J. Chem. Phys. **100,** 1797 (1994).

[5] G. S. Ickingkonert, H. Handschuh, P. S. Bechthold, G. Gantefor, B. Kessler, and W. Eberhardt, Surface Review and Letters **3,** 483 (1996).

[6] E. C. Honea, A. Ogura, C. A. Murray, K. Raghavachari, W. O. Sprenger, M. F. Jarrold, and W. L. Brown, Nature **366,** 42 (1993).

[7] S. Li, R. J. Vanzee, W. Weltner, and K. Raghavachari, Chem. Phys. Lett. **243,** 275 (1995).

[8] R. S. Grev and H. F. Schaefer, Chem. Phys. Lett. **119,** 111 (1985).

[9] K. Raghavachari, J. Chem. Phys. **84,** 5672 (1986).

[10] J. R. Sabin, J. Oddershede, G. H. F. Diercksen, and N. E. Gruner, J. Chem. Phys. **84,** 354 (1986).

[11] K. Balasubramanian, Chem. Phys. Lett. **125,** 400 (1986).

[12] K. Balasubramanian, Chem. Phys. Lett. **135,** 283 (1987).

[13] G. Pacchioni and J. Koutecky, J. Chem. Phys. **84,** 3301 (1986).

[14] P. Ballone, W. Andreoni, R. Car, and M. Parrinello, Phys. Rev. Lett. **60,** 271 (1988).

[15] K. Raghavachari and C. McMichael Rohlfing, J. Chem. Phys. **89,** 2219 (1988).

[16] K. Raghavachari and C. M. Rohlfing, J. Chem. Phys. **94,** 3670 (1991).

[17] C. M. Rohlfing and K. Raghavachari, J. Chem. Phys. **96,** 2114 (1992).

[18] D. A. Dixon and J. L. Gole, Chem. Phys. Lett. **188,** 560 (1992).

[19] R. Fournier, S. B. Sinnott, and A. E. Depristo, J. Chem. Phys. **97,** 4149 (1992).

[20] S. D. Li, R. L. Johnston, and J. N. Murrell, Journal Of the Chemical Society-Faraday Transactions **88,** 1229 (1992).

[21] L. Adamowicz, Chem. Phys. Lett. **188,** 131 (1992).

[22] A. Rubio, J. A. Alonso, X. Blase, L. C. Balbas, and S. G. Louie, Phys. Rev. Lett. **77,** 247 (1996).

[23] R. B. Metz, A. Weaver, S. E. Bradforth, T. N. Kitsopoulos, and D. M. Neumark, J. Phys. Chem. **94,** 1377 (1990).

[24] C. Xu, G. R. Burton, T. R. Taylor, and D. M. Neumark, J. Chem. Phys. **107,** 3428 (1997).

[25] D. L. Osborn, D. J. Leahy, D. R. Cyr, and D. M. Neumark, J. Chem. Phys. **104,** 5026 (1996).

[26] J. Cooper and R. N. Zare, in *Lectures in Theoretical Physics*, Vol. XI-C, edited by S. Geltman, K. T. Mahanthappa, and W. E. Brittin (Gordon and Breach, New York, 1969), pp. 317-337.

[27] C. Rohlfing, private communication .

[28] GAUSSIAN 92, M. J. Frisch, G. W. Trucks, M. Head-Gordon, P. M. W. Gill, M. W. Wong, J. B. Foresman, B. G. Johnson, H. B. Schlegel, M. A. Robb, E. S. Replogle, R. Gomperts, J. L. Andres, K. Raghavachari, J. S. Binkley, C. Gonzalez, R. L. Martin, D. J. Fox, D. J. Defrees, J. Baker, J. J. P. Stewart, and J. A. Pople (Gaussian, Inc., Pittsburgh, 1992).

[29] G. H. F. Diercksen, N. E. Grüner, J. Oddershede, and J. R. Sabin, Chem. Phys. Lett. **117,** 29 (1985).

[30] K. Raghavachari, J. Chem. Phys. **83,** 3520 (1985).

[31] L. Adamowicz, Chem. Phys. Lett. **180,** 466 (1991).

5 Anion Photoelectron Spectroscopy of $In_xP_y^-$ (x,y = 1-4)

Abstract

Small indium phosphide clusters having 2 – 8 atoms are studied using anion photoelectron spectroscopy of $In_xP_y^-$ (x,y = 1-4). From these spectra, the electron affinities are determined. Both ground and low-lying excited states of the neutral clusters are observed. An electronic gap is shown in the even cluster anion spectra.

I. Introduction

The electronic and vibrational spectroscopy of semiconductor clusters has been an extremely active area in physical chemistry, as it offers an opportunity to learn how the properties of matter evolve from the molecular limit to the larger size regimes which are of interest in technological applications. A vital component in experimental studies of these species is the ability to combine size-selectivity with spectral resolution, so that one can follow the dependence of the electronic and vibrational structure of clusters as a function of size. Three techniques which have proved particularly valuable in probing the spectroscopy of semiconductor clusters are (i) photodissociation spectroscopy,[1-3] in which one records the depletion of a cluster of a given mass as a function of dissociation wavelength, (ii) negative ion photodetachment spectroscopy, in which the photoelectron

spectrum,[4-8] or (at higher resolution) the zero electron kinetic energy (ZEKE) spectrum[9-11] of a size-selected anion cluster probes the electronic and vibrational structure of the resulting neutral species, and (iii) Raman spectroscopy of size-selected clusters deposited onto a matrix.[12] In this Communication, we report the photoelectron spectra of a series of size-selected indium phosphide cluster anions.

While much of the experimental and theoretical work thus far on semiconductor clusters has focused on pure elemental clusters of silicon and germanium, mixed semiconductor clusters are also intriguing targets for study due to their greater complexity. Smalley and co-workers[5,13,14] have performed photoionization and photodetachment experiments on gallium arsenide clusters, finding that clusters with an odd number of atoms consistently have lower ionization potentials and higher electron affinities than even clusters. Several theoretical groups have carried out *ab initio* studies of gallium arsenide and other mixed clusters.[15-18] Mandich and co-workers[1,2] have performed a photodissociation spectroscopy study of indium phosphide clusters ranging in size from 5-14 atoms. The spectra showed the rising edge of an electronic absorption band which was typically quite close to the band gap of bulk crystalline indium phosphide, 1.34 eV at 300 K.[19] These striking results, which suggest that very small indium phosphide clusters exhibit properties reminiscent of the bulk material, motivate the work described in this Communication. We report the photoelectron spectra of indium phosphide cluster anions having 2-8 atoms ($In_xP_y^-$, x,y=1-4). We determine the electron affinities from the photoelectron spectra, and observe both ground and low-lying excited electronic states of the neutral clusters. While our results are generally

consistent with the photodissociation studies, they provide a more complete picture of the electronic spectroscopy of indium phosphide clusters and nicely illustrate the complementary nature of the two techniques.

II. Experiment

The apparatus used in the present work is a fixed-frequency negative ion photoelectron spectrometer that has been described in detail elsewhere.[20] Indium phosphide cluster anions are generated in a laser vaporization source by focusing the second harmonic (532 nm) of a YAG laser onto a rotating and translating indium phosphide rod. The resulting plasma is entrained in a pulse of helium carrier gas from a piezoelectric valve, and expanded through a clustering channel into the source vacuum chamber of the spectrometer. The anions generated in the plasma are extracted into a time-of-flight mass spectrometer and accelerated to an energy of about 1 keV. The ions separate according to mass and are detected by a microchannel plate detector. The resulting ion beam is crossed by a second pulsed YAG laser beam. By controlling the laser firing time, the cluster ion of interest is selectively detached. A small fraction (~0.4 %) of the ejected photoelectrons is collected with a 70 mm diameter microchannel plate detector 1 m from the interaction region, and the kinetic energy of these photoelectrons is determined via their time-of-flight. The instrumental resolution is 8-10 meV for an electron kinetic energy (eKE) of 0.65 eV and degrades as $(eKE)^{3/2}$.

III. Results

Figure 1 shows the mass spectrum of the indium phosphide cluster anions. An interesting feature in Fig. 1 is that four of the five most intense peaks correspond to

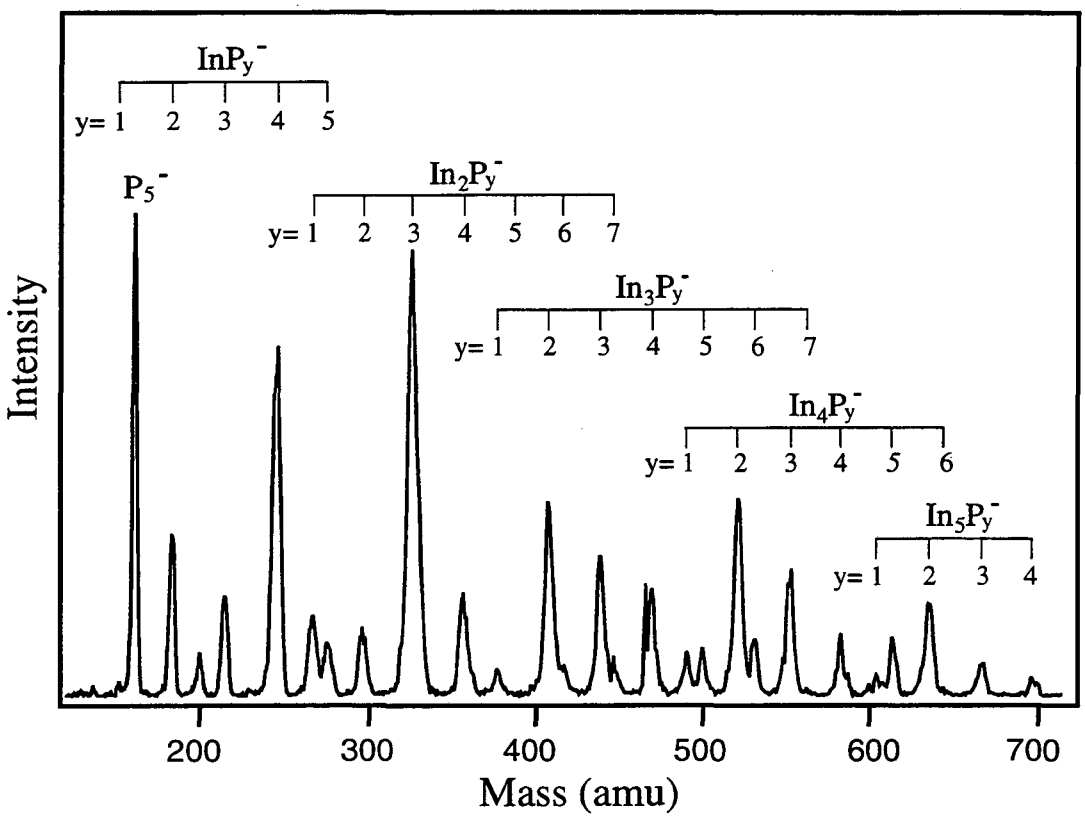

FIG. 1. Mass spectrum of indium phosphide anion clusters ranging in mass from 130 to 700 amu.

anions with five atoms, namely, P_5^-, InP_4^-, $In_2P_3^-$, and $In_3P_2^-$. This suggests that these anions are particularly stable.

Figure 2 shows the 16 photoelectron spectra of indium phosphide clusters ranging from InP^- to $In_4P_4^-$. The electron kinetic energy (eKE) is given by

$$eKE = h\nu - EA - E^{(o)} + E^{(-)}$$

where $h\nu$ is the photon energy (4.657 eV), EA is the electron affinity of the neutral cluster, and $E^{(o)}$ and $E^{(-)}$ are the internal (electronic + vibrational) energies of the neutral and anion, respectively. The spectra show resolved peaks, most of which represent transitions from the anion ground electronic state to various electronic states of the neutral. In the $In_2P_2^-$ spectrum, for example, the peaks labeled as X, A and B correspond to transitions to the In_2P_2 ground state and first two excited electronic states, respectively. The onset of band X yields the adiabatic electron affinity.

Some of the smaller features in Fig. 2 require additional explanation. There is a pair of small peaks (labeled with *) at the same electron kinetic energy of 2.865 eV and 2.985 eV in the photoelectron spectra of the larger $In_xP_y^-$ anions. These are most likely due to a two-photon absorption process, in which the first photon dissociates these clusters into the same daughter anion which is subsequently photodetached by the second photon. The electron binding energy of this daughter anion is 1.69 eV. It therefore cannot be In^- or P^- (EA(In)=0.30 eV, EA(P)=0.7465 eV[21]), and a comparison with the other spectra in Fig. 2 shows that it is not InP^- or In_2P^-. Based on the smallest clusters which show this feature, the remaining possibility is In_2^-, for which no photoelectron spectrum exists. However, the splitting of 120 meV between the two peaks is in good agreement with the calculated energy separation of 129 meV between the $^3\Pi_u$ ground electronic state and the $^3\Sigma_g^-$ first excited state of In_2,[22] so assigning the daughter anion to In_2^- appears reasonable.

The other anomalous feature is the broad peak around eKE = 3.8 eV in the InP_2^- spectrum. The intensity of this peak depended upon the source conditions and it was not

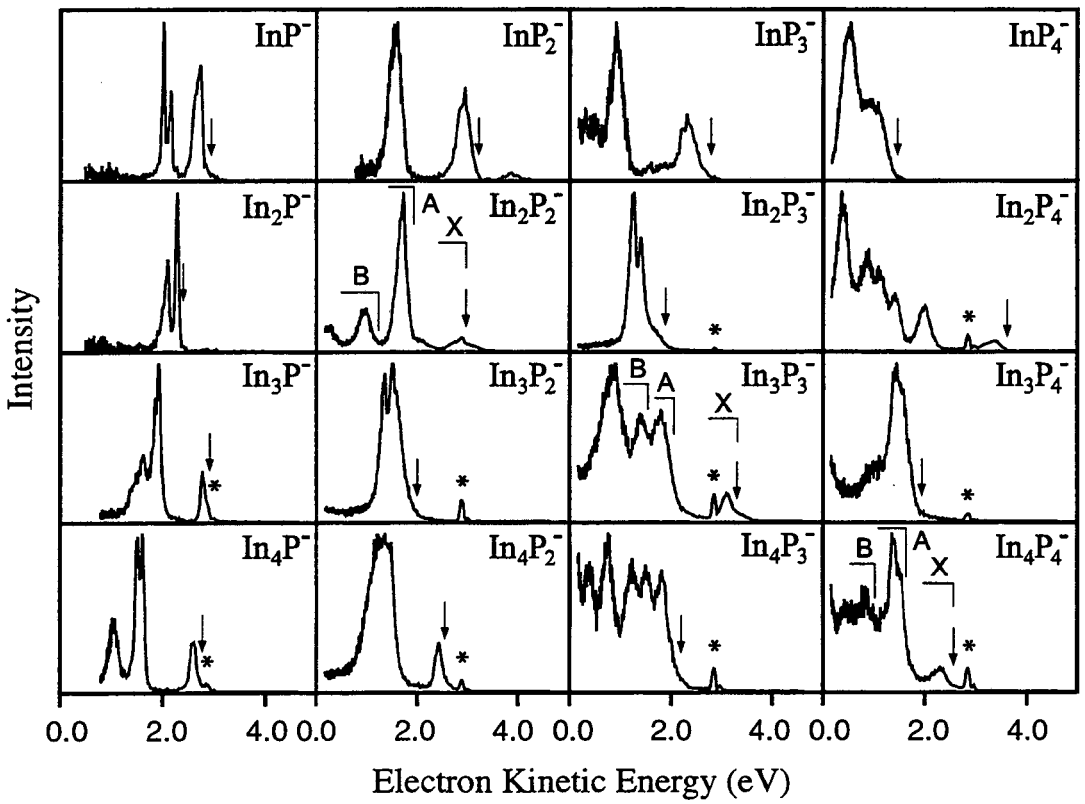

FIG. 2. Photoelectron spectra of 16 $In_xP_y^-$ (x, y = 1-4) clusters at 4.657 eV photodetachment energy. Arrows indicate electron kinetic energies corresponding to adiabatic electron affinities, and the asterisks indicate the two-photon peaks generated by In_2^-.

observed when the expansion carrier gas was changed from helium to argon; we therefore assign this band to the transition from a low-lying electronic state of the InP_2^- anion. Peaks similar in appearance to this in other spectra (such as the highest electron kinetic energy peak in the $In_2P_4^-$ spectrum) were insensitive to source conditions and are therefore assigned to transitions between the anion and neutral ground states.

Table I. Adiabatic electron affinities of indium phosphide clusters In_xP_y (x,y=1-4) determined in the present work. The values are estimated to be accurate to ±0.05 eV.

Cluster	Electron affinity (eV)	Cluster	Electron affinity (eV)	Cluster	Electron affinity (eV)	Cluster	Electron affinity (eV)
InP	1.95	InP_2	1.61	InP_3	1.86	InP_4	3.22
In_2P	2.36	In_2P_2	1.68	In_2P_3	2.72	In_2P_4	1.08
In_3P	1.77	In_3P_2	2.07	In_3P_3	1.30	In_3P_4	2.72
In_4P	1.88	In_4P_2	2.00	In_3P_4	2.43	In_4P_4	2.07

The adiabatic electron affinities of the neutral clusters were determined as the energy difference between the photon energy and onset of the leading edge of the highest kinetic energy band in the photoelectron spectrum (with the exception of the cases just discussed). In some cases, notably $In_3P_3^-$, the exact onset is unclear because the band tails off slowly towards high electron kinetic energy; these tails are attributed to vibrationally hot anions. The best estimates for the true onsets are indicated by arrows in Fig. 2, and the corresponding electron affinities of the 16 indium phosphide clusters are listed in Table I. Table I shows that clusters having an even total number of atoms have smaller electron affinities than the adjacent odd clusters; the only exceptions are InP_2 and In_4P (see below). Table I also shows that, for the five atom clusters, the electron affinity increases with phosphorous content, reaching a maximum value of 3.8 eV for P_5 (not listed in Table I). The high electron affinities for In_2P_3, InP_4, and P_5 are consistent with the intense anion peaks in the mass spectrum.

· The second general trend is that, for all the even clusters, there is a noticeable gap between the bands corresponding to transitions to the ground and first excited states of the neutral. This gap is absent in all of the odd cluster spectra except for InP_2 and In_4P. Figure 3 shows these gaps for clusters with four, six, and eight atoms. The gaps range from 0.75-1.6 eV, and for clusters with the same number of atoms, the gap decreases as the number of indium atoms increases.

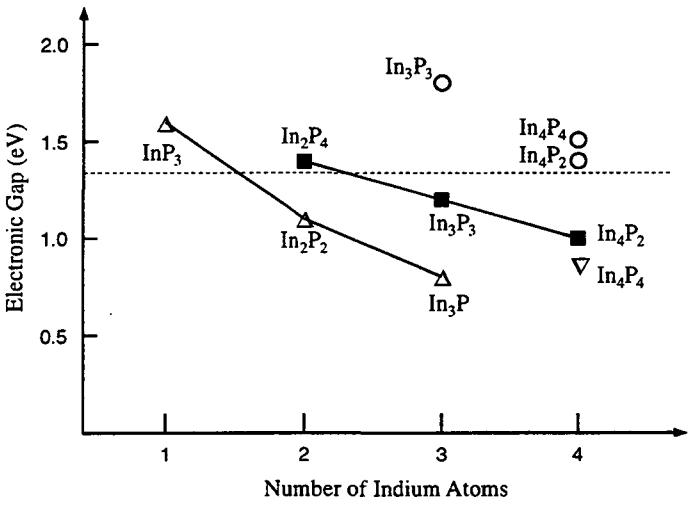

FIG. 3. Electronic gaps in the even-numbered indium phosphide clusters as a function of the number of indium atoms. Δ: 4-atom clusters, ■: 6-atom clusters, ∇: 8-atom clusters. Dotted line indicates the bulk band gap of indium phosphide (1.34 eV) (Ref. 19). Absorption onsets reported by Mandich (Ref. 1,2) are indicated by O.

Both general trends can be explained if the neutral, even clusters are closed-shell species with a substantial highest occupied molecular orbital-lowest unoccupied molecular orbital (HOMO-LUMO) gap while odd clusters are open-shell radicals. This is precisely what has been predicted in the *ab initio* calculations by Lou *et al.*[17,18] on gallium arsenide clusters. Thus, an even cluster anion is formed by adding an electron to the LUMO of the neutral cluster, whereas in an odd cluster anion, the added electron goes

into a half-filled valence orbital. Hence, the even clusters have a smaller electron affinity than the odd clusters (the opposite trend is seen in linear carbon clusters,[23] but the reasoning is still the same).

This simple picture also explains the electronic gap in the even cluster anion spectra. The ground state of the neutral is formed by removal of the LUMO electron, while the first excited state is formed by removal of an electron from the HOMO. Hence the gap in the photoelectron spectrum should, to first order, correspond to the HOMO-LUMO gap in the neutral cluster. In contrast, photodetachment of an odd cluster anion cannot access the LUMO of the neutral cluster by a one-electron transition, so the photoelectron spectrum should look quite different. We point out that Smalley's gallium arsenide cluster anion photoelectron spectra[5] did not show this even-odd alternation in the appearance of an electronic gap. However, due to the similarities in the masses of gallium and arsenic, each spectrum corresponds to a range of stoichiometries. Figure 3 shows that the gap in indium phosphide clusters is strongly dependent on cluster composition, so one might expect the pattern we observe to be averaged out in Smalley's spectra.

It is instructive to compare our results to the photodissociation experiments of Mandich[1,2] in more detail. The latter experiments probed the energy range between 1.0-1.8 eV for clusters ranging in size from 5-14 atoms; all the clusters studied showed the onset of an electronic absorption band in this energy range. In contrast, the anion photoelectron spectrum maps out the ground and excited states of the neutral cluster over a wider energy range, typically 2-3 eV depending on the electron affinity of the cluster.

For the even clusters studied by both methods (In_4P_2, In_3P_3, and In_4P_4), Fig. 3 shows that the gap in the photoelectron spectrum between the ground and first excited states is noticeably less than the onset observed in the photodissociation experiments. However, the gap between peaks X and B in the $In_3P_3^-$ and $In_4P_4^-$ spectra is 1.9 and 1.5 eV, respectively, which is much closer to the onsets in Mandich's experiments. A possible explanation for this is that peaks A and B in our spectra correspond to transitions to triplet and singlet excited states, respectively, each with one unpaired electron in the HOMO and one in the LUMO. The triplet states would not be seen in the photodissociation experiments if the $\Delta S = 0$ selection rule applies. In the $In_4P_2^-$ spectrum, the large peak below 2.0 eV appears anomalously broad, suggesting that it is composed of two or more overlapping transitions terminating in the analogous triplet and singlet excited states.

A comparison of the odd cluster spectra obtained by the two methods is more problematic. The onsets in the photodissociation spectra presumably correspond to a transition between one of the valence orbitals to the LUMO, but the resulting upper state is not accessible from the anion by a one-electron transition. The peaks in the photoelectron spectrum correspond instead to removal of electrons from the various valence orbitals of the anion. Some of the excited neutral states generated by such a transition should be optically accessible from the neutral ground state but at a lower frequency than could be reached with the lasers used in the photodissociation work. It would be interesting to perform the two-color photodissociation experiments using a

lower frequency infrared laser as the first excitation pulse to see which, if any, of the low-lying states in the photoelectron spectra appear.

The results of the photodissociation experiments indicate that the HOMO-LUMO gap in these very small clusters is similar to the bulk band gap in indium phosphide. In bulk indium phosphide, the band gap transition corresponds to a transition between a $p\sigma$ bonding orbital with dominant P character and a non-bonding $s\sigma$ orbital largely localized on the In atoms.[24] The photodissociation experiments imply that similar transitions occur in very small indium phosphide clusters, even though a high percentage of the atoms are "surface" atoms, suggesting that In-P bonding is the dominant chemical interaction in these clusters. Our results are in qualitative agreement in that the even cluster anion photoelectron spectra reveal the existence of electronic states at energies close to those seen in the photodissociation spectra. However, the photoelectron spectra cover a considerably wider range of energies, and they demonstrate that the electronic structure in these clusters is more complex than implied by the photodissociation experiments.

Finally, we consider the InP_2 and In_4P clusters which, as mentioned above, deviate from the observed even-odd trends; their electron affinities are anomalously low and they exhibit a significant electronic gap. We have recently obtained a vibrationally-resolved zero electron kinetic energy spectrum of InP_2^- in which the observed frequencies suggest strong P-P bonding in InP_2 and InP_2^-.[25] This suggests that the InP_2 neutral and anion are acute C_{2v} structures with the In atom bound to a P_2 unit, an interpretation consistent with *ab initio* calculations on isovalent $GaAs_2$ and $GaAs_2^-$.[16] Given that P-P bonding may be stronger than In-P bonding for these species, one can understand how the

photoelectron spectrum might differ significantly from the other clusters. In In_4P, one might also expect that In-In interactions outweigh effects due to In-P bonding. Hence, both exceptions can be rationalized in that In-P bonding may not be the dominant chemical interaction in the anion and neutral clusters.

Acknowledgements

This research is supported by the National Science Foundation under Grant No. DMR-92001159. We thank Dr. M. Mandich for providing the first indium phosphide rod. C. X. thanks the Abraham and Lo Foundations for fellowships, and E. d. B. thanks the Miller Institute for Basic Research in Science for a postdoctoral fellowship.

Reference

[1] K. D. Kolenbrander and M. L. Mandich, J. Chem. Phys. **92,** 4759 (1990).

[2] K. D. Rinnen, K. D. Kolenbrander, A. M. Desantolo, and M. L. Mandich, J. Chem. Phys. **96,** 4088 (1992).

[3] M. L. Mandich and K.-D. Rinnen, Z. Physics D **26,** 147 (1993).

[4] O. Cheshnovsky, S. H. Yang, C. L. Pettiette, M. J. Craycraft, Y. Liu, and R. E. Smalley, Chem. Phys. Lett. **138,** 119 (1987).

[5] C. Jin, K. J. Taylor, J. Conceicao, and R. E. Smalley, Chem. Phys. Lett. **175,** 17 (1990).

[6] T. N. Kitsopoulos, C. J. Chick, A. Weaver, and D. M. Neumark, J. Chem. Phys. **93,** 6108 (1990).

[7] T. N. Kitsopoulos, C. J. Chick, Y. Zhao, and D. M. Neumark, J. Chem. Phys. **95,** 1441 (1991).

[8] C. C. Arnold, T. N. Kitsopoulos, and D. M. Neumark, J. Chem. Phys. **99,** 766 (1993).

[9] T. N. Kitsopoulos, C. J. Chick, Y. Zhao, and D. M. Neumark, J. Chem. Phys. **95,** 5479 (1991).

[10] C. C. Arnold and D. M. Neumark, J. Chem. Phys. **99,** 3353 (1993).

[11] C. C. Arnold and D. M. Neumark, J. Chem. Phys. **100,** 1797 (1994).

[12] E. C. Honea, A. Ogura, C. A. Murray, K. Raghavachari, W. O. Sprenger, M. F. Jarrold, and W. L. Brown, Nature **366,** 42 (1993).

[13] S. C. O'Brien, Y. Liu, Q. Zhang, J. R. Heath, F. K. Tittel, R. F. Curl, and R. E. Smalley, J. Chem. Phys. **84,** 4074 (1986).

[14] Y. Liu, Q. L. Zhang, F. K. Tittel, R. F. Curl, and R. E. Smalley, J. Chem. Phys. **85,** 7434 (1986).

[15] K. K. Das and K. Balasubramanian, J. Chem. Phys. **94,** 6620 (1991).

[16] U. Meier, S. D. Peyerimhoff, and F. Grein, Chem. Phys. **150,** 331 (1991).

[17] L. Lou, L. Wang, L. P. F. Chibante, R. T. Laaksonen, P. Nordlander, and R. E. Smalley, J. Chem. Phys. **94,** 8015 (1991).

[18] L. Lou, P. Nordlander, and R. E. Smalley, J. Chem. Phys. **97,** 1858 (1992).

[19] D. Kirillov and J. L. Merz, Journal of Applied Physics **54,** 4104 (1983).

[20] R. B. Metz, A. Weaver, S. E. Bradforth, T. N. Kitsopoulos, and D. M. Neumark, J. Phys. Chem. **94,** 1377 (1990).

[21] R. D. Mead, A. E. Stevens, and W. C. Lineberger, , Vol. III, edited by M. T. Bowers (Academic Press, London, 1984), pp. .

[22] K. Balasubramanian, Chem. Rev. **90,** 93 (1990).

[23] D. W. Arnold, S. E. Bradforth, T. N. Kitsopoulos, and D. M. Neumark, J. Chem. Phys. **95,** 8753 (1991).

[24] M. L. Cohen and J. R. Chelikowsky, in *Electronic Structure and Optical Properties of Semiconductors* (Springer-Verlag, Berlin, 1988), pp. 79-139.

[25] C. C. Arnold and D. M. Neumark, Canadian Journal Of Physics **72,** 1322 (1994).

6 Photoelectron Spectroscopy of Si_nH^- (n=2-4) Anions

Abstract

Vibrationally-resolved photoelectron spectra of Si_nH^- (n=2-4) have been measured at a photodetachment wavelength of 355 nm (3.493 eV). The electron affinities of Si_2H, Si_3H, and Si_4H are 2.31 ± 0.01 eV, 2.53 ± 0.01 eV, and 2.68 ± 0.01 eV, respectively. Vibrational frequencies for the neutral ground states and a low-lying state of Si_2H are also determined. Assignment of the electronic states and vibrational frequencies is facilitated by comparison with *ab initio* calculations. The calculations show that the H atom in Si_4H and Si_4H^- is bonded to a single Si-atom, in contrast to the bridged structures found for the smaller clusters. These calculations along with photoelectron energy and angular distributions yield a definitive assignment of the ground and nearly degenerate first excited states of Si_2H.

I. Introduction

Silicon hydrides serve as reaction intermediates in chemical vapor deposition of amorphous silicon from silanes.[1] Silicon hydride anions have been implicated in the formation of dust particles in the plasma etching and deposition of silicon.[2,3] A full understanding of the reaction mechanisms in these processes requires the characterization of the ground and low-lying electronic states of the neutral and negatively charged silicon hydrides. In addition, the nature of the silicon-hydrogen bonding in silicon hydrides in which there is more than one Si atom is of significant interest. High resolution spectra have been obtained for disilyne (Si_2H_2),[4] and numerous theoretical studies of this molecule have been carried out;[5,6] these indicate a "dibridged" structure in which each H atom is bound to two Si atoms.

In this paper we present experimental studies of silicon monohydrides (Si_nH) using negative ion photoelectron spectroscopy. Although there have been a small number of theoretical studies of these species, [7-9] they have proved resistant to experimental characterization due to their high reactivity. *Ab initio* calculations predict Si_2H and Si_3H to have hydrogen-bridged ground states for both neutral and anion[7-9]. This is quite different from the bonding of hydrogen to extended silicon surfaces in which single Si-H bonds are favored.[10-15] The calculations also predict that the silicon core structures differ only slightly from the bare silicon clusters in these small silicon monohydride systems, for example, Si_3H and Si_3H^- ground states are planar C_{2v} symmetry. However, the two studies[8,9] of Si_2H do not agree on the neutral ground state assignment.

The work presented here represents the first spectroscopic investigation of silicon monohydrides. We report anion photoelectron spectra of Si_2H^-, Si_3H^-, and Si_4H^- at a photodetachment wavelength of 355 nm (3.493 eV). We have obtained electron affinities and vibrational frequencies of the ground states for all three silicon monohydrides. Photoelectron angular distributions were used to distinguish transitions to the nearly degenerate ground and first excited states of Si_2H. *Ab initio* calculations were also performed on the three anion and neutral species to aid in assigning the electronic and vibrational structure in the photoelectron spectra.

II. Experiment

The experiments were carried out on a time-of-flight negative ion photoelectron spectrometer.[16,17] The anions or interest are generated by expanding a dilute mixture of SiH_4 (5% SiH_4, 95% He) through a pulsed piezoelectric valve/pulsed electrical discharge source.[18] In this source, the gas pulse from the beam valve passes through two stainless steel plates between which a high voltage (about 600 V) pulse is applied. The pulse then expands into a vacuum chamber. The resulting free jet is collimated by a 2 mm diameter skimmer located 1.5 cm downstream from the ion source and then enters a differentially pumped region. Here, the ions are extracted from the beam and enter a time-of-flight mass spectrometer with a linear reflectron stage; the overall mass resolution is ~2000. The accelerated ions separate in time and space according to their mass to charge ratios, and are selectively detached by a pulsed Nd:YAG laser.

The third harmonic (355 nm, 3.493 eV) from a pulsed Nd:YAG laser is used in these experiments. The photoelectron kinetic energy is measured by time-of-flight in a field-free flight tube 100 cm in length. The instrumental resolution is 8 - 10 meV for an electron kinetic energy (eKE) of 0.65 eV and degrades as $(eKE)^{3/2}$. The polarization angle θ between the laser polarization and the direction of electron collection can be varied using a half-wave plate. The variation of peak intensities with θ is used to separate the contributions of different electronic states to the photoelectron spectra.

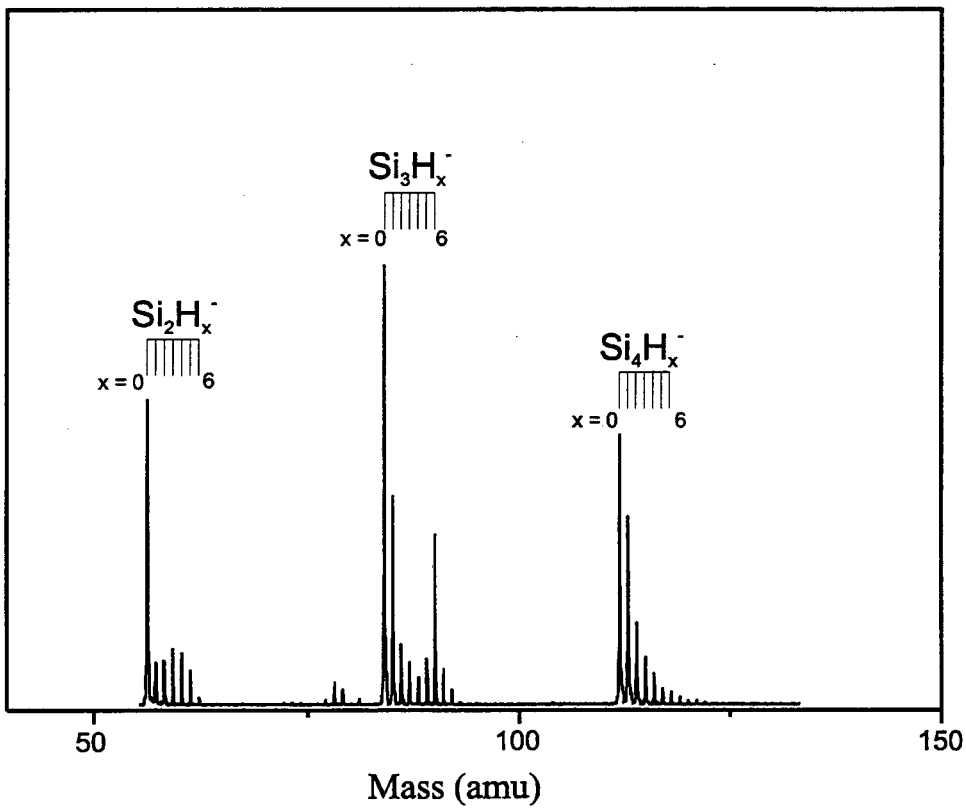

FIG. 1. Mass spectra of silicon hydride anions and corresponding bare silicon anion clusters generated from the discharge ion source.

III. Results

The anion mass spectrum obtained from the discharge source is shown in Fig. 1. Bare silicon clusters as well as partially hydrogenated species $Si_xH_y^-$ are observed. Since

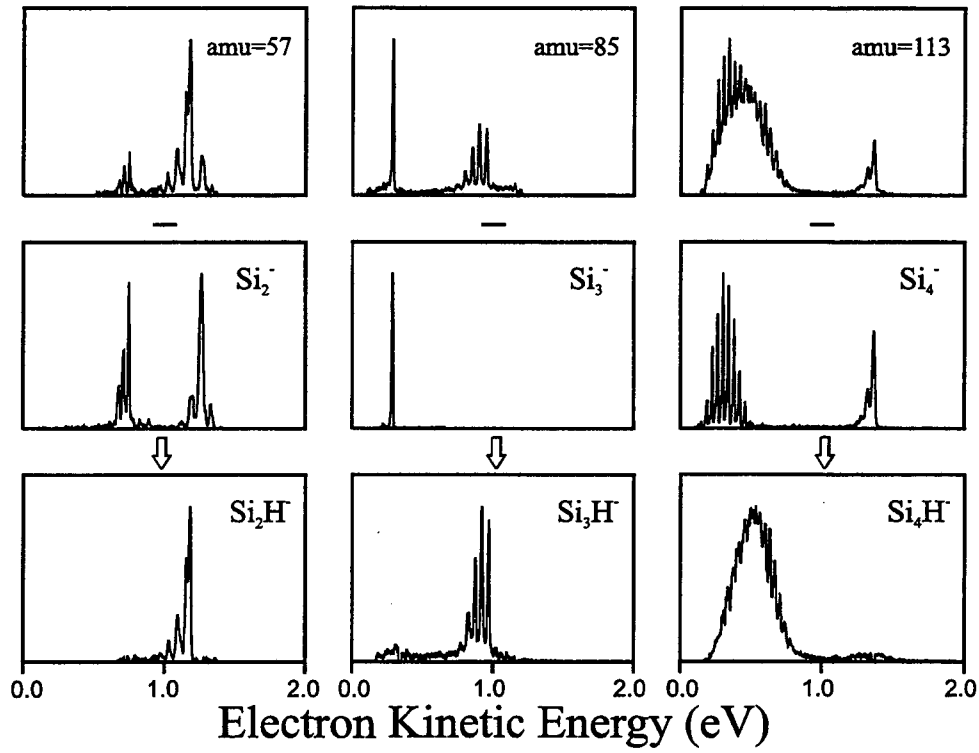

FIG. 2. Photoelectron spectra of Si_nH^- (n=2-4) taken at 355 nm. Laser polarization angle θ is 55° (magic angle) with respect to direction of electron collection. The three rows show how the Si_nH^- spectra are generated by subtracting the corresponding Si_n^- spectrum (see text for details).

silicon has three isotopes with atomic mass units (amu) of 28 (92%), 29 (5%), and 30 (3%), respectively, the silicon hydride mass peaks in the mass spectrum are contaminated by bare silicon clusters with the same number of Si atoms. The peak at 57 amu, for ex-

ample, is a mixture of $^{28}Si_2H^-$ and $^{28}Si^{29}Si^-$ anions. The photoelectron spectrum for Si_2H^- can be obtained by subtracting the appropriately scaled Si_2^- spectrum at 56 amu from the spectrum at 57 amu, and likewise for the larger clusters. Fig. 2 shows the raw spectra (top panel), the Si_n^- spectra (middle panel), and the Si_nH^- (n = 2 - 4) spectra after subtraction (bottom panel) at a photodetachment wavelength of 355 nm (3.493 eV). The spectra shown in Fig. 2 were taken at laser polarization angle θ of 54.7° (magic angle).

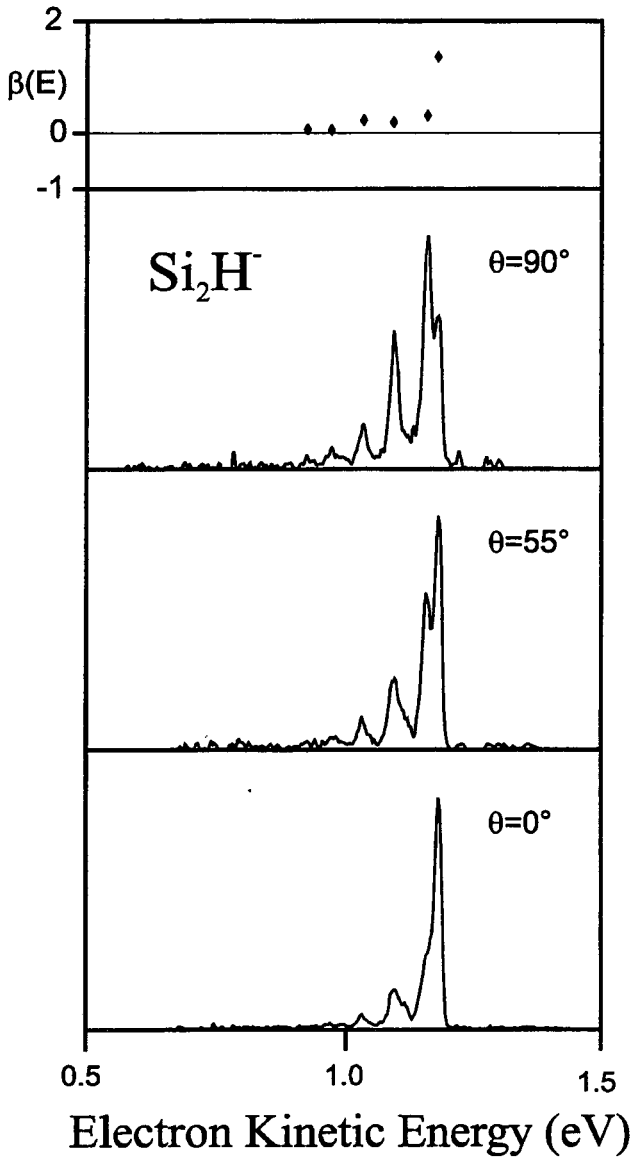

FIG. 3. Photoelectron spectra of Si_2H^- taken at 355 nm. Laser polarization angles are θ = 90°, 55°, and 0°. Top panel shows anisotropy parameters β for each peak in spectrum..

The Si_nH^- spectra consist of bands corresponding to transitions from the anion to various neutral electronic states. Vibrational structure is

resolved in many of these bands. For each peak, the electron kinetic energy (eKE) is given by:

$$eKE = h\nu - EA - T_o^{(o)} + T_o^{(-)} - E_v^{(o)} + E_v^{(-)}, \qquad (1)$$

where hν is the laser photon energy (3.493 eV), EA is the adiabatic electron affinity of the neutral species, $T_o^{(o)}$ and $T_o^{(-)}$ are the term values of the neutral and anion electronic states, and $E_v^{(o)}$ and $E_v^{(-)}$ are the neutral and anion vibrational energies, respectively, above the zero point energy. The photoelectron angular distribution is given by[19]

$$\frac{d\sigma}{d\Omega} = \frac{\sigma_{total}}{4\pi}[1 + \beta(E)P_2(\cos\theta)], \qquad (2)$$

where σ_{total} is the total photodetachment cross section and β(E) is the asymmetry parameter, varying from –1 to 2. One can determine β for each peak in the photoelectron

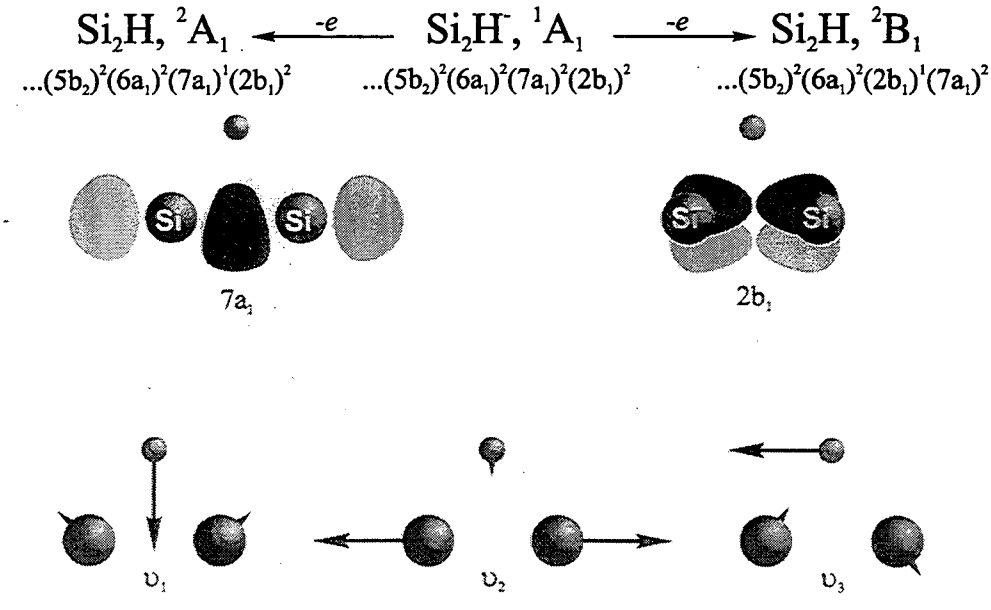

FIG. 4. High-lying electronic orbitals (top) of Si_2H/Si_2H^- and vibrational modes (bottom).

spectrum through its intensity variation with laser polarization angle.

Of the three anions studied here, Si_2H^- shows the most interesting photoelectron angular distributions, as shown in Fig. 3. These spectra show two overlapped bands X and A, with markedly different angular distributions. Band X has an origin at 1.18 ± 0.01 eV electron energy, and a rapid drop of intensity towards lower eKE. The vibrational origin of band X becomes the largest feature at θ = 0° with a β parameter of 1.4. Band A,

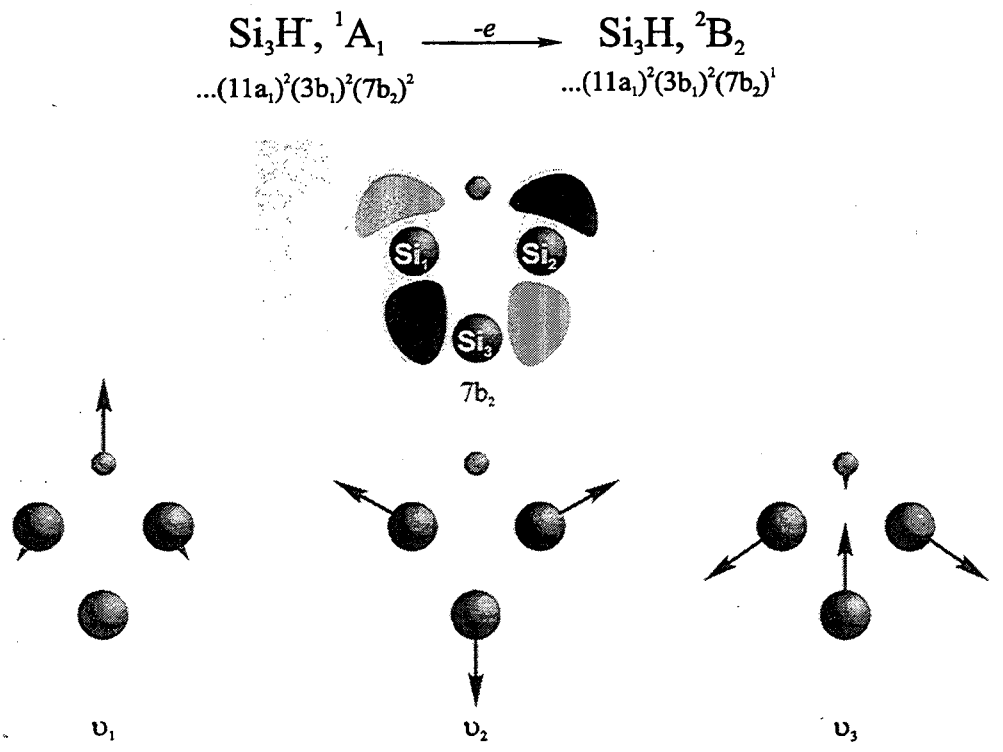

which is most apparent at θ=90°, consists of a more extended progression of five peaks, starting at 1.16 ± 0.01 eV. The peaks are spaced by 520 ± 20 cm^{-1} and have β parameters very close to 0. The β parameter of each peak is shown in the top panel of Fig. 3.

The Si_3H^- spectrum in Fig. 2 shows a single band labeled X with its origin at 0.97 ± 0.01 eV electron energy. A vibrational progression of five peaks spaced by 398 ± 20

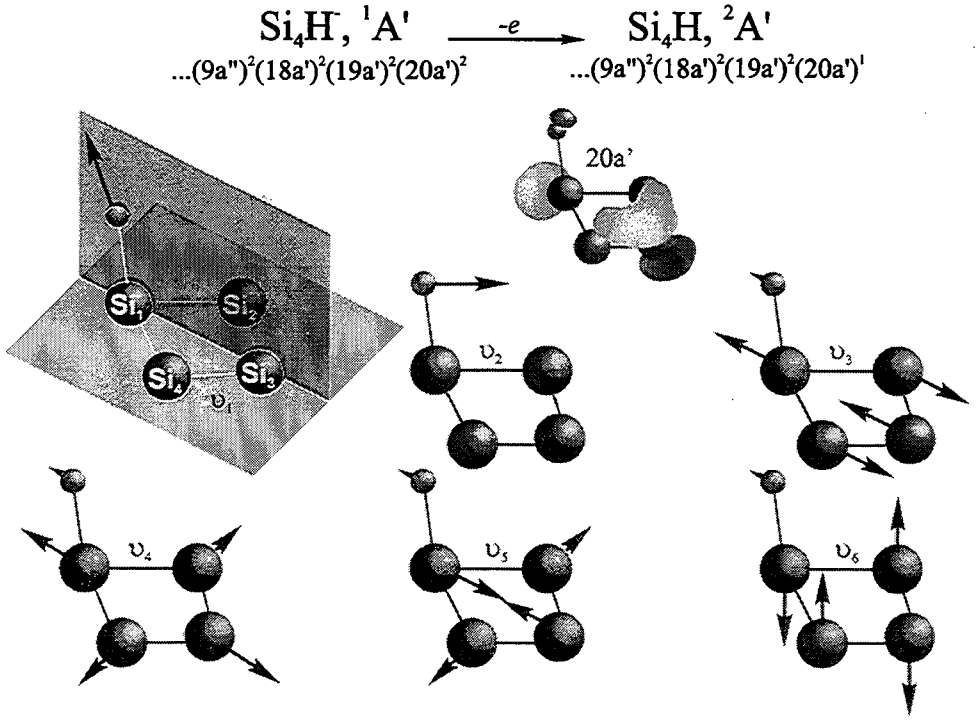

FIG. 6 HOMO of Si_4H/Si_4H^- and totally symmetric vibrational modes (bottom).

cm^{-1} is clearly resolved. Measurement of the photoelectron angular distributions shows that all peaks have approximately the same anisotropy, with an average β parameter of -0.4. The baseline noise at low eKE, (~0.3 eV) results from background subtraction of a strong Si_3^- transition.

The Si_4H^- spectrum in Fig. 2 shows a single band. Eight peaks with a spacing of 310 ± 20 cm^{-1} are apparent starting at eKE = 0.81 ± 0.01 eV; the structure below 0.5 eV is more irregular. The average anisotropy parameter for this band is β = -0.4.

In order to aid assignments of electronic and vibrational structure, we performed geometry optimization and frequency calculations on each anion and neutral at the QCISD(T)/6-31G* level of theory, using the Gaussian 94 package[20]. The optimized geometries are then adopted to obtain more reliable electronic state energies using a larger basis set of 6-311+G(3DF) at the same level of theory. For Si_4H and Si_4H^-, a ground state structure search was performed at the MP2/6-31G* level. The results are summarized in Table I - III. The geometries of the silicon monohydride clusters used in these Tables are shown in Fig. 4 - 6. These calculations also yield normal coordinate displacements for photodetachment to each neutral state. The displacements are calculated within the parallel mode approximation, in which the force constants for the neutral state are assumed for both the anion and neutral. One can then perform Franck-Condon simulations of the spectrum based on the *ab initio* calculations and compare with experiment. All simulations assume no vibrational excitation of the anions. The electron affinities and adiabatic excitation energies from the calculations aid in the assignments of electronic states. This type of comparison with theory proved very useful in our recent work on Si_n^- photoelectron spectroscopy.[21]

IV. Analysis and Discussion

A. General

In this section, the photoelectron spectra will be analyzed and assigned to various electronic states. The ground state structures of anions and neutrals are determined by *ab*

initio calculations. Franck-Condon simulations provide vibrational profiles, which are very helpful in assigning the spectra. For Si_2H^-, the assignments of overlapped bands were aided by photoelectron angular distributions. The discussion is concluded by comparisons between the bare silicon clusters and the silicon monohydrides.

B. Si_2H^-

Fig. 3 shows transitions to two nearly degenerate electronic states of Si_2H. Both bands are well resolved, but the origins are separated by only 0.02 eV. However, band A has a noticeably longer progression than band X, indicating a larger geometry change upon photodetachment to band A.

Only a few *ab initio* calculations have been performed on Si_2H^- and the low-lying states of Si_2H.[8,9,22] The anion ground state is predicted to have the symmetrically-bridged (C_{2v}) structure shown in Fig. 4. The valence electron configuration is $...(5b_2)^2(6a_1)^2(7a_1)^2(2b_1)^2$, resulting in a $^1A_1$ state. The $^2B_1$ and $^2A_1$ states of the neutral, both of which are also predicted to have this bridged C_{2v} structure, are formed by photodetachment from the $2b_1$ and $7a_1$ orbitals, respectively. As shown in Fig. 4, the $2b_1$ orbital is a π-bonding orbital between the two Si atoms, while the $7a_1$ orbital is a σ-orbital. Previous *ab initio* calculations (see Table I) predict the two neutral states to be nearly isoenergetic. Kalcher and Sax found the $^2A_1$ state to be 0.02 eV more stable than the $^2B_1$ state, using CASSCF geometry optimization followed by MRCI evaluation of the energies.[8] A later study by Ma *et al.* at the TZ2P(f,d) CCSD level of theory predicted that the $^2B_1$ state lies 0.07 eV lower in energy.[9] Our higher level calculations, also summarized in

Table I, predict the $^2A_1$ state to be the ground state, but only by 0.01 eV. With such a small splitting, it is fair to say that one cannot definitively assign the ground state based solely on the calculated energetics. Moreover, the experimental peak spacing of 520 ± 20 cm^{-1} in band A can be assigned to the ν_2 Si-Si stretching mode of either state.

However, the *ab initio* calculations also show that photodetachment to the $^2A_1$ state results in a smaller geometry change than to the $^2B_1$ state. Our calculations in Table I show that R_{Si-Si} decreases by 0.027 Å upon detachment to the $^2A_1$ and increases by 0.059 Å upon detachment to the $^2B_1$ state. As a result, the calculated normal coordinate displacement ΔQ_2 is substantially larger for the $^2B_1$ state, 0.22 amu·$Å^{1/2}$ *vs.* 0.10 amu·$Å^{1/2}$ for the $^2A_1$ state. Since a larger normal coordinate displacement produces a longer progression, we assign band X to the $^2A_1$ state and band A to the $^2B_1$ state, which is also consistent with our energy calculations. The resulting electron affinity of 2.31 ± 0.01 eV agrees well with the value of 2.25 eV from our calculations, and slightly above the MRCI(D) values of 2.14 eV by Kalcher and Sax[8]. The electron affinity of Si_2H is 0.11 eV higher than that for Si_2, 2.20 eV.[23]

Franck-Condon simulations of these two electronic transitions are superimposed on the experimental spectrum in Fig. 7. The simulation parameters are shown in Table IV. The excellent agreement between these parameters and the calculated values in Table I confirms our assignment. Our term energy of T_o ($^2B_1$) = 0.020 ± 0.005 eV is in good agreement with the values of 0.02 eV obtained by Kalcher and Sax[8] and 0.01 eV from our calculations.

Table I QCISD(T)/6-31G* optimization geometries, frequencies, and normal coordinate displacements for Si_2H. Term energies are derived from the QCISD(T)/6-311+G(3DF) energies using the QCISD(T)/6-31G* optimized geometries.

		T_e				Frequencies (cm^{-1}) / ΔQ (Å•$amu^{1/2}$)				
	States	(eV)	R_{Si-H} (Å)	R_{Si-Si} (Å)	∠SiHSi	υ_1	ΔQ_1	υ_2	ΔQ_2	υ_3
Si_2H^-	$^1A_1$ (C_{2v})	-2.25	1.690	2.182	80.4°	1479		558		1103
Reference [8]			1.706	2.215	81.0°					
Si_2H	$^2A_1$ (C_{2v})	0.0	1.693	2.155	79.1°	1592	0.01	554	0.10	1048
Reference [8]			1.708	2.194	79.4°					
Reference [9]			1.658	2.123	79.6°					
	$^2B_1$ (C_{2v})	0.01	1.703	2.241	82.3°	1491	0.01	525	0.22	1032
Reference [8]			1.723	2.273	82.6°					
Reference [9]			1.677	2.218	82.4°					

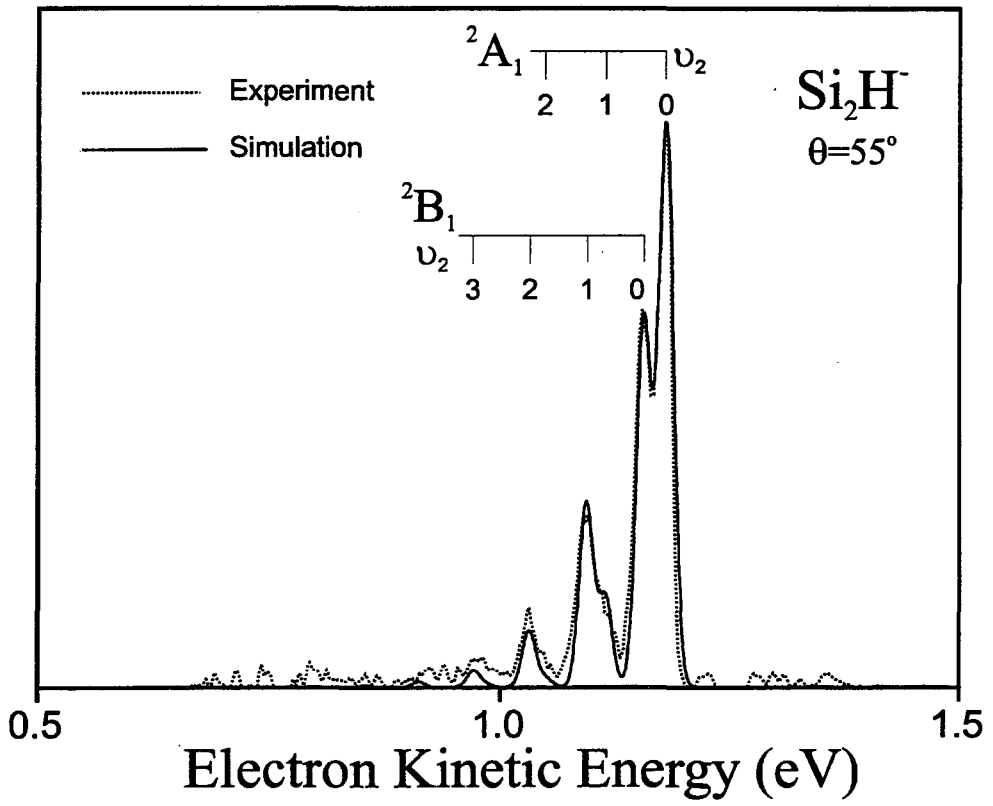

FIG. 7. Franck-Condon simulation of the Si_2H^- spectrum. Parameters given in Table IV.

C. Si_3H^-

The photoelectron spectrum of Si_3H^- in Fig.2 shows a single band with a progression of five evenly spaced peaks. The peak spacing is 398 ± 20cm^{-1}, and the apparent band origin occurs at eKE=0.97 eV. Measurement of the photoelectron angular distributions show that all five peaks have the same anisotropy parameter of approximately –0.4, indicating they are associated with a single electronic state.

Theoretical studies on Si_3H and its anion are extremely limited. Kalcher and Sax have performed *ab initio* calculations on Si_3H/Si_3H^- at the CCSD-(T) level of theory.[7] Several structures have been studied for both neutral and anion species. The ground state of the anion is predicted to have a planar cyclic hydrogen-bridge C_{2v} structure as shown in Fig. 5. The valence orbital configuration is $...(11a_1)^2(3b_1)^2(7b_2)^2$, yielding a $^1A_1$ electronic state. The $^2B_2$ ground state of neutral Si_3H, which also has C_{2v} symmetry, is accessed by removal of an electron from the $7b_2$ orbital in the anion. The $7b_2$ orbital and the three totally symmetric vibrational modes of Si_3H/Si_3H^- are shown in Fig. 5. Comparison of Table I and II shows that the addition of one silicon atom to Si_2H does not lengthen the Si-H bond, but simply enlarges the Si-H-Si angle.

The extended progression in the experimental spectrum indicates a large geometry change between the anion and neutral electronic states. The $^2B_2$ ground state is formed by photodetaching an electron from the $7b_2$ orbital, of the anion. Our QCISD(T)/6-31G* calculations show that detachment to the $^2B_2$ state results in a large normal coordinate displacement of $\Delta Q_3 = 0.42$ Å·cm$^{1/2}$. The observed peak spacing of 398 ± 20 cm^{-1} is in good agreement with the ν_3 frequency of 409 cm^{-1} from our calculation (Table II). We therefore assign this band to the $^2B_2$ state. Kalcher and Sax[7] predicted the lowest lying excited state with C_{2v} symmetry lies about 1 eV above the $^2B_2$ ground state, which would not show up in our photoelectron spectrum due insufficient photon energy. Although other low-lying states are predicted, they have very different geometries from the anion. Photodetachment to these states would result in very extended and broad bands in the

photoelectron spectrum. The spectrum thus represents a single electronic transition to the $^2B_2$ ground state, consistent with the photoelectron angular distribution.

The Franck-Condon simulation of the $^2B_2$ ground state, using our calculations as a starting point, is shown in Fig. 7. The simulation parameters are shown in Table IV. The

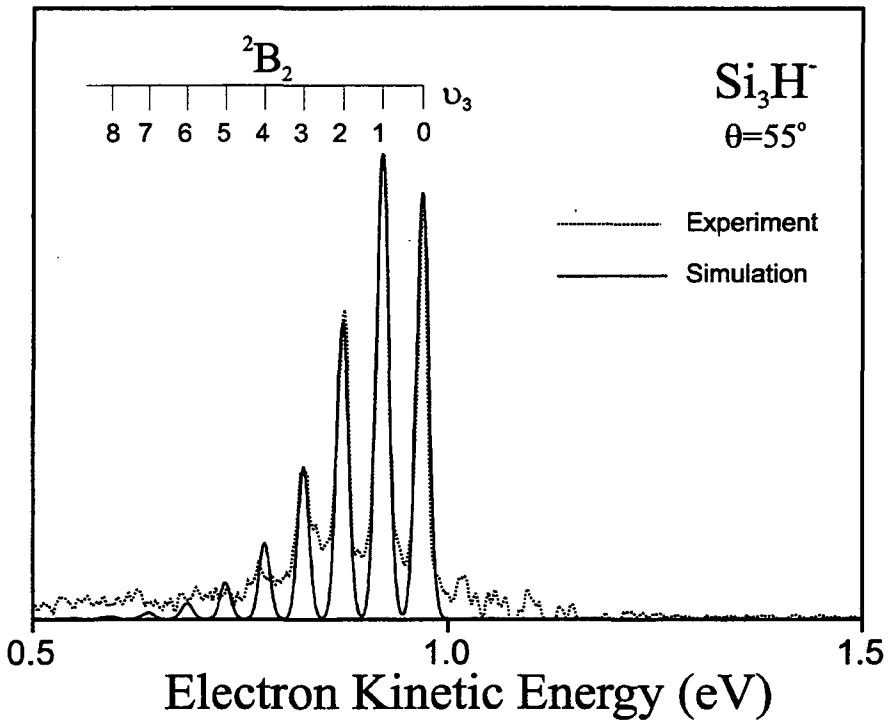

FIG. 8. Franck-Condon simulation of the Si_3H^- spectrum. Parameters given in Table IV.

normal coordinate displacement, ΔQ_3, used in the simulation is very close to the *ab initio* value in Table II. The vibrational origin of band X at eKE=0.96 eV yields EA (Si_3H) = 2.53 ± 0.01 eV for the electron affinity, which lies between the values of 2.65 eV from Kalcher and Sax and 2.48 eV from our calculations. The electron affinity of Si_3H is 0.24 eV greater than that of Si_3, 2.29 eV.[24]

Table II QCISD(T)/6-31G* optimization geometries, frequencies, and normal coordinate displacements for Si_3H/Si_3H^- and Si_3/Si_3^- [a]. Term energies are derived from the QCISD(T)/6-311+G(3DF) energies using the QCISD(T)/6-31G* optimized geometries.

	States	T_e (eV)	R(1-2) (Å)	R(1-3) (Å)	R(1-H) (Å)	∠(1-H-2)	Frequencies (cm^{-1}) / ΔQ (Å•$amu^{1/2}$)
Si_3H^-	$^1A_1$ (C_{2v})	-2.48	2.498	2.284	1.699	94.7°	1410(a_1), 521(a_1), 379(a_1), 952(b_2), 539(b_1), 411(b_2)
Si_3H	$^2B_2$ (C_{2v})	0.0	2.403	2.305	1.667	92.2°	1499(a_1) / 0.02, 498(a_1) / 0.02, 409(a_1) / 0.42, 1003(b_2), 463(b_1), 301(b_2)
Si_3^-	$^2A_1$ (C_{2v})	-2.21	2.437	2.261			533(a_1), 297(a_1), 370(b_2)
Si_3	$^3A_2'$ (D_{3h})	0.02	2.290	2.290			522(a_1), 285(e)

[a] Reference 27.

D. Si_4H^-

No *ab initio* calculations have been published for Si_4H or Si_4H^-. We therefore carried out such calculations on both species in order to better understand the photoelectron spectrum. An initial search for the global minimum energy structures of the anion and neutral was performed at the MP2/6-31G* level of theory. After the ground states of the anion and neutral were located, more accurate electronic state energies were calculated at the QCISD(T) level of theory using the larger 6-311+G(3DF) basis set using these geometries. The results are summarized in and Table III.

Both the anion and neutral have minimum energy structures of C_s symmetry shown in Fig. 6. The four Si atoms lie in a planar rhombus structure, with the H atom is singly-bonded to a Si atom (Si_1 in Fig. 6). The optimized geometry shows that the Si_4 unit is distorted, in that the Si-Si bonds involving Si_1 are slightly longer than the other two Si-Si bonds. The hydrogen-bridged structures found in Si_2H and Si_3H are found to be saddle points for Si_4H. The Si-H bond length is 1.535 Å in Si_4H^- and 1.500 Å in Si_4H, in both cases about 0.15 Å shorter than in the bridged structures for the smaller clusters. For comparison, the Si-H single bond lengths have been reported to be 1.43 Å on a Si(111) surface[11] and 1.6 ± 0.2 Å on a Si(100) surface.[10]

Table III MP2/6-31G* optimization geometries, frequencies, and normal coordinate displacements for Si_4H/Si_4H^- and Si_4/Si_4^-

[a] Term energies are derived from the QCISD(T)/6-311+G(3DF) energies using the MP2/6-31G* optimized geometries.

	States	T_e (eV)	R(1-2) (Å)	R(1-3) (Å)	R(2-3) (Å)	R(2-4) (Å)	R(1-H) (Å)	∠(H-1-3)	Frequencies (cm^{-1}) / ΔQ (Å•$amu^{1/2}$) [b]
Si_4H^-	$^1A'$ (C_s)	-2.53	2.391	4.020	2.274	2.366	1.535	96.6°	1919(a'), 603(a'), 520(a'), 504(a"), 446(a'), 410(a"), 335(a'), 237(a"), 143(a')
Si_4H	$^2A'$ (C_s)	0.0	2.313	3.839	2.263	2.492	1.500	125.1°	2100(a') / 0.16, 1291(a"), 727(a"), 537(a') / 0.10, 510(a') / 0.64, 448(a') / 0.15, 385(a"), 314(a') / 0.79, 142(a') / 0.18
Si_4^-	$^2B_{2g}$ (D_{2h})	-2.06	2.303	3.960	2.303	2.352			485(a_g), 361(a_g)
Si_4	$^3B_{3u}$ (D_{2h})	0.85	2.265	3.748	2.265	2.544			480(a_g), 330 (a_g) [c]

[a] Reference 27.

[b] MP2 frequencies are scaled by 0.95.

[c] QCISD/6-31G* frequencies from private communication with C. Rohlfing.

The anion $^1A'$ ground state has a valence electron configuration of $...(9a'')^2(18a')^2(19a')^2(20a')^2$. Photodetachment of an electron from the 20a' orbital yields the $^2A'$ ground state of the neutral species. The $^2A'$ state has six totally symmetric modes, all of which can be active upon photodetachment. The optimized geometries, vi-

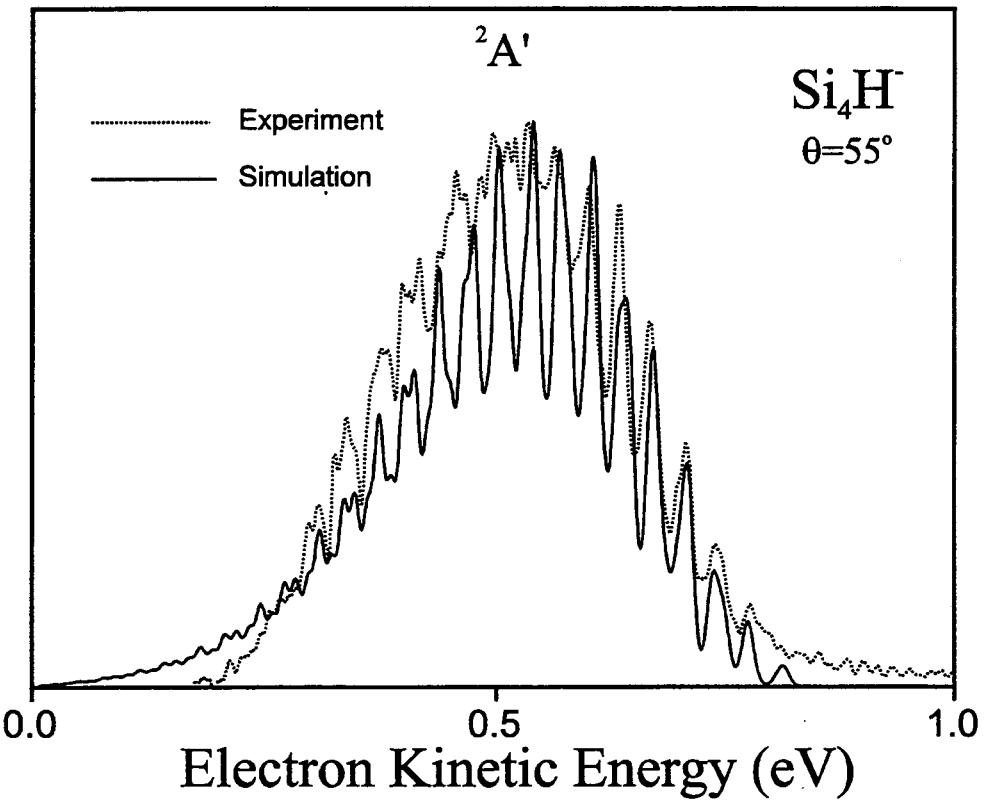

FIG. 9. Franck-Condon simulation of the Si_4H^- spectrum. Parameters given in Table IV.

brational frequencies and resulting normal coordinate displacements at the QCISD/6-31G* level are shown in Table III. The largest displacement is predicted for the ν_5 mode, which corresponds to a symmetric distortion of the Si_4 framework; this can be seen from the calculated geometries which show the neutral to be more "square" than the anion.

The Si_4H^- photoelectron spectrum at 355 nm (Fig. 2) shows a resolved vibrational progression with a peak spacing of 310 ± 20 cm^{-1}. Comparison to Table III shows that this frequency is close to the calculated ν_5 frequency, 334 cm^{-1}. Since this mode has the largest calculated displacement, we assign the observed progression to the ν_5 mode. As shown in Table III, other totally symmetric modes are also active, resulting a broad and partial resolved progression in the simulated spectrum (Fig. 9). The simulation parameters are shown in Table IV. Only the four modes with the largest displacements were used to perform the Franck-Condon simulation. Moderate adjustments of the ΔQ values from the calculations were made to achieve the best fit to the experimental vibrational profile. Note that ΔQ_1 used in the simulation is substantially less than the calculated value, suggesting a smaller H-Si-Si bond angle change than predicted by the calculation. Also, the experimental and simulated spectra deviate at electron kinetic energies below 0.5 eV, where the contribution from one of the bands from Si_4^- photodetachment is very strong (see Fig. 2). We attribute this deviation to imperfect subtraction of the Si_4^- contribution to the Si_4H^- spectrum.

Table IV Electron affinities, term energies, vibrational frequencies, and normal coordinate changes obtained from Franck-Condon simulation.

			Frequencies (cm^{-1}) / ΔQ (Å•$amu^{1/2}$)									
	States	T_o (eV)	υ_1	ΔQ_1	υ_2	ΔQ_2	υ_3	ΔQ_3	υ_5	ΔQ_5	υ_6	ΔQ_6
Si_2H	$^2A_1$ (C_{2v})	0.0	1592	0.01	540 x_2=3[a]	0.12						
EA = 2.31 ± 0.01 eV	$^2B_1$ (C_{2v})	0.02	1491	0.01	520 x_2=5[a]	0.23						
Si_3H	$^2B_2$ (C_{2v})	0.0	1500	0.02	500	0.02	398 x_3=2[a]	0.43				
EA = 2.53 ± 0.01 eV												
Si_4H [b]	$^2A'$ (C_s)	0.0	2100	0.05			510	0.64	314	0.79	142	0.18
EA = 2.68 ± 0.01 eV												

[a] x_2 and x_3 are the anharmonicities used in the simulations.

[b] The four modes with the largest normal coordinate displacements are used in the simulation.

To obtain the best fit, we chose the vibrational origin at eKE=0.81 eV, yielding an electron affinity of EA (Si_4H) = 2.68 ± 0.01 eV. Although alternative simulations assuming the vibrational origin shifted by a vibrational quantum in either direction satisfactorily matched the experimental progression, this required using normal coordinate displacements that differed more from the *ab initio* values. The adiabatic electron affinity from our assignment is 0.15 eV higher than the value of 2.53 eV predicted by our calculation. The electron affinity of Si_4H is 0.55 eV greater than that of Si_4, 2.13 eV.[21]

E. Comparison between Si_n and Si_nH

There are several points of comparison between the photoelectron spectra of Si_nH^- and Si_n^- (n=2-4).[21,23,25,26] The electron affinities monohydrides are all slightly larger than those of the corresponding bare clusters, with the difference increasing with n: 0.11 eV (n=2), 0.24 eV (n=3), and 0.55 eV (n=4). There are also noticeable similarities between the vibrational structure in the two sets of spectra. Vibrational frequencies of the most active modes are very close for all n. The single band in the Si_3H^- spectrum has a progression of five peaks spaced by 398 cm^{-1}. A of similar extent with a peak spacing of 360 cm^{-1} is seen in the Si_3^- spectrum for the transition to the $^3A_2$' state of Si_3.[25] The Si_4H^- spectrum looks remarkably like the band in the Si_4^- spectrum corresponding to the transition to the $^3B_{3u}$ first excited state, as seen in Fig. 2; the peak spacing is 310 cm^{-1} in both cases. However, there are generally more electronic bands in the Si_n^- spectra over the same energy range.

The similarities in the vibrational progressions suggest that addition of an H atom does not strongly perturb the geometry of the Si_n core, and that the orbitals from which detachment occurs are similar in the bare clusters and monohydrides. This is borne out by the *ab initio* calculations. The Si_3/Si_3^- and Si_4/Si_4^- geometries and vibrational frequencies from previous work[27] are listed on the bottom of Table II and III for comparison with the monohydrides. In Si_3^-, Si_3H^-, and Si_3H, the Si_3 core is a C_{2v} structure with similar Si-Si bond lengths. The Si_4 core in Si_4H^- and Si_4H is a slightly distorted planar rhombus; Si4 and Si_4^- have more symmetric D_{2h} planar rhombus structures. The calculations also indicate that the highest occupied molecular orbitals in the monohydride anions are localized on the Si_n core (see Fig. 4 - 6), and that these orbitals always resemble one of the high-lying occupied orbitals in the Si_n^- species.

There are, however, differences in the electronic structure of the monohydrides and bare clusters, the most important of which is that the Si_nH^- anions are closed-shell singlets, whereas the Si_n^- are open-shell doublets. This probably accounts for the higher electron affinities of the monohydrides. Si_2^- has two nearly degenerate electronic states separated by only 216.5 cm^{-1},[28] the $X\ ^2\Sigma_g^-$ and $A\ ^2\Pi_u$ states. The Si_2^- photoelectron spectrum[23] shows contributions from both states, but the Si_2H^- spectrum appears to arise from only a single anion electronic state, consistent with the closed-shell configuration of the anion. The molecular orbital configurations of Si_3^- and Si_4^- are $...(3b_1)^2(7b_2)^2(11a_1)^1$ and $(a_g)^2(b_{1u})^2(b_{2g})^1$, respectively. A comparison with the configuration for Si_3H^- (see Section IV) indicates that the half-filled $11a_1$ orbital in Si_3^- is stabilized by the addition of an H atom and is no longer the HOMO in Si_3H^-. Instead, the HOMO in Si_3H^- is the $7b_2$ orbital;

removal of this electron yields a photoelectron spectrum that resembles the band in the Si_3^- spectrum resulting from detachment from the corresponding orbital, the transition to the $^3A_2'$ state of Si_3. The situation for Si_4H^- is more complicated because of its lower symmetry compared to Si_4^-. The HOMO in Si_4H is the 20a' orbital (see Fig. 6), which shares characteristics of the b_{2g} and b_{1u} orbitals in Si_4^-. Nonetheless, the extended progression in the Si_4H^- spectrum is more similar to the band in the Si_4^- spectrum corresponding to the $^3B_{1u}$ excited state of Si_4 than to the ^1A_g ground state.

These considerations also explain the smaller number of electronic bands in the Si_nH^- spectra. In the Si_n^- spectra, photodetachment from the half-filled orbital yields a closed-shell singlet ground state, and one then can form pairs of triplet and singlet states via photodetachment from the high-lying fully occupied orbitals. In the Si_nH^- spectra, the transition to the closed shell singlet is absent, and photodetachment from the HOMO yields one doublet state rather than a triplet-singlet pair. We can therefore understand many of the similarities and differences between the spectra of the bare clusters and monohydrides.

Finally, we point out that hydrogen atoms form single Si-H bonds on bulk silicon surfaces. The work here shows that, bridged structures are more favored for small silicon hydrides such as Si_2H and Si_3H, but that Si_4H has a single Si-H bond. This suggests that Si_4H represent the transition between bridged and single silicon-hydrogen bonds. However, further work on larger clusters is needed to confirm this conjecture.

V. Conclusions

The anion photoelectron spectra of Si_nH^- (n=2-4) reported here represent the first experimental characterization of the silicon monohydrides. We obtain electron affinities and vibrational frequencies for the Si_nH ground states and for a low-lying excited state of Si_2H. *Ab initio* calculations carried out on the anion and neutral species aid in the assignment of electronic and vibrational spectral features. Our calculations show that the ground states of Si_2H/Si_2H^- and Si_3H/Si_3H^- have planar hydrogen-bridged structures, in agreement with previous theoretical work, but that Si_4H/Si_4H^- have non-bridged C_s structures in which the H atom is bonded to a single silicon atom. The overall good agreement between our experimental spectra and simulations based on the a*b initio* calculations supports the validity of these structures.

The photoelectron spectra of Si_3H^- and Si_4H^- are comprised of vibrationally-resolved transitions from the anion to the ground state of the neutral, but in the Si_2H^- spectrum there are strongly overlapped transitions to the ground and first excited state of Si_2H. The two electronic transitions can be distinguished by their photoelectron angular distributions, and comparison with the calculated normal coordinate displacements for the two transitions identifies the ground state as the $^2A_1$ state and the excited state as the $^2B_1$ state with a term value of 0.02 eV.

There are many points of similarity between the Si_nH^- and Si_n^- photoelectron spectra, indicating that HOMO in the silicon monohydride anions is primarily localized on the Si core; this inference is supported by the *ab initio* calculations. However, the

electron affinities of the monohydrides are systematically larger than those of the bare clusters, and the photoelectron spectra of the monohydrides are in general less complex with fewer electronic bands. These trends can be understood by simple molecular orbital considerations.

Acknowledgments

This work is supported by the National Science Foundation under Grant No. DMR-9521805. The theoretical calculations were performed at the National Energy Research Scientific Computing Center (NERSC).

References

[1] J. M. Jasinski, B. S. Meyerson, and B. A. Scott, Annu. Rev. Phys. Chem. **38,** 109 (1987).

[2] G. S. Selwyn, J. Singh, and R. S. Bennett, Journal of Vacuum Science and Technology A **7,** 2758 (1989).

[3] A. A. Howling, L. Sansonnes, J.-L. Dorier, and C. Hollenstein, Journal of Applied Physics **75,** 1340 (1994).

[4] M. Bogey, H. Bolvin, C. Demuynck, and J. L. Destombes, Phys. Rev. Lett. **66,** 413 (1991).

[5] B. T. Colegrove and H. F. Schaefer, J. Phys. Chem. **94,** 5593 (1990).

[6] M. M. Huhn, R. D. Amos, R. Kobayashi, and N. C. Handy, J. Chem. Phys. **98,** 7107 (1993).

[7] J. Kalcher and A. F. Sax, Chem. Phys. Lett. **259,** 165 (1996).

[8] J. Kalcher and A. F. Sax, Chem. Phys. Lett. **215,** 601 (1993).

[9] B. Y. Ma, N. L. Allinger, and H. F. Schaefer, J. Chem. Phys. **105,** 5731 (1996).

[10] W. R. Wampler, Phys. Rev. B **51,** 4998 (1995).

[11] W. R. Wampler, Phys. Rev. B **55,** 9693 (1997).

[12] X. Blase, X. J. Zhu, and S. G. Louie, Phys. Rev. B **49,** 4973 (1994).

[13] K. Hricovini, R. Gunther, P. Thiry, A. Talebibrahimi, G. Indlekofer, J. E. Bonnet, P. Dumas, Y. Petroff, X. Blase, X. J. Zhu, S. G. Louie, Y. J. Chabal, and P. A. Thiry, Phys. Rev. Lett. **70,** 1992 (1993).

[14] X. M. Zheng and P. V. Smith, Surf. Sci. **279,** 127 (1992).

[15] Z. Jing and J. L. Whitten, Physical Review B (Condensed Matter) **46,** 9544 (1992).

[16] R. B. Metz, A. Weaver, S. E. Bradforth, T. N. Kitsopoulos, and D. M. Neumark, J. Phys. Chem. **94,** 1377 (1990).

[17] C. Xu, G. R. Burton, T. R. Taylor, and D. M. Neumark, J. Chem. Phys. **107,** 3428 (1997).

[18] D. L. Osborn, D. J. Leahy, D. R. Cyr, and D. M. Neumark, J. Chem. Phys. **104,** 5026 (1996).

[19] J. Cooper and R. N. Zare, in *Lectures in Theoretical Physics*, Vol. XI-C, edited by S. Geltman, K. T. Mahanthappa, and W. E. Brittin (Gordon and Breach, New York, 1969), pp. 317-337.

[20] GAUSSIAN 94, M. J. Frisch, G. W. Trucks, H. B. Schlegal, P. M. W. Gill, B. G. Johnson, M. A. Robb, J. R. Cheeseman, T. Keith, G. A. Petersson, J. A. Montgomery, K. Raghavachari, M. A. Al-Laham, V. G. Zakrzewski, J. V. Ortiz, J. B. Foresman, J. Cioslowski, B. B. Stefanov, A. Nanayakkara, M. Challacombe, C. Y. Peng, P. Y. Ayala, W. Chen, M. W. Wong, J. L. Andres, E. S. Replogle, R. Gomperts, R. L. Martin, D. J. Fox, J. S. Binkley, D. J. Defrees, J. Baker, J. P. Stewart, M. Head-Gordon, C. Gonzalez, and J. A. Pople (Gaussian, Inc., Pittsburgh, 1995).

[21] C. Xu, T. R. Taylor, G. R. Burton, and D. M. Neumark, J. Chem. Phys. , submitted (1997).

[22] A. F. Sax and J. Kalcher, Theochem-Journal Of Molecular Structure **67,** 123 (1990).

[23] C. C. Arnold, T. N. Kitsopoulos, and D. M. Neumark, J. Chem. Phys. **99,** 766 (1993).

[24] C. C. Arnold and D. M. Neumark, J. Chem. Phys. **100,** 1797 (1994).

[25] T. N. Kitsopoulos, C. J. Chick, A. Weaver, and D. M. Neumark, J. Chem. Phys. **93,** 6108 (1990).

[26] T. N. Kitsopoulos, C. J. Chick, Y. Zhao, and D. M. Neumark, J. Chem. Phys. **95,** 1441 (1991).

[27] C. M. Rohlfing and K. Raghavachari, J. Chem. Phys. **96,** 2114 (1992).

[28] Z. Liu and P. B. Davies, J. Chem. Phys. **105,** 3443 (1996).

7 Photoelectron Spectroscopy of PO_2^-

I. Introduction

In this chapter, we report the photoelectron spectrum of PO_2^- anion. The electron affinity of PO_2 is determined from the spectrum. The anion geometry is obtained by Franck-Condon simulations of the photoelectron spectrum and is compared with *ab initio* calculations and previous experimental work.

The oxidation reactions of phosphorus and phosphine have been studied for centuries. However, the mechanisms for these reactions were poorly understood until recently, when PO_2 was strongly suggested to play a key role.[1,2] Unlike the isovalent NO_2 molecule, which has been investigated extensively, only a few spectroscopic studies have been performed on PO_2. The UV absorption spectrum of PO_2 was first observed by Verma and McCarthy[3] using a flash photolysis technique. More recently, Kawaguchi *et al.*[4] obtained an accurate ground state geometry and estimates of the lowest vibrational frequencies from far-infrared laser magnetic resonance (FIR LMR) and microwave spectroscopy. Laser induced fluorescence (LIF) and infrared absorption spectra observed by Hamilton and co-workers[1] also give similar ground state vibrational frequencies. Knight *et al.*[5] have investigated PO_2 in a Ne matrix using electron spin resonance. Several *ab initio* calculations[6-8] of geometries and frequencies show reasonable agreement with experiment.

Considerably less information is available on the PO_2^- anion. Spectroscopic studies of PO_2^- have been limited to the solid phase: Geometries and vibrational frequencies of PO_2^- in a potassium chloride crystal have been obtained from spectroscopic and optically detected magnetic resonance studies by Francis and co-workers.[9,10] *Ab initio* calculations carried out by Lohr[7] give ground state constants and vibrational frequencies. They also predict PO_2 has a very large electron affinity (3.6 ± 0.2 eV). The work presented here represents the first experimental characterization of PO_2^- in the gas phase.

II. Experimental

The apparatus used in the present work is a fixed-frequency negative ion photoelectron spectrometer that has been described in detail elsewhere.[11] PO_2^- is a byproduct of our previous study of indium phosphide clusters[12] and was generated in a pulsed beam valve/laser vaporization source. A second harmonic (532 nm) of a YAG laser is focused onto a rotating and translating indium phosphide rod. The resulting plasma is entrained in a supersonic pulse of helium gas. Anions in the beam are injected into a time-of-flight mass spectrometer. After being accelerated by 1 keV energy, ions separate according to mass and are detected by a microchannel plate detector. The resulting ion beam is crossed by a second pulsed laser, the fourth harmonic (266 nm, 4.657 eV) of a YAG laser beam. By controlling the laser firing time, PO_2^- is selectively photodetached. The kinetic energy of the photoelectrons is determined via their time-of-flight. The instrumental

resolution is 8-10 meV for an electron kinetic energy (eKE) of 0.65 eV and degrades as $(eKE)^{3/2}$.

III. Results

Figure 1(a) shows the 266 nm photoelectron spectrum of PO_2^- at laser polarization angle $\theta = 90°$ with respect to the detection angle. The electron kinetic energy (eKE) is given by

$$eKE = h\nu - EA\,(PO_2) - E^{(0)} + E^{(-)},$$

where $h\nu$ is the laser photon energy (4.657 eV) and EA (PO_2) is the electron affinity of PO_2. $E^{(0)}$ and $E^{(-)}$ are the internal energies of PO_2 and PO_2^- respectively. The spectrum corresponds to the transition between the ground electronic states of the anion and neutral, with an extended vibrational progression over the kinetic energy range from 0.7 eV to 1.4 eV. The spacing between adjacent peaks is about 400 cm^{-1} except for peaks G and H, which are separated by only 330 cm^{-1}. This indicates that there might be more than one active vibrational mode. Peak A is assigned to the 0-0 transition. It has a kinetic energy of 1.24 eV, yielding an electron affinity of 3.42 eV for PO_2. The smaller peak "*a*" occurs at 520 cm^{-1} higher kinetic energy than the origin. It has been assigned as a hot band transition, which indicates that the vibrational frequency of the main active mode is higher in the anion than in the neutral.

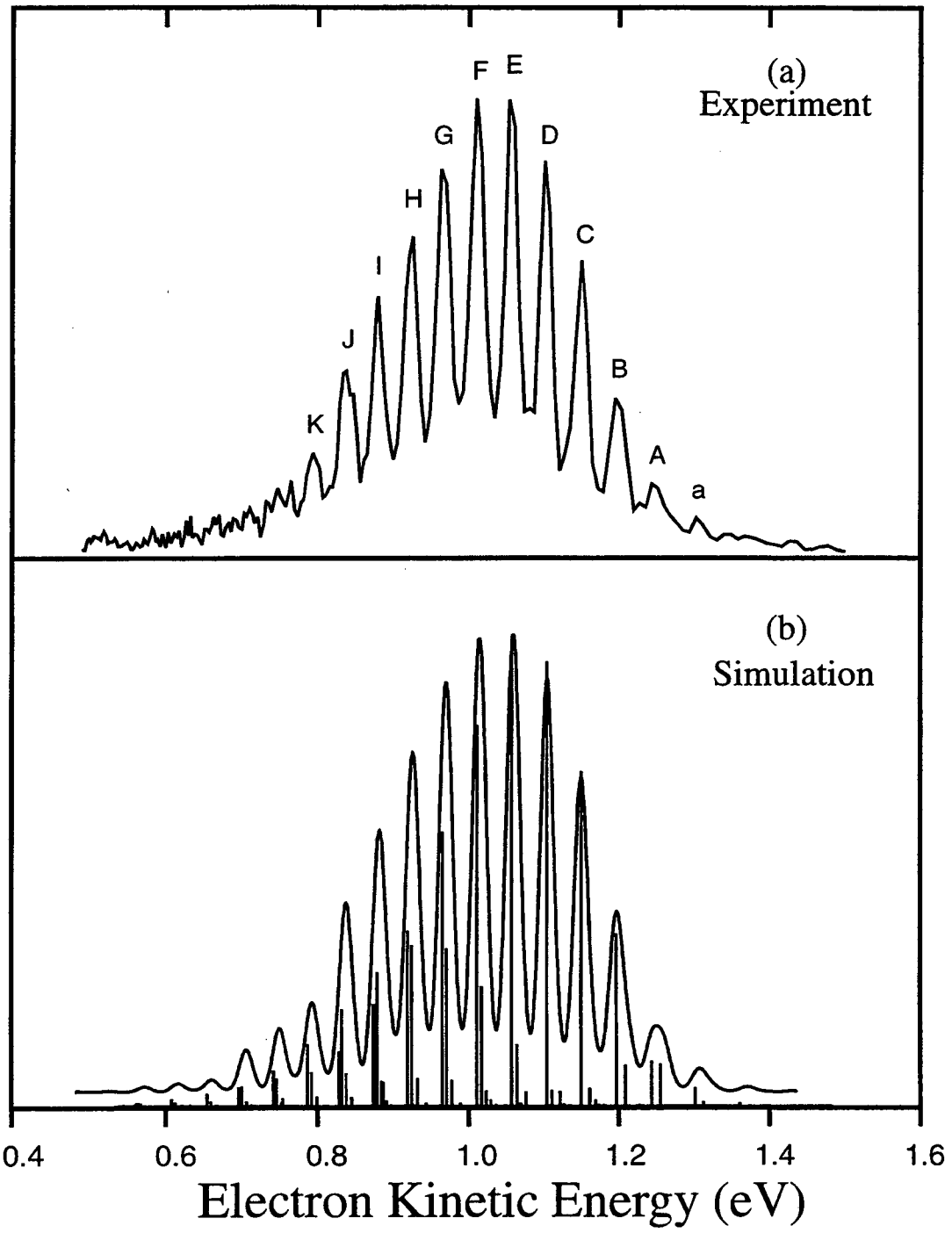

FIG. 1. (a) Photoelectron spectrum of PO_2^- measured using a photodetachment energy of 4.657 eV at laser polarization angle $\theta = 90°$, (b) Frank-Condon simulation with 2 active modes ν_1 and ν_2, convoluted with the experimental resolution (curve line) and the corresponding stick spectrum.

We have also performed *ab initio* calculations on PO_2 and PO_2^-. The calculations are aimed at determining the geometries, force constants, and vibrational frequencies of the ground electronic states. The results are summarized in Tables I & II. The geometries are optimized at the MP2 and CISD levels of theory, and harmonic vibrational frequencies are obtained at both levels of theory.

Table I. Molecular parameters for the ground $^2A_1$ state of PO_2^-.

Method / Basis Set	r_{PO} (Å)	θ_{OPO}	$\nu_1(cm^{-1})$	$\nu_2(cm^{-1})$	$\nu_3(cm^{-1})$
SCF / 6-31G* [a]	1.446	134.4	1048	396	1260
HF / 6-31G* [b]	1.440	135.8	1126.5	445.6	---
SCF [c] (valence electrons)	1.454	135.6	1210	460	1540
SCF+CORR [c] (valence electrons)	1.496	134.3	1060	380	1340
SCF [c] (all electrons)	1.439	135.4	1256	463	1564
HF / 6-31+G* [d]	1.446	134.86	1201	451	1451
MP2 / 6-31+G* [d]	1.496	136.83	1075	396	1585
MP2 / 6-311+G* [d]	1.480	136.65	1091	398	1570
CISD / 6-31G* [d]	1.471	134.7	1136	425	1421
FILMR, microwave[e]	1.4665	135°17'	1090	377	1278
LIF, IR absorption[f]	---	---	1117	387	1300/1345

[a] Reference 7.

[b] Reference 8.

[c] Reference 6.

[d] This work.

[e] Reference 4.

[f] Reference 1.

Tables I and II also show the geometry and vibrational frequencies of PO_2 ground state ($^2A_1$) and PO_2^- ground state ($^1A_1$) obtained from previous work. Compared with the

FIR LMR and microwave study of PO_2 by Kawaguchi *et al.*,[4] our MP2 level calculations give good agreement with frequencies and geometries. The CISD level calculation with a small basis set gives better results on geometry, but not on frequencies. There are no gas phase experiments for PO_2^- to compare with the calculations. Based on the calculations, PO_2^- has a longer bond length and smaller bond angle in the solid phase than in the gas phase.

Table II. Spectral constants of the ground $^1A_1$ state of PO_2^-.

Method / Basis Set	r_{PO} (Å)	θ_{OPO}	$\nu_1(cm^{-1})$	$\nu_2(cm^{-1})$	$\nu_3(cm^{-1})$
SCF / 6-31G* [a]	1.483	118.9	1051	465	1192
HF / 6-31G* [b]	1.483	119	1097	501	---
HF / 6-31+G* [c]	1.4867	118.7			
MP2 / 6-31+G* [c]	1.5381	119.483	999.03	436.0	1151.7
MP2 / 6-311+G* [c]	1.5194	119.177	1046.0	465.0	1207.8
CISD / 6-31G* [c]	1.5048	119.381	1135.1	497.5	1303.0
PO_2^- in KCl [d]	1.65	110	1097	501	1207

[a] Reference 7.

[b] Reference 8.

[c] This work.

[d] Reference 9,10.

IV. Analysis and Discussion

Ab initio calculations predict that the PO_2 and PO_2^- ground electronic states have C_{2v} symmetry. PO_2^- has a $^1A_1$ ground state with a $...(3b_2)^2(1a_2)^2(4a_1)^2$ valence electron configuration. Photodetachment from the $4a_1$ orbital will form the PO_2 $^2A_1$ ground state. *Ab initio* calculations also show that the $4a_1$ orbital is O-O bonding and P-O antibonding,

so photodetachment should result in a O-P-O bond angle increase and a P-O bond length decrease, in agreement with the calculated geometries.

The isovalent species NO_2 also has a $^2A_1$ ground electronic state with the same electron configuration as PO_2. However, the composition of the molecular orbitals differs in the two molecules. The $4a_1$ orbital in PO_2 is formed by mixing of $3s$(P) and $2p\sigma$(O) orbitals; whereas in NO_2, the $2p$(N) and $2p$(O) orbitals are close in energy, and the $4a_1$ orbital is primarily a linear combination of these orbitals.

PO_2 and PO_2^- each have three vibrational modes: the symmetric stretch (ν_1), bend (ν_2) and asymmetric stretch (ν_3). The ν_1 and ν_2 modes are totally symmetric and can therefore be active in the photoelectron spectrum. Calculations show ν_1 is around 1100 cm^{-1} for both PO_2 and PO_2^-; ν_2 is around 400 cm^{-1} for PO_2 and 500 cm^{-1} for PO_2^-. Recall the peak spacing of the spectrum is around 400 cm^{-1}, so the ν_2 mode appears to be the main activated mode. The assignment of peak "*a*" as a hot band transition is also supported. Since the ratio between ν_1 and ν_2 is about 3:1, overlap between the combination bands is expected, making it difficult to ascertain the contribution of the ν_1 mode by inspection alone.

To be more quantitative, we perform a Franck-Condon analysis to determine the normal coordinate displacements between PO_2 and PO_2^-. The normal coordinate displacements in the ν_1 and ν_2 modes are varied to obtain the best fit with the experimental spectrum. While the spectrum is reasonably well fit assuming only the ν_2 mode is active, the fit is improved with a small normal coordinate displacement in the ν_1 mode. The

computer code we used has been discussed elsewhere.[13] Figure 1(b) shows the simulated spectrum from Franck-Condon analysis. The fitting yields electron affinity EA = 3.42 ± 0.01 eV. Due to the $1_0^0 2_0^{n+3}$ / $1_0^1 2_0^n$ overlapping and sequence bands, the observed width of the peaks is around 25 meV. From the intensity of peak "*a*", assigned as the $1_0^0 2_1^0$ hot band transition, we estimate the anion temperature T = 300 K. Other fitting parameters are ν_1' = 1070 cm^{-1}, ν_2' = 380 cm^{-1}, x_2' = 0.8 ± 0.2 cm^{-1} for PO_2 and ν_1" = 1000 cm^{-1}, ν_2" = 470 cm^{-1} for PO_2^-. The normal coordinate displacements from the anion to the neutral are ΔQ_1 = -0.16, ΔQ_2 = 0.79, which correspond to a bond angle increase and a bond length decrease.

From the normal coordinate displacements, one can obtain geometry changes between the anion and neutral given the force constants. The force constants can be determined from either experimental vibrational frequencies or *ab initio* calculations.

We first construct the force constant matrix in internal coordinates, based on the vibrational frequencies and geometry obtained by Kawaguchi *et al.*[4] We use the *FG* matrix method,[14] assume that the bend-stretch force constant (*h*) equals half of the bend force constant (*H*). The *F* matrix in the units of mdyne/Å is calculated to be:

$$F = \begin{pmatrix} K & k & h \\ k & K & h \\ h & h & H \end{pmatrix} = \begin{pmatrix} 9.077 & 0.9105 & 0.4109 \\ 0.9105 & 9.077 & 0.4109 \\ 0.4109 & 0.4109 & 0.8217 \end{pmatrix}, \qquad (1)$$

where *K* and *k* are the stretch and the stretch-stretch force constants respectively. Since the neutral geometry is known from microwave experiments, we use the normal coordi-

nate displacements (ΔQ_1 = -0.16, ΔQ_2 = 0.79) to find the PO_2^- geometry: r_{PO} = 1.504 Å and θ_{OPO} = 120.0°. Changing the approximation condition for the bend-stretch force constant to $h = 0$ and $h = H$ gives similar results which are shown in Table III. We use averages as the reported values.

Table III. Anion geometry comparison from FG matrix method calculation.

Assumptions	r_{PO} (Å)	θ_{OPO}
$h = 0$	1.492	120.1
$h = H/2$	1.504	120.0
$h = H$	1.519	120.1
Average	1.50 ± 0.01	120.0 ± 0.1

As a comparison, we can use the force constant matrix from our MP2/6-311+G* level calculation on PO_2. This yields the following anion geometry: r_{PO} = 1.523 Å, θ_{OPO}= 120.4°. These values are in reasonable agreement with those from *FG* matrix method but are very different from solid-state geometry, indicating strong perturbations in the potassium chloride crystal. The *FG* results are slightly preferred as they are from force constants determined from experimental frequencies.

V. Conclusions

This work represents the first spectral observation of gas phase PO_2^-. PO_2^- is found out to be a very stable gas phase anion having a large electron affinity, 3.42 ± 0.01 eV. The anion geometry is determined to be: r_{PO} = 1.50 ± 0.01 Å, θ_{OPO} = 120.0 ± 0.1°.

MP2 level *ab initio* calculations on PO_2 and PO_2^- based on different basis sets have been performed as comparisons. They are consistent with previous experimental work done by other groups and the one reported in this Note.

Acknowledgement

This work is supported by the National Science Foundation under Grant No. DMR-92001159.

Reference

[1] P. A. Hamilton, J. Chem. Phys. **86,** 33 (1987).

[2] H. B. Qian, P. B. Davies, I. K. Ahmad, and P. A. Hamilton, Chem. Phys. Lett. **235,** 255 (1995).

[3] R. D. Verma and C. F. McCarthy, Canadian Journal of Physics **61,** 1149 (1983).

[4] K. Kawaguchi, S. Saito, E. Hirota, and N. Ohashi, J. Chem. Phys. **82,** 4893 (1985).

[5] L. B. Knight, G. C. Jones, G. M. King, R. M. Babb, and A. J. McKinley, J. Chem. Phys. **103,** 497 (1995).

[6] Y. Kabbadj and J. Levin, Phys. Scrip. **40,** 259 (1989).

[7] L. L. Lohr, J. Phys. Chem. **88,** 5569 (1984).

[8] S. A. Jarrett-Sprague, I. H. Hillier, and I. R. Gould, Chem. Phys. **140,** 27 (1990).

[9] S. J. Hunter, K. W. Hipps, and A. H. Francis, Chem. Phys. **39,** 209 (1979).

[10] S. J. Hunter, K. W. Hipps, and A. H. Francis, Chem. Phys. **40,** 367 (1979).

[11] R. B. Metz, A. Weaver, S. E. Bradforth, T. N. Kitsopoulos, and D. M. Neumark, J. Phys. Chem. **94,** 1377 (1990).

[12] C. Xu, E. Debeer, D. W. Arnold, C. C. Arnold, and D. M. Neumark, J. Chem. Phys. **101,** 5406 (1994).

[13] D. W. Arnold, Ph. D. Dissertation, Univeristy of California, Berkeley, 1994.

[14] E. B. Wilson Jr., J. C. Decius, and P. C. Cross, in *Molecular Vibrations* (Dover, New York, 1980), pp. 54-76.

Appendix A

Fortran codes for normal coordinate displacement analysis

```
      PROGRAM normal

C
C     Compile with f77 -O normal.f -o normal -llapack -lblas
C
C     FCF calculation program
C
C     10/20/96    C.X.
C
C     Based on f7.f, f8.f, f9.f program by SEB, DWA, and DLO.
C     This program reads the neutral and anion force constants in
C     cartesian coordinates from an ab initio calculation (Gaussian
92/94)
C     output, which is in atomic units.  Given the anion and neutral
C     cartesian coordinates, and masses and number of atoms, it
C     calculates the normal coordinate changes from anion to neutral.
C     At the end, Duschinsky rotarion matrix is calculated.
C
C     This program can also be used to calculation the neutral geometry
C     given the anion geometry, force constants and normal coordinates
C     changes.
C
C     Max number of atoms set with ndim, currently 10.  LWORK is the
C     dimention of the working array used by LAPACK library.
C
C     Files description:
C     ##.ageom    ("##" is the name of the molecule, ie. si4)
C           It contains the anion geometry in cartesian coordinates.
C     ##.ngeom
C           It contains the neutral geometry in cartesian coordinates.
C     ##.info
C           It contains the number of atoms, masses, comment line
C           and some options on the calculation.
C     ##.nfc
C           It contains the neutral force constant matrix from ab initio
C           calculations.  They are in atomic units (Hatrees/Bohr).
C     ##.afc
C           It contains the anion force constant matrix from ab initio
C           calculations.  They are in atomic units (Hatrees/Bohr).
C     ##.out
C           Output file.
C     ##.ageom.out
C           Output file of second type of calculation (derive anion
C           geometry from known neutral geometry, force constants
C           and normal coordinate changes).
C     ##.ngeom.out
C           Output file of neutral geometry similar to ##.ageom.out
C           (derive neutral geometry from known anion geometry,
C           force constants, and normal coordinate changes).
C
C
C
```

```
C     Usage:
C     1). Get the ##.ageom, ##.afc, ##.ngeom, and ##.nfc from ab initio
C         calculations such as Gaussian.
C     2). Use infogen program to generate ##.info file for normal
C         program.
C     3). Use rotate program to align and rotate ##.ngeom, so that the
C         center of mass and the principal axises won't change from
C         anion to neutral. This program will generate a ##.rot file.
C     4). Run normal program to get the normal coordinate changes or
C         geometry info.
C     5). Repeat 3), 4) until the change of transition and rotation
C         modes are zero or very close to.
C

C
C     Input file example:
C
C       si3.info
C           3            Number of atoms
C            28.0000     Mass of each atom
C            28.0000     Mass of each atom
C            28.0000     Mass of each atom
C           N            [L]inear or [N]onlinear molecule
C           y            Whether to print normal mode vectors
C            Si3 1-B1 state FCF simulation using MP2/6-31G* results
C           y            Whether to use extended FC analysis
C           A            [A]nion or [N]eutral has known geometry
C            7    7      0.300
C            9    9      0.460
C
C
C       si3.ageom
C           0.000000    0.000000    0.000000
C           0.000000    0.000000    2.239718
C           2.040293    0.000000    0.923871
C
C
C       si3.ngeom
C           -0.019857    0.000000   -0.029774
C           -0.044764    0.000000    2.290526
C            2.104914    0.000000    0.902837
C
C
C       si3.afc
C                    1           2           3           4           5
C           1  0.143146D+00
C           2  0.000000D+00  0.777120D-05
C           3  0.268979D-01  0.000000D+00  0.167506D+00
C           4  0.508382D-04  0.000000D+00  0.853046D-04  0.468654D-01
C           5  0.000000D+00 -0.388558D-05  0.000000D+00  0.000000D+00 -0.188783D-04
C           6  0.378814D-01  0.000000D+00 -0.155377D+00 -0.302964D-01  0.000000D+00
C           7 -0.143197D+00  0.000000D+00 -0.269832D-01 -0.469163D-01  0.000000D+00
C           8  0.000000D+00 -0.388558D-05  0.000000D+00  0.000000D+00  0.227638D-04
C           9 -0.647792D-01  0.000000D+00 -0.121289D-01  0.302111D-01  0.000000D+00
C                    6           7           8           9
C           6  0.192048D+00
C           7 -0.758501D-02  0.190113D+00
C           8  0.000000D+00  0.000000D+00 -0.188783D-04
```

```
C            9 -0.366709D-01  0.345682D-01  0.000000D+00  0.487998D-01
C
C
C       si3.nfc
C                    1             2             3             4             5
C            1  0.912150D-01
C            2  0.000000D+00  0.763011D-05
C            3  0.384028D-01  0.000000D+00  0.123948D+00
C            4 -0.180089D-02  0.000000D+00 -0.271968D-02  0.352190D-01
C            5  0.000000D+00 -0.381509D-05  0.000000D+00  0.000000D+00 -0.767068D-05
C            6  0.165597D-02  0.000000D+00 -0.105781D+00 -0.213257D-01  0.000000D+00
C            7 -0.894141D-01  0.000000D+00 -0.356831D-01 -0.334181D-01  0.000000D+00
C            8  0.000000D+00 -0.381509D-05  0.000000D+00  0.000000D+00  0.114858D-04
C            9 -0.400588D-01  0.000000D+00 -0.181674D-01  0.240453D-01  0.000000D+00
C                    6             7             8             9
C            6  0.120568D+00
C            7  0.196697D-01  0.122832D+00
C            8  0.000000D+00  0.000000D+00 -0.767074D-05
C            9 -0.147876D-01  0.160134D-01  0.000000D+00  0.329550D-01
C
```

```
      PARAMETER (ndim=30, LWORK=100)
      CHARACTER*79 comment
      CHARACTER*20 fname1, fname2, fname3, fname4, fname7, fname8
      CHARACTER*20 fname9, fname10
      CHARACTER*10 molecule
      CHARACTER*1 linear, modeprint, extend, knowngeom
      INTEGER noatoms, imollen, threen, iunit, transrotnum, INFO
      DOUBLE PRECISION conv, conv2
      DOUBLE PRECISION m(ndim), RM(ndim), WORK(LWORK)
      DOUBLE PRECISION q(ndim), freq(ndim), rn(ndim), ra(ndim), QQ(ndim)
      DOUBLE PRECISION c(ndim,ndim), fm(ndim,ndim), Ct(ndim,ndim)
      DOUBLE PRECISION evals(ndim), evecs(ndim,ndim), evecsa(ndim,ndim)
      DOUBLE PRECISION evecsn(ndim,ndim), duschinsky(ndim,ndim)
      DOUBLE PRECISION QQXA(ndim), QQXN(ndim), dq(ndim)
      DOUBLE PRECISION R(ndim,ndim), A(ndim,ndim,ndim)

C     Read in molecule name: this defines input files
      write(*,*) 'Molecule:  '
      read(*,'(A10)') molecule

      imollen=index(molecule,' ')-1
C     Anion geometry file
      fname1=molecule(1:imollen) //'.ageom'
      open(1,file=fname1)
C     Mass information and comments file
      fname2=molecule(1:imollen) //'.info'
      open(2,file=fname2)
C     Neutral Force constant matrix file
      fname3=molecule(1:imollen) //'.nfc'
      open(3,file=fname3)
C     Anion force constant matrix file
      fname4=molecule(1:imollen) //'.afc'
      open(4,file=fname4)
C     Neutral geometry file
      fname7=molecule(1:imollen) //'.ngeom'
      open(7,file=fname7)
```

```
C     Output file
      fname8=molecule(1:imollen) //'.out'
      open(8,file=fname8)
      fname9=molecule(1:imollen) //'.ngeom.out'
      fname10=molecule(1:imollen) //'.ageom.out'

C     Start by reading in masses from *.info (the old *.2) file
      read(2,*) noatoms
      threen=3*noatoms
      do num=1,noatoms
          read(2,*) m(3*num-2)
          m(3*num-1)=m(3*num-2)
          m(3*num)=m(3*num-2)
      enddo
C     Set verbose flag in *.info (*.2), to indicate whether normal mode
C     vectors to be printed
      read(2,*) linear
      read(2,*) modeprint
      read(2,'(A79)') comment
      read(2,'(A1)') extend
      if ((extend .eq. 'Y').or.(extend .eq. 'y')) then
          read(2,'(A1)') knowngeom
          do i=1,threen
            QQXA(i)=0.0
            QQXN(i)=0.0
          enddo
          do i=1,threen
            read(2,*,end=10) j, k, QQXA(j)
            QQXN(k)=QQXA(j)
          enddo
   10 endif
      close(2)
C     Finish reading *.info file

C     Write up output header
      write(*,*) comment
      write(*,*) 'Masses used in this run are:'
      write(*,'(9(f6.2,2x),/)') (m(3*i),i=1,noatoms)
      write(*,*)
      write(8,*) comment
      write(8,*) 'Masses used in this run are:'
      write(8,'(9(f6.2,2x),/)') (m(3*i),i=1,noatoms)
      write(8,*)


C     Conversion factors are for hartrees/bohr/bohr to N/m
C     and for mass in amu to kg
      conv=1.66056d-27
      conv2=27.2116*96.4885d03/6.022d23/5.29177d-11/5.29177d-11


C     Start main do loop over anion and neutral
      do 1000 istate=1,2

          if (istate .eq. 1) then
            write(*,*) '**** ANION ****'
            write(8,*) '**** ANION ****'
          else
            write(*,*) '**** NEUTRAL ****'
            write(8,*) '**** NEUTRAL ****'
          endif
```

```
C     Set up which file force constants are coming from
          if (istate .eq. 1) iunit=4
          if (istate .eq. 2) iunit=3

          call inarrs(iunit,ndim,c,threen,threen)

          write(*,*) 'Force constant matrix from input file:'
          call showarrs(ndim,c,threen,threen)

C     Convert force constant matrix from theoretical calculation output
C     to mass weighted with the units of N/m
          do i=1,threen
            RM(i)=1.0/(sqrt(m(i)))
          enddo
          do j=1,threen
            do i=1,j
               c(i,j)=c(i,j)*conv2
               fm(i,j)=RM(i)*c(i,j)*RM(j)
C     The input real symmetric matrix for LAPACK library
               evecs(i,j)=fm(i,j)
            enddo
          enddo

C     Diagonalise mass weighted force constant matrix with LAPACK
C     library

          call dsyev('V','U',threen,evecs,ndim,evals,WORK,LWORK,INFO)

C     Hold eigenvectors to evecsa(i,j) for anion, and evecsn(i,j) for
C     neutral
C     This is for the later Duschinsky analysis
          if (istate .eq. 1) then
            do i=1,threen
               do j=1,threen
                 evecsa(i,j)=evecs(i,j)
               enddo
            enddo
          else
            do i=1,threen
               do j=1,threen
                 evecsn(i,j)=evecs(i,j)
               enddo
            enddo
          endif

          do i=1,threen
            if (evals(i) .lt. 0.0) then
               write(*,500) i
               write(8,500) i
            endif
          enddo
  500 format('Mode ',i2,' has negative eigenvalue! :(')

C     Convert eigenvalues to the units of cm-1 (frequencies)
          do i=1,threen
            freq(i)=sqrt(abs(evals(i)))*130.27809
          enddo

          write(*,*)
          write(*,*) 'Harmonic frequencies in cm-1:'
```

```
          write(*,510) (freq(i),i=1,threen)
          write(8,*)
          write(8,*) 'Harmonic frequencies in cm-1:'
          write(8,510) (freq(i),i=1,threen)
  510 format(30(f7.1,2x))

          write(*,*) 'Eigenvectors are:'
          do i=1,threen
            write(*,511) (evecs(i,j),j=1,threen)
          enddo
          write(*,*)
          if ((modeprint .eq. 'Y') .or. (modeprint .eq. 'y')) then
            write(8,*) 'Eigenvectors are:'
            do i=1,threen
                write(8,511) (evecs(i,j),j=1,threen)
            enddo
            write(8,*)
          endif
  511 format(30(f7.3,2x))


C     Now read ion and neutral geometry and calculate difference
C     Read the cartesian cordinates of atoms in anion from *.ageom
C     (the old *.1) file to array ra, and the neutral from *.ngeom
C     (the old *.7) file to array rn.  Finally, convert those to
C     mass weighted coordinates, in units of A*(amu)^0.5.
          if (istate .eq. 1) then
            do i=1,noatoms
                 read(1,*) ra(3*i-2), ra(3*i-1), ra(3*i)
                 read(7,*) rn(3*i-2), rn(3*i-1), rn(3*i)
            enddo
            close(1)
            close(7)

            do i=1,threen
                q(i)=(rn(i)-ra(i))*sqrt(m(i))
                if (icad .eq. 1) q(i)=q(i)*.529177
            enddo
          endif

         write(*,*) 'The mass weighted displacement from anion to neutral'
         write(*,*) ' #   X       Y       Z'
         write(*,520) (i, q(3*i-2), q(3*i-1), q(3*i), i=1,noatoms)
  520 format(i3,f9.3,f9.3,f9.3)
          write(*,*)

          write(8,*) 'Anion Cartesian coordinates:'
          write(8,*) ' #   Mass      X       Y       Z'
          write(8,521) (i, m(3*i), ra(3*i-2), ra(3*i-1), ra(3*i),
i=1,noatoms)
  521 format(i3, f8.2, f9.3, f9.3, f9.3)
          write(8,*) 'Neutral Cartesian coordinates:'
          write(8,521) (i, m(3*i), rn(3*i-2), rn(3*i-1), rn(3*i),
i=1,noatoms)

          write(8,*)


C     Calculate the transpose of the C matrix that diagonalises F
C     Lambda=C^t F C  and QQ=C^t q
```

```
          call transpos(ndim,evecs,Ct)

          call matmult(ndim,Ct,q,QQ)

          write(*,*)'The normal coord. displacement from anion to
neutral'
          if (istate .eq.1) then
            write(*,*)'In terms of normal coordinates of anion are:'
          else
            write(*,*)'In terms of normal coordinates of neutral are:'
          endif
          if ((linear .eq. 'L') .or. (linear .eq. 'l')) then
            transrotnum=5
          else
            transrotnum=6
          endif
          write(*,*)'Trans. and rots.'
          write(*,530) (' N(',0,')', QQ(i), freq(i),i=1,transrotnum)
          write(*,*) 'Mode       dQ       Frequency'
          write(*,530) ('dQ(',i-6,')', QQ(i), freq(i), i=transrotnum+1
,threen)
  530 format(a3,i2,a1,2x,f8.3,8x,f9.2)
          write(*,*)

          write(8,*)'The normal coord. displacement from anion to
neutral'
          if (istate .eq.1) then
            write(8,*)'In terms of normal coordinates of  anion  are:'
          else
            write(8,*)'In terms of normal coordinates of neutral are:'
          endif
          write(8,*)'Trans. and rots.'
          write(8,530) (' N(',0,')', QQ(i), freq(i),i=1,transrotnum)
          write(8,*) 'Mode       dQ          Frequency'
          write(8,530) ('dQ(',i-6,')', QQ(i), freq(i),
i=transrotnum+1,threen)
          write(8,*)


C     End of anion basis now do for istate=2 (neutral basis)
 1000 continue


C     Begin the process of the optional analysis to determine
C     the geometry of one of the species if one knows the dQ's
C     and the geometry (and FC's) of the other.  Set up to do
C     all of the 4 possible calculations since it takes
C     ~no time.(ie, fix anion-1)neutral FC's;2)anion FC's...
C     fix neutral-1)neutral FC's;2)anion FC's.)

      if ((extend .ne. 'Y') .and. (extend .ne. 'y')) go to 110
      write(*,*) '**** Entering Extended NC Analysis ****'
      write(*,*) '  Assume:'
      if ((knowngeom .eq. 'A') .or. (knowngeom .eq. 'a')) then
          write(*,*) 'Case I: find neutral geom. from known anion geom.'
          write(*,550) (' N(',0,')=', QQXN(i), i=1,transrotnum)
          write(*,550) ('dQ(',i-6,')=', QQXN(i), i=transrotnum+1,threen)
  550 format(a3,i2,a2,f8.3)
          open(9,file=fname9)
          write(9,*) 'Case I: find neutral geom. from known anion geom.'
          write(9,550) (' N(',0,')=', QQXN(i), i=1,transrotnum)
```

```
          write(9,550) ('dQ(',i-6,')=', QQXN(i), i=transrotnum+1,threen)

          write(*,*) 'Anion geometry given in ##.ageom file'
          write(*,*) ' #   Mass       X        Y        Z'
          write(*,521) (i, m(3*i), ra(3*i-2), ra(3*i-1), ra(3*i),
i=1,noatoms)
          write(*,*) 'The neutral geometry'

          write(9,*) 'Anion geometry given in ##.ageom file'
          write(9,*) ' #   Mass       X        Y        Z'
          write(9,521) (i, m(3*i), ra(3*i-2), ra(3*i-1), ra(3*i),
i=1,noatoms)
          write(9,*) 'The neutral geometry'

          write(*,*) '    Using anion FCs and fixing anion geometry'
          write(9,*) '    Using anion FCs and fixing anion geometry'
          call matmult(ndim,evecsa,QQXN,dq)
          do i=1,threen
            rn(i)=dq(i)/sqrt(m(i))+ra(i)
          enddo
          write(*,521) (i, m(3*i), rn(3*i-2), rn(3*i-1), rn(3*i),
i=1,noatoms)
          write(9,521) (i, m(3*i), rn(3*i-2), rn(3*i-1), rn(3*i),
i=1,noatoms)

          call internal(ndim,noatoms,9,rn,R,A)

          write(*,*) '    Using neutral FCs and fixing anion geometry'
          write(9,*) '    Using neutral FCs and fixing anion geometry'
          write(9,*) ' #   Mass       X        Y        Z'
          call matmult(ndim,evecsn,QQXN,dq)
          do i=1,threen
            rn(i)=dq(i)/sqrt(m(i))+ra(i)
          enddo
          write(*,521) (i, m(3*i), rn(3*i-2), rn(3*i-1), rn(3*i),
i=1,noatoms)
          write(9,521) (i, m(3*i), rn(3*i-2), rn(3*i-1), rn(3*i),
i=1,noatoms)

          call internal(ndim,noatoms,9,rn,R,A)

          close(9)

      else
          write(*,*) 'Case II: find anion geom. from known neutral
geom.'
          write(*,550) (' N(',0,')=', QQXN(i), i=1,transrotnum)
          write(*,550) ('dQ(',i-6,')=', QQXN(i), i=transrotnum+1,threen)
          open(10,file=fname10)
          write(10,*) 'Case II: find anion geom. from known neutral
geom.'
          write(10,550) (' N(',0,')=', QQXN(i), i=1,transrotnum)
          write(10,550) ('dQ(',i-6,')=', QQXN(i),
i=transrotnum+1,threen)

          write(*,*) 'Neutral geometry given in ##.ngeom file'
          write(*,*) ' #   Mass       X        Y        Z'
          write(*,521) (i, m(3*i), rn(3*i-2), rn(3*i-1), rn(3*i),
i=1,noatoms)
          write(*,*) 'The anion geomtry'
```

```
          write(10,*) 'Neutral geometry given in ##.ngeom file'
          write(10,*) ' #   Mass       X        Y        Z'
          write(10,521) (i,m(3*i), rn(3*i-2), rn(3*i-1), rn(3*i),
i=1,noatoms)
          write(10,*) 'The anion geomtry'

          write(*,*) '    Using anion FCs and fixing neutral geometry'
          write(10,*) '    Using anion FCs and fixing neutral geometry'
          call matmult(ndim,evecsa,QQXN,dq)
          do i=1,threen
            ra(i)=rn(i)-dq(i)/sqrt(m(i))
          enddo
          write(*,521) (i, m(3*i), ra(3*i-2), ra(3*i-1), ra(3*i),
i=1,noatoms)
          write(10,521) (i,m(3*i), ra(3*i-2), ra(3*i-1), ra(3*i),
i=1,noatoms)

            call internal(ndim,noatoms,10,rn,R,A)

          write(*,*) '    Using neutral FCs and fixing neutral geometry'
          write(10,*) '    Using neutral FCs and fixing neutral
geometry'
          write(10,*) ' #   Mass       X        Y        Z'
          call matmult(ndim,evecsn,QQXN,dq)
          do i=1,threen
            ra(i)=rn(i)-dq(i)/sqrt(m(i))
          enddo
          write(*,521) (i, m(3*i), ra(3*i-2), ra(3*i-1), ra(3*i),
i=1,noatoms)
          write(10,521) (i,m(3*i), ra(3*i-2), ra(3*i-1), ra(3*i),
i=1,noatoms)

          call internal(ndim,noatoms,10,rn,R,A)

          close(10)

      endif


C     Now multiply evecs of neutral by those of anion to calculate
C     degree of Duschinsky rotation J"= L"^t L'

  110 write(*,*) '**** Duschinsky Analysis ****'
      write(8,*) '**** Duschinsky Analysis ****'

      call transpos(ndim,evecsa,Ct)
      call matm(ndim,Ct,evecsn,duschinsky)

      write(*,*) 'Compare anion and neutral normal coordinates :'
      write(*,*) 'Duschinsky Rotation matrix J" is :'
      do i=1,threen
          write(*,540) (duschinsky(i,j),j=1,threen)
      enddo
      write(*,*) 'Part corresponding to vibrations only:'
      do i=transrotnum+1,threen
          write(*,540) (duschinsky(i,j),j=transrotnum+1,threen)
      enddo
  540 format(30(f6.2))
      write(*,*)

      write(8,*) 'Compare anion and neutral normal coordinates :'
```

```
      write(8,*) 'Duschinsky Rotation matrix J"'
      write(8,*) 'Part corresponding to vibrations only :'
      do i=transrotnum+1,threen
         write(8,540) (duschinsky(i,j),j=transrotnum+1,threen)
      enddo
      write(8,*)



      STOP
      END



C *********************************************
      SUBROUTINE inarrs(iunit,ndim,a,nra,nca)
C *********************************************
C     Reads the Force constants matrix output from Gaussian calculations

      DOUBLE PRECISION a(ndim,ndim)
      INTEGER iunit, ndim, nra, nca, temp(5)

      do ig=1,nca/5
          read(iunit,*) (temp(ic), ic=1,5)
          do ir=5*(ig-1)+1,nra
            imax = ir - 5*(ig-1)
            if (imax.gt.5) imax=5
            read(iunit,*) temp(1),(a(ic+5*(ig-1),ir), ic = 1,imax)
          enddo
      enddo
      ileft = nca - 5*(nca/5)
      if (ileft.gt.0) then
          read(iunit,*) (temp(ic),ic=1,ileft)
          do ir=5*(nca/5)+1, nra
            imax = ir - 5*(nca/5)
            read(iunit,*) temp(1),(a(ic+5*(nca/5),ir), ic = 1,imax)
          enddo
      endif

      return
      end


C ***************************************
      SUBROUTINE matm(ndim,a,b,c)
C ***************************************
C     Finds C = AB, where A,B, C are matrices.

      INTEGER ndim
      DOUBLE PRECISION a(ndim,ndim), b(ndim,ndim), c(ndim,ndim)

      do i=1,ndim
         do j=1,ndim
           c(i,j)=0.0
         enddo
      enddo

      do icc=1,ndim
```

```
            do ir=1,ndim
              do ic=1,ndim
                  c(ir,icc)=c(ir,icc)+a(ir,ic)*b(ic,icc)
              enddo
            enddo
        enddo

        return
        end

C ****************************************
        SUBROUTINE matmult(ndim,a,b,c)
C ****************************************
C       Finds c = Ab, where A is matrix and c, b are vectors.

        INTEGER ndim
        DOUBLE PRECISION a(ndim,ndim), b(ndim), c(ndim)

        do i=1,ndim
            c(i)=0.0
        enddo

        do ir=1,ndim
            do ic=1,ndim
              c(ir)=c(ir)+a(ir,ic)*b(ic)
            enddo
        enddo

        return
        end


C ***********************************************
        SUBROUTINE showarrs(ndim,a,nra,nca)
C ***********************************************
C       Shows the lower triangle of a N-by-N symmetric matrix

        INTEGER ndim, ileft, imax, nra, nca
        DOUBLE PRECISION a(ndim,ndim)

        do ig=1,nca/9
            write(*,'(x,9(5x,i3))') (ic+9*(ig-1), ic=1,9)
            do ir = 9*(ig-1)+1,nra
              imax = ir - 9*(ig-1)
              if (imax.gt.9) imax=9
              write(*,'(i3,9(f8.3))') ir,(a(ic+9*(ig-1),ir), ic = 1,imax)
            enddo
        enddo

        ileft = nca - 9*(nca/9)
        if (ileft.gt.0) then
            write(*,'(x,9(5x,i3))') (ic+9*(nca/9), ic=1,ileft)
            do ir = 9*(nca/9)+1, nra
              imax = ir - 9*(nca/9)
              write(*,'(i3,9(f8.3))') ir,(a(ic+9*(nca/9),ir), ic = 1,imax)
            enddo
        endif

        return
        end
```

```
C ************************************
      SUBROUTINE transpos(ndim,a,at)
C ************************************
C     Finds At = A (transpose)

      INTEGER ndim
      DOUBLE PRECISION a(ndim,ndim), at(ndim,ndim)

      do ir=1,ndim
          do ic=1,ndim
            at(ir,ic)=a(ic,ir)
          enddo
      enddo

      return
      end


C ************************************************************
      SUBROUTINE internal(ndim,noatoms,iodevice,array,R,A)
C ************************************************************
C     Converts a Cartesian coordinate array to internal coordinates
C     and shows the internal bond length and bond angle to the screen
C     and I/O device with iodevice

      PARAMETER (nmax=10)
      INTEGER ndim, noatoms,iodevice
      DOUBLE PRECISION array(ndim), X(nmax), Y(nmax), Z(nmax)
      DOUBLE PRECISION R(nmax,nmax), A(nmax,nmax,nmax)
      DOUBLE PRECISION cosA(nmax,nmax,nmax)

C     Read in Cartesian coordinates from array
      do i=1,noatoms
          X(i)=array(3*i-2)
          Y(i)=array(3*i-1)
          Z(i)=array(3*i)
      enddo

C     Calculate internal coordinates: bond length
      write(*,*) 'Output Internal coordinates:'
      write(*,*) 'Definition                Value'
      write(*,*) 'Bond length             Angstroms'
      write(iodevice,*) 'Output Internal coordinates:'
      write(iodevice,*) 'Definition                Value'
      write(iodevice,*) 'Bond length             Angstroms'
      do i=1,noatoms
          do j=i+1,noatoms
            R(i,j)=sqrt((X(i)-X(j))**2+(Y(i)-Y(j))**2+(Z(i)-Z(j))**2)
            write(*,510) i, j, R(i,j)
            write(iodevice,510) i, j, R(i,j)
          enddo
      enddo
  510 format(' R(',I2,',',I2,')',T28,f5.3)

C     Calculate internal coordinates: bond angle
      if (noatoms .le. 2) go to 10

      write(*,*) 'Bond Angle                Degrees'
      write(iodevice,*) 'Bond Angle                Degrees'
```

```
      do i=1,noatoms
          do j=1,noatoms
            if (j .eq. i) go to 20
                  do k=i+1,noatoms
                if (k .eq. j) go to 30
                R(i,j)=sqrt((X(i)-X(j))**2+(Y(i)-Y(j))**2+(Z(i)-
Z(j))**2)
                R(j,k)=sqrt((X(j)-X(k))**2+(Y(j)-Y(k))**2+(Z(j)-
Z(k))**2)
                R(k,i)=sqrt((X(k)-X(i))**2+(Y(k)-Y(i))**2+(Z(k)-
Z(i))**2)
                cosA(i,j,k)=(R(i,j)**2+R(j,k)**2-R(k,i)**2)/
     x                        (2*R(i,j)*R(j,k))
                A(i,j,k)=acos(cosA(i,j,k))*360/2/3.141592654
                write(*,520) i, j, k, A(i,j,k)
                write(iodevice,520) i, j, k, A(i,j,k)
   30         enddo
   20       enddo
      enddo
  520 format(' A(',I2,',',I2,',',I2,')',T26,f7.3)

      write(*,*)
      write(iodevice,*)

   10 return
      end
```

```
      Program ROTATE
      Implicit double precision (A-H,O-Z)

c     Program to do molecule translation and rotation so that
c     center of mass is same and that there is no rotation of
c     molecule when calculating NC changes.
c     to the zeros.

c     For 6 atom molecule, modified by DLO, 7/27/96
c     For n atom molecule, along 3 axises, modified by C.X. 10/12/96

      integer nmax, n1
c     Max number of atoms set with nmax, currently 10.
      parameter(nmax=10)
      real*8 MASS(nmax)

      dimension X1(nmax),Y1(nmax),Z1(nmax)
      dimension X2(nmax),Y2(nmax),Z2(nmax)
      dimension XN1(nmax),YN1(nmax),ZN1(nmax)
      dimension XN2(nmax),YN2(nmax),ZN2(nmax)
      dimension RX2(nmax),RY2(nmax),RZ2(nmax)
      dimension XROT(2,2), YROT(2,2), ZROT(2,2)
      dimension XYN(2,nmax), YZN(2,nmax), ZXN(2,nmax)
      dimension XY(2,nmax), YZ(2,nmax), ZX(2,nmax)

      character*20 FNAMEIN1,FNAMEIN2,FNAMEINFO,FNAMEOUT
      character*1 redo

      pi=3.141592654

      write(*,*) 'Name of file from which to get geometry of #1?'
      write(*,*) 'This will be the FIXED axis'
      read(*,*) FNAMEIN1

      write(*,*) 'Name of file from which to get geometry of #2?'
      write(*,*) 'This axis will be SHIFTED'
      read(*,*) FNAMEIN2

      write(*,*) 'Name of file from which to get mass info?'
      write(*,*) 'The same file (*.info) to do normal mode calculation'
      read(*,*) FNAMEINFO

 1000 write(*,*) 'Rotate clockwise along X axis by what angle
(degrees)?'
      read(*,*) ALPHA

      write(*,*) 'Rotate clockwise along Y axis by what angle
(degrees)?'
      read(*,*) BETA

      write(*,*) 'Rotate clockwise along Z axis by what angle
(degrees)?'
      read(*,*) GAMMA

      INAME=index(FNAMEIN2,' ')-1
      FNAMEOUT=FNAMEIN2(1:INAME)//'.rot'


      open(14,file=FNAMEINFO)
      read(14,*) n1
      write(*,*)
```

```
      write(*,*) 'Number of atoms: ', n1
      do 50 i=1,n1
       read(14,*) MASS(i)
       write(*,*) 'Mass(', i, '): ', MASS(i)
   50 continue
      close(14)
      write(*,*)

      write(*,*) '  Original Coordinate for #1:'
      open(10,file=FNAMEIN1)
      do 100 i=1,n1
      read(10,*) X1(i),Y1(i),Z1(i)
      write(*,103) X1(i),Y1(i),Z1(i)
  100 continue
      close(10)
      write(*,*)
      write(*,*) '  Original Coordinate for #2:'
      open(12,file=FNAMEIN2)
      do 101 i=1,n1
      read(12,*) X2(i),Y2(i),Z2(i)
      write(*,103) X2(i),Y2(i),Z2(i)
  101 continue
      close(12)
      write(*,*)
  102 format(I3,2x,f9.6,3x,f9.6,3x,f9.6,3x,f9.6)
  103 format(f9.6,3x,f9.6,3x,f9.6)


c     Determine Center of Mass of molecule #1
      TMPX=0.
      TMPY=0.
      TMPZ=0.

      do 110 i=1,n1
      TMPX=TMPX+MASS(i)*X1(i)
      TMPY=TMPY+MASS(i)*Y1(i)
      TMPZ=TMPZ+MASS(i)*Z1(i)
  110 continue

c     Calculate the total mass
      SUMMASS=0.
      do 112 i=1,n1
      SUMMASS=SUMMASS+MASS(i)
  112 continue

      CMX1=TMPX/SUMMASS
      CMY1=TMPY/SUMMASS
      CMZ1=TMPZ/SUMMASS

      TMPX=0.
      TMPY=0.
      TMPZ=0.

c     Determine Center of Mass of molecule #2

      do 113 i=1,n1
      TMPX=TMPX+MASS(i)*X2(i)
      TMPY=TMPY+MASS(i)*Y2(i)
      TMPZ=TMPZ+MASS(i)*Z2(i)
  113 continue
```

```
      CMX2=TMPX/SUMMASS
      CMY2=TMPY/SUMMASS
      CMZ2=TMPZ/SUMMASS

      write(*,*) '   Center of mass of #1 located at:'
      write(*,120) CMX1
      write(*,121) CMY1
      write(*,122) CMZ1
      write(*,*)

      write(*,*) '   Center of mass of #2 located at:'
      write(*,120) CMX2
      write(*,121) CMY2
      write(*,122) CMZ2
      write(*,*)
  120 format(2x,'X:  ',f9.6)
  121 format(2x,'Y:  ',f9.6)
  122 format(2x,'Z:  ',f9.6)

c     Shift molecule #2 wrt #1 so that cm are at same point

      DX=CMX1-CMX2
      DY=CMY1-CMY2
      DZ=CMZ1-CMZ2

      do 130 i=1,n1
       XN1(i)=X1(i)
       YN1(i)=Y1(i)
       ZN1(i)=Z1(i)
       XN2(i)=X2(i)+DX
       YN2(i)=Y2(i)+DY
       ZN2(i)=Z2(i)+DZ
  130 continue

      write(*,*) '  New Coordinates for #1 (fixed, no changed):'

      do 140 i=1,n1
       write(*,103) XN1(i),YN1(i),ZN1(i)
  140 continue
      write(*,*)
      write(*,*) '  New Coordinates for #2:'
      do 150 i=1,n1
      write(*,103) XN2(i),YN2(i),ZN2(i)
  150 continue
      write(*,*)

c     Determine NEW Center of Mass of molecule #1
      TMPX=0.
      TMPY=0.
      TMPZ=0.

      do 160 i=1,n1
      TMPX=TMPX+MASS(i)*XN1(i)
      TMPY=TMPY+MASS(i)*YN1(i)
      TMPZ=TMPZ+MASS(i)*ZN1(i)
  160 continue

      CMX1=TMPX/SUMMASS
      CMY1=TMPY/SUMMASS
      CMZ1=TMPZ/SUMMASS
```

```
      TMPX=0.
      TMPY=0.
      TMPZ=0.

c     Determine NEW Center of Mass of molecule #2

      do 163 i=1,n1
      TMPX=TMPX+MASS(i)*XN2(i)
      TMPY=TMPY+MASS(i)*YN2(i)
      TMPZ=TMPZ+MASS(i)*ZN2(i)
  163 continue

      CMX2=TMPX/SUMMASS
      CMY2=TMPY/SUMMASS
      CMZ2=TMPZ/SUMMASS

      write(*,*) '   NEW Center of mass of #1 (fixed) located at:'
      write(*,120) CMX1
      write(*,121) CMY1
      write(*,122) CMZ1
      write(*,*)

      write(*,*) '   NEW Center of mass of #2 located at:'
      write(*,120) CMX2
      write(*,121) CMY2
      write(*,122) CMZ2
      write(*,*)

c     To rotate, first move #2 so that cm is at origin
      do 170 i=1,n1
      RX2(i)=XN2(i)-CMX2
      RY2(i)=YN2(i)-CMY2
      RZ2(i)=ZN2(i)-CMZ2
  170 continue


c     Test that NEW Center of Mass of molecule #2 is at (0,0,0)
      TMPX=0.
      TMPY=0.
      TMPZ=0.

      do 173 i=1,n1
      TMPX=TMPX+MASS(i)*RX2(i)
      TMPY=TMPY+MASS(i)*RY2(i)
      TMPZ=TMPZ+MASS(i)*RZ2(i)
  173 continue

      RCMX2=TMPX/SUMMASS
      RCMY2=TMPY/SUMMASS
      RCMZ2=TMPZ/SUMMASS

      write(*,*) '   Shift Center of mass of #2 for rotation step to:'
      write(*,120) RCMX2
      write(*,121) RCMY2
      write(*,122) RCMZ2
      write(*,*) '  With atom positions:'
      do 195 i=1,n1
       write(*,103) RX2(i),RY2(i),RZ2(i)
  195 continue
      write(*,*)
```

```
c     Use rotation matrix to rotate the molecule by THETA degrees
c           cos  -sin
c           sin   cos

      ALPHARAD=(ALPHA*2.0*pi)/360.0
      BETARAD=(BETA*2.0*pi)/360.0
      GAMMARAD=(GAMMA*2.0*pi)/360.0

      XROT(1,1)=cos(ALPHARAD)
      XROT(1,2)=-sin(ALPHARAD)
      XROT(2,1)=sin(ALPHARAD)
      XROT(2,2)=cos(ALPHARAD)

      YROT(1,1)=cos(BETARAD)
      YROT(1,2)=-sin(BETARAD)
      YROT(2,1)=sin(BETARAD)
      YROT(2,2)=cos(BETARAD)

      ZROT(1,1)=cos(GAMMARAD)
      ZROT(1,2)=-sin(GAMMARAD)
      ZROT(2,1)=sin(GAMMARAD)
      ZROT(2,2)=cos(GAMMARAD)

      write(*,*)'  Rotation matrix (along X axis by', ALPHA, '
degrees):'
      write(*,179) XROT(1,1), XROT(1,2)
      write(*,179) XROT(2,1), XROT(2,2)
  179 format(2x,f9.6,1x,f9.6)
      write(*,*)
      write(*,*)'  Rotation matrix (along Y axis by', BETA, ' degrees):'
      write(*,179) YROT(1,1), YROT(1,2)
      write(*,179) YROT(2,1), YROT(2,2)
      write(*,*)
      write(*,*)'  Rotation matrix (along Z axis by', GAMMA, '
degrees):'
      write(*,179) ZROT(1,1), ZROT(1,2)
      write(*,179) ZROT(2,1), ZROT(2,2)
      write(*,*)

c     Make planar matrix to multiply

      do 1 i=1,2
       do 2 j=1,n1
        XYN(i,j)=0.0
        ZXN(i,j)=0.0
        YZN(i,j)=0.0
    2  continue
    1 continue

c     Start rotation along X axis
      do 180 i=1,n1
       YZ(1,i)=RY2(i)
       YZ(2,i)=RZ2(i)
  180 continue

      do 10 i=1,2
       do 20 j=1,n1
        TEMP=0.0
        do 30 k=1,2
         YZN(i,j)=TEMP+XROT(i,k)*YZ(k,j)
```

```
          TEMP=YZN(i,j)
    30    continue
    20   continue
    10  continue
c       Finish rotation along X axis

c       Update new coordinates
        do 190 i=1,n1
         RY2(i)=YZN(1,i)
         RZ2(i)=YZN(2,i)
   190  continue

c       Start rotation along Y axis
        do 182 i=1,n1
         ZX(1,i)=RZ2(i)
         ZX(2,i)=RX2(i)
   182  continue

        do 12 i=1,2
         do 22 j=1,n1
          TEMP=0.0
          do 32 k=1,2
           ZXN(i,j)=TEMP+YROT(i,k)*ZX(k,j)
           TEMP=ZXN(i,j)
    32    continue
    22   continue
    12  continue
c       Finish rotation along Y axis

c       Update new coordinates
        do 192 i=1,n1
         RZ2(i)=ZXN(1,i)
         RX2(i)=ZXN(2,i)
   192  continue

c       Start rotation along Z axis
        do 184 i=1,n1
         XY(1,i)=RX2(i)
         XY(2,i)=RY2(i)
   184  continue

        do 14 i=1,2
         do 24 j=1,n1
          TEMP=0.0
          do 34 k=1,2
           XYN(i,j)=TEMP+ZROT(i,k)*XY(k,j)
           TEMP=XYN(i,j)
    34    continue
    24   continue
    14  continue
c       Finish rotation along Z axis

c       Update new coordinates
        do 194 i=1,n1
         RX2(i)=XYN(1,i)
         RY2(i)=XYN(2,i)
   194  continue

        write(*,*)'  Rotated and Translated Coordinates of Molecule #2, CM
at (0,0,0):'
        do 240 i=1,n1
```

```
      write(*,103) RX2(i),RY2(i),RZ2(i)
  240 continue
      write(*,*)

c     Move back such that CM is same as cm of #1
      do 175 i=1,n1
       XN2(i)=RX2(i)+CMX2
       YN2(i)=RY2(i)+CMY2
       ZN2(i)=RZ2(i)+CMZ2
  175 continue

      open(16,file=FNAMEOUT)
      write(*,*)'  Rotated and Translated Coordinates of Molecule #2:'
      write(*,*)' #     Mass          X           Y           Z'
      do 245 i=1,n1
       write(16,103) XN2(i),YN2(i),ZN2(i)
       write(*,102) i, mass(i), XN2(i),YN2(i),ZN2(i)
  245 continue
      close(16)
      write(*,*)

C     Ask for retry
      write(*,*) 'Redo rotation with new angles [Y/n]? '
      read(*,'(A1)') redo
      if ((redo .ne. 'n') .and. (redo .ne. 'N')) then
          goto 1000
      endif

      stop'o.k.'
      end
```

```
      PROGRAM infogen
C     This program generates the ##.info file for normal mode
calculation
C     program normal.
C
C     11/15/96    C.X.
C

      PARAMETER (nmax=10, ndim=30)
      INTEGER noatoms, imollen, anionmode(ndim), neutralmode(ndim),
numdq
      CHARACTER*1 linear, modeprint, extend, knowngeom, moredq
      CHARACTER*10 molecule
      CHARACTER*20 fname
      CHARACTER*79 comment
      REAL m(nmax), dq(ndim)


C     Read in molecule name: this defines the file name
      write(*,*) 'Molecule: '
      read(*,'(A10)') molecule

C     Generate info file name
      imollen=index(molecule,' ')-1
      fname=molecule(1:imollen) //'.info'
      open(1,file=fname)

C     Ask for number of atoms
      write(*,*) 'Number of atoms? '
      read(*,*) noatoms
      write(1,500) noatoms, 'Number of atoms'
  500 format(I2, 18X, A)

C     Ask for mass of each atom
      do i=1,noatoms
          write(*,*) 'Mass of #', i, ' atom: '
          read(*,*) m(i)
          write(1,510) m(i), 'Mass of each atom'
      enddo
  510 format(f8.4, 12X, A)

C     Ask for linear or nonlinear
  100 write(*,*) 'Is it a [L]inear or [N]onlinear molecule?'
      read(*,*) linear
      if ((linear.ne.'L').and.(linear.ne.'l').and.(linear.ne.'N').and.
     x            (linear.ne.'n')) go to 100
      if ((linear .eq. 'L') .or. (linear .eq. 'l')) then
          write(1,520) 'L', '[L]inear or [N]onlinear molecule'
      else
          write(1,520) 'N', '[L]inear or [N]onlinear molecule'
      endif
  520 format(A1, 19X, A)

C     Ask for whether normal mode vectors to be printed
      write(*,*) 'Print normal mode vectors to output file [N,y]?'
      read(*,*) modeprint
      if ((modeprint .eq. 'Y') .or. (modeprint .eq. 'y')) then
          write(1,520) 'y', 'Whether normal mode vectors to be printed'
      else
          write(1,520) 'n', 'Whether normal mode vectors to be printed'
      endif
```

```
C     Ask for comments
      write(*,*) 'Please input the comment line'
      read(*,'(A79)') comment
      write(1,*) comment

C     Ask for whether use extended FC analysis to derive geometry
      write(*,*) 'Use extended FC analysis to derive geometry info
[N/y]?'
      read(*,*) extend
      if ((extend .eq. 'Y') .or. (extend .eq. 'y')) then
          write(1,520) 'y',
     x                 'Whether use extended FC analysis to derive
geometry'
      else
          write(1,520) 'n',
     x                 'Whether use extended FC analysis to derive
geometry'
      endif

C     Ask for which species has known geometry
  200 if ((extend .eq. 'Y') .or. (extend .eq. 'y')) then
          write(*,*) 'Which species has known geometry [A]nion or
[N]eutral?'
          read(*,*) knowngeom
          if ((knowngeom.ne.'A').and.(knowngeom.ne.'a').and.
     x            (knowngeom.ne.'N').and.(knowngeom.ne.'n')) go to 200
          if ((knowngeom .eq. 'N') .or. (knowngeom .eq. 'n')) then
            write(1,520) 'N', '[A]nion or [N]eutral has known geometry'
          else
            write(1,520) 'A', '[A]nion or [N]eutral has known geometry'
          endif
      endif

C     Ask for dQ information for extended FC analysis
      if ((extend .eq. 'Y') .or. (extend .eq. 'y')) then
          write(*,*) 'Input dQ information'
          do i=1,3*noatoms
            write(*,*) 'dQ(',i,'): '
            write(*,*) '      correspond to which mode in anion?'
            read(*,*) anionmode(i)
            write(*,*) '      correspond to which mode in neutral?'
            read(*,*) neutralmode(i)
            write(*,*) '      dQ value in this mode: '
            read(*,*) dq(i)
            numdq=i
            write(*,*) 'More [Y/n]?'
            read(*,*) moredq
            if ((moredq .eq. 'N') .or. (moredq .eq. 'n')) go to 300
          enddo

  300     write(1,530) (anionmode(i), neutralmode(i), dq(i), i=1,numdq)
  530 format(I2,6X,I2,4X,f8.3)

      endif

      close(1)

      STOP
      END
```

Ernest Orlando Lawrence Berkeley National Laboratory
One Cyclotron Road | Berkeley, California 94720

Prepared for the U.S. Department of Energy under Contract No. DE-AC03-76SF00098